공학박사 학위논문

Surface Modification of Magnesium for Biomedical Applications: Its Degradation Behavior and Biological Response

생체 의료용 마그네슘의 표면처리:

이의 분해거동과 생체반응

2016 년 8 월

서울대학교 대학원

재료공학부

김 새 미

Abstract

Surface Modification of Magnesium for Biomedical Applications: Its Degradation Behavior and Biological Response

Sae-Mi Kim

Department of Materials Science and Engineering

Seoul National University

Magnesium (Mg) have received great attention as a suitable material for biomedical application in accordance with the increasing demand for biodegradable materials in recent years. No toxicity, similar mechanical properties to those of natural bone and biodegradability, which enables complete dissolution after the damaged tissue heals, are the most attractive characteristics of Mg. Despite these favorable features, high corrosion rate in physiological conditions restricts its practical use in clinical field. Numerous studies have been conducted to regulate

corrosion resistance of Mg, mainly categorized as alloying and surface modification. In this study, surface modification was vigorously explored because it can effectively modulate corrosion resistance, also can give an additional function to Mg such as improved bioactivity. Coating of the materials having excellent biocompatibility, such as hydroxyapatite (HA; $Ca_{10}(PO_4)_6(OH)_2$), could achieve both goals, corrosion protection and enhanced biological response.

The first study aimed at fabricating a biocompatible and corrosion protective coating for pure Mg substrate by introducing HA. HA was coated onto Mg in an aqueous solution containing calcium and phosphate sources to improve its *in vitro* and *in vivo* biocorrosion resistance, biocompatibility and bone response. A layer of needle-shaped HA crystals was created uniformly on the Mg substrate even when the Mg sample had a complex shape of a screw. This HA coating layer remarkably reduced the corrosion rate of the Mg tested in a simulated body fluid (SBF). Moreover, the biological responses, including cell attachment, proliferation and differentiation, of the HA coated samples were considerably enhanced compared to the samples without a coating layer. The preliminary *in vivo* experiments also showed that the biocorrosion of the Mg implant was significantly retarded by HA coating, which resulted in good mechanical stability. In addition, in the case of the HA coated implants, biodegradation was mitigated, particularly over the first 6 weeks of implantation. This considerably promoted bone growth at the interface between the implant and bone. These results confirmed that HA coated Mg is a promising material for biomedical implant applications.

In the second study, the attention was focused on producing the coating layer which is biocompatible, corrosion protective and strain-resistant at the same time by employing surface patterning. Micro-patterned HA and poly(L-lactic) acid (PLLA) coating has been introduced to pure Mg by the combination of photolithography and solution treatment, stated in above paragraph. Periodically arrayed HA rods with a diameter of 10 μm, were well fabricated on Mg with PLLA filling between the rods. In order to mimic real case and possible deformation during implantation, a 5% tensile strain was applied to the HA/PLLA patterned Mg. Compared with single HA coating and PLLA coating, HA/PLLA patterning showed good stability under strain and remarkably reduced the corrosion rate of Mg with no crack formation or delamination, resulting in negligible evolution of hydrogen gas in SBF. Moreover the biological response level of the patterned Mg, including cell attachment, proliferation, was stably maintained, while that of single HA coated and PLLA coated Mg dropped significantly under deformation. These results confirmed that HA/PLLA patterning on Mg has widened its feasibility to the real clinical operation.

In the third study, we explored the applicability of the HA pattern, produced through the second study, to other materials, such as PLLA. As HA dots array on PLLA surface periodically, better biocompatibility can be naturally achieved without altering polymer's intrinsic flexibility. HA patterns were formed on silicon wafer as described in the second study and transferred to PLLA. HA patterned PLLA showed similar level of stiffness and tensile strength to those of pure PLLA, while the

mechanical properties of HA powder mixed PLLA was significantly deteriorated, stiffer and weaker. Furthermore, HA pattern effectively increased biological responses of PLLA, including cell attachment and proliferation. Interestingly, biocompatibility of the samples varied depending on the pattern geometry. With the fixed HA content on the surface, better bioactivity was observed as the size of HA rod decreased. These results are suggesting that cellular responses of the materials, PLLA in this case, can be directly modulated by introducing different HA patterns on the surface.

Keywords: Magnesium (Mg), Hydroxyapatite (HA) coating, Poly(L-lactic) acid (PLLA), Patterning, Biodegradability, Biocompatibility,

Student number: 2010-22756

Contents

Chapter 3. HA coating on Mg for orthopedic application

Chapter 4. Behavior of HA/PLLA patterned Mg under deformation

List of Tables

List of Figures

Chapter 1.

Introduction

1.1. Using Mg as a biodegradable implant and the difficulties

Today, more than 200 years after the first production of metallic Mg by Sir Humphry Davy in 1808 (a full review of the history of biodegradable Mg implants can be found in [2]), biodegradable Mg-based metal implants are currently breaking the paradigm in biomaterial science to develop permanently stable metals. [3,4] The increasing demands for temporary metallic implants have provided a strong motivation to develop a biodegradable Mg implants, having suitable properties depending on the applications, and it became one of the most vigorously studied research areas in biomedical community. [5] The main factors making Mg attractive over other metals, ceramics or polymers are the favorable combination of its biocompatibility, suitable mechanical properties, and biodegradability. [6] Presence of the Mg in human body implies its non-toxicity, but it rather stimulates the biological action, such as bone tissue growth. [6,7] Also, the elastic modulus and the compressive strength of Mg are close to those of natural bone, [8] so the risk of stress shielding is mitigated. Biodegradability is the most important characteristic of Mg implants, enabling to fully function during surgical region recovers or heals, then gradually dissolve, be consumed or absorbed.

Despite the large amount of studies focusing on the subject, no Mg-based implants have been developed for commercial use so far. It is mainly because the degradation rate of Mg is too rapid to be matched with the rate of tissue healing. [3,4] Once it is exposed to a biological medium, Mg implant loses its functionality before

the bone tissue is fully restored, producing excessive amount of by-products, including hydrogen bubbles and hydroxide ions. [9] Although the disintegration of Mg and the safe excretion of its resultant products by the kidney grantee its best advantage of being biodegradable, too fast degradation dramatically reduces its use as an implant. [10-12] Therefore a suitable degradation rate of Mg is determinant for the promising future of Mg as body implants.

1.2. Outline of the thesis

The goal of this thesis is to develop a system that responds to the problem mentioned above, that is the high corrosion rate of Mg. From the thesis objectives, the document is organized in four chapters that are now presented.

Chapter 2 comprehensively reviews a background theory of Mg as a biodegradable implant material and the corrosion controlling technologies. The first section of this chapter starts with introducing the currently used metallic implants and its limitations, namely too long duration in the body. The following section provides the general information regarding Mg as a biodegradable implant and the problems facing, rapid corrosion behavior. The last section is related with the strategies to mitigate the corrosion, alloying and surface coating.

Chapter 3 aims at fabricating corrosion protective HA layer on pure Mg for enhancing the corrosion resistance, *in vitro* biocompatibility, and *in vivo* bone responses. The corrosion properties of Mg samples with and without an HA coating layer were investigated by measuring the amounts of hydrogen gas and hydroxide ions that were released in the SBF. The biological response of the samples was evaluated by *in vitro* cell tests using MC3T3-E1 preosteoblast cells to observe cell attachment, viability and differentiation. In addition, animal tests were performed to assess *in vivo* behaviors (e.g., biodegradation and bone response) of Mg bone implants, as well as their *in vivo* mechanical stability.

Chapter 4 focuses on the fabrication of a coating to reduce its corrosion rate, provide good biocompatibility, and sustain its corrosion protection under deformation. Micro-patterned HA and PLLA coating has been introduced on pure Mg by the combination of photolithography and solution treatment containing calcium and phosphate sources. The objective of the study is to increase both coating stability and bioactivity under the tensile strain mode, where patterned HA improves corrosion resistance and bioactivity of the coating layer and PLLA tolerates the deformation of the Mg substrate. The corrosion resistance of the samples was investigated by measuring the amount of hydrogen gas released from the corrosion medium, SBF. Furthermore, the biological responses were assessed through *in vitro* cell tests using MC3T3-E1 preosteoblast cells to observe cell attachment and viability under the deformation.

Chapter 5 is devoted to introduce HA patterns on pure PLLA by the combination of photolithography, Mg deposition and solution treatment containing calcium and phosphate sources. The objective of the study is to control bioactivity of pure PLLA by varying the geometry of HA patterns, whereas the PLLA matrix continues to exhibit its favorable mechanical characteristics. The microstructure of the HA patterned PLLA was investigated, while its mechanical properties were examined by tensile strength testing. Furthermore, the *in vitro* biocompatibility of HA patterned PLLA sample was also evaluated in terms of the attachment and proliferation of preosteoblast MC3T3- E1 cells.

Finally chapter 6 summarizes the conclusions of this thesis and proposes future research direction of the works described here.

Chapter 2.

Theoretical review

2.1. Currently used metallic implant

Metal has been used extensively in the manufacturing of load bearing orthopedic implants and coronary stents in a multitude of different forms. [13] The vigorous use of metallic alloys in modern times is related to the availability and success of several different alloys made of the noble metals at the beginning of the 20th century. [14-16] Implants made from stainless steels, cobalt-chromium alloys, and titanium alloys are commonly used. The use of metallic alloys for a whole range of medical implants is justified by their superior mechanical properties (strength, hardness, stiffness, etc.) compared, for example, to polymers. [17-19] Other properties such as biocompatibility or visibility in X-ray images also can be mentioned. Clinical studies have demonstrated that alloys made from these metals can be used safely and effectively in the manufacturing of orthopedic implants that are left *in vivo* for extended periods. [14,18,20,21] The mechanical, biological, and physical properties of these materials play significant roles in the longevity of these implants.

However, their superior stability in human body is now considered as a disadvantage. In situations when the implants are used to temporarily assist tissue healing, such as plates, screws, and pins, a second surgical procedure is inevitable after the tissue has healed [8], leading to burden additional pain and increased cost on patients. In addition, specific drawbacks of permanent metallic stents, including the risk of stent thrombosis and bleeding complications, as well as the cost of a prolonged hospitalization, limit their widely acceptance.[22] Also, the wear particles

produced during service and/or release of toxic metallic ions from the alloys as a result of corrosion may cause health hazards, such as chronic inflammation.[23] Moreover, the mechanical strength, fracture toughness, and elastic modulus are key characteristics of medical implants, and loss of the implant's functionality, notably through stress shielding effect, may be a consequence of a mismatch in these properties between the implant material and the natural bone.[23] Therefore, biodegradable materials that can be resorbed in the body when the function of the implant is fulfilled have become a subject of intensive research.

2.2. The potential of Mg as a biodegradable implant

The development of biodegradable implants is one of the important areas in medical science as discussed above. [24] A biodegradable material can gradually be dissolved and adsorbed after implanting, not causing permanent physical irritation or chronic inflammatory discomfort. Also, it eliminates the typical problems that are associated with permanent implants, such as stress shielding,[23] the accumulation of toxic metal ions,[25] and the need for a second surgery in order to remove the implant.[8] Currently, the biodegradable implants are mainly made of synthetic polymers, [26,27] such as poly-L-Lactic acid (PLLA), [28] poly glycolic acid (PGA) and poly caprolactone (PCL). However, these polymer based implants usually have an unsatisfactory mechanical strength and are more suitable for low load bearing applications.

Mg and its alloys will readily dissolve or corrode in aqueous solutions especially that contain chloride ions. [29] This rapid corrosion property has inspired the biomaterial researchers recently to develop a new concept of degradable implants. Mg and its alloys are expected to be used for implants with a temporary function, such as plates and stents, which provide a temporary mechanical support and degrade completely after the tissue healing. The advantages attributed to Mg as a materials for biomedical application are listed below:

- **Presence of Mg in human body and its roles**

The use of Mg as a degradable metal is based on the fact that Mg is an essential element in the living organism and has a high systemic toxic level. Mg^{2+} is present in large amount in the body, approximately 35 g per 70 kg body weight, 50~60% contained in the bones and most of the rest in soft tissues.[7] The recommended daily allowance (RDA) of Mg is within 300–450 mg/day throughout the world and generally excessive Mg is almost entirely excreted through the kidneys [8]. Since Mg is a cofactor for over 300 enzymatic reaction in the body, it is involved in many metabolic reactions and biological mechanisms, such as DNA and RNA synthesis, protein synthesis, cell growth and reproduction, cellular energy production, and storage.[7,30,31] Mg also plays a primary role in controlling nerve transmission, cardiac excitability, neuromuscular conduction, muscular contraction, vasomotor tone, and blood pressure [8]. Moreover Mg could stimulate bone tissue growth. [6] Several studies have demonstrated that Mg has a good biocompatibility since the release of Mg ions is not detrimental to the human body but rather helps the formation of biological apatite, the main bone mineral component. [32,33] An *in vivo* study conducted by Witte et al. [4] showed an osteoblastic response to the degrading Mg alloys inserted into the guinea pig femur, with an increased bone mass around the specimens.

- **Suitable mechanical properties**

The mechanical properties of Mg over commercially used metallic or

polymeric implants are one of the most important advantages with the consideration of load bearing orthopedic application. Its best attractive feature subsists in its elastic modulus of 30-45 GPa that is very close to that of the bone (5-20 GPa). A mismatch in the elastic moduli can lead to a stress shielding of the injured bone which consists in a reduction of its density as a result of the implant carrying a greater portion of the load due to its high modulus (which is very common with titanium based implants owing to their high elastic modulus of 100-125GPa). [8,23] The fracture toughness of Mg is greater than that of ceramic biomaterials such as HA, while compressive yield strength is still closer to that of natural bone. Table 2.1 summarized the mechanical properties of various implant material compared to the one of natural bone. [8] Moreover, Mg is the easiest structural material to machine [34] which allows the fabrication of complex shapes. It represents a big advantage when one knows that implant structures must be tailored to fit the size and shape of the body of each patient.

Due to the superior characteristics as mentioned above, Mg used to be introduced as implants into orthopedic and trauma surgery in the first half of the last century. [35] However, the use of Mg in biomedical applications has been restricted because of its high corrosion rate in biological ambiance. [3,4,36] The Mg surface rapidly reacts with aqueous solutions, revealing a strong tendency for localized corrosion. As a consequence, a fast degeneration of mechanical integrity has been observed for Mg alloys [2,30,37] and leads to failure of implants before tissue has healed. [38,39] Another issue is the rapid by-products formation, such as hydroxide ion and

hydrogen gas, [37] which could be hazardous to the host tissue. When the hydrogen evolution is too fast for tissue to absorb, a gas balloon will be seen [4,40] and a strong alkaline pH shift is harmful to the biological surroundings by reducing the cell viability significantly. In particular, these Mg corrosion reactions are accelerated in chloride-containing solutions (e.g. human body fluid, blood plasma).[41] The following reactions summarize the corrosion reactions of Mg [1] :

$$\mathrm{Mg} \rightarrow Mg^{2+} + 2e^{-} \ (\boldsymbol{anodic\ reaction}) \quad \textbf{(1)}$$

$$2H_2O + 2e^{-} \rightarrow H_2 + 2OH^{-} \ (\boldsymbol{cathodic\ reaction}) \quad \textbf{(2)}$$

$$Mg^{2+} + 2OH^{-} \rightarrow Mg(OH)_2 \ (\boldsymbol{product\ formation}) \quad \textbf{(3)}$$

$$Mg(OH)_2 + 2Cl^{-} \rightarrow MgCl_2 + 2OH^{-} \ (\boldsymbol{product\ dissolution}) \quad \textbf{(4)}$$

The above electrochemical reactions occur arbitrarily over the entire Mg alloys surface where a galvanic coupling forms due to different potentials between the Mg matrix and intermetallic phase, or grain boundary [42]. Mg hydroxide accumulates on the surface of Mg alloys as the protective layers in water. However, the body fluid contains a high amount of chloride (~150 mmol/L), which is fatal to Mg hydroxide. The Mg hydroxide starts to convert to soluble Mg chloride when the chloride concentration in corrosive medium is higher than 30 mmol/L [43]. Thus, chloride adsorption causes the breakdown of $Mg(OH)_2$ layer and leads to pitting

corrosion. Based on the above reactions, it is expected that the degradation of Mg is much accelerated in the human body, naturally containing chloride ions.

Since rapid corrosion is almost an intrinsic response of Mg to a chloride containing solution, it has inspired the biomaterial researchers to develop a new concept of degradable implant. Obviously, achieving a suitable degradation rate is a critical issue, enabling to fully function before surgical region recovers or heals, then gradually dissolve, be consumed or absorbed. Therefore, controlling the corrosion resistance of Mg in body fluid has become an extensive research field in development of Mg implants.

Table 2.1. Summary of the physical and mechanical properties of various implant materials in comparison with natural bone. [1]

Properties	Natural bone	Magnesium	Ti alloy	Co-Cr alloy	Stainless steel	Synthetic hydroxyapatite
Density (g/cm^3)	1.8-2.1	1.74-2.0	4.4-4.5	8.3-9.2	7.9-8.1	3.1
Elastic modulus (GPa)	3-20	41-45	110-117	230	189-205	73-117
Compressive yield strength (MPa)	130-180	65-100	758-1117	450-1000	170-310	600
Fracture toughness ($MPam^{1/2}$)	3-6	15-40	55-115	N/A	50-200	0.7

2.3. Strategies to control corrosion rate of Mg

2.3.1. Alloying

Alloying is one of the most effective solutions to reduce the corrosion rate of Mg. [3,4,9,40,41,44-47] Numerous Mg alloys have been reported to have improved corrosion resistance and biocompatibility. In the process, alloying elements show profound influence on the corrosion properties with different mechanisms. For example, calcium (Ca) exists primarily in the skeleton where it serves a structure-function role, resulting in Ca becoming an intriguing alloying element for orthopedic Mg alloys. Li et al. [40] have developed the binary Mg–Ca alloys with Ca contents ranging from 1–3 wt%, showing the increase in Ca addition results in higher amount of Mg_2Ca precipitation along the grain boundary, which exhibits a pronounced effect on mechanical property and corrosion of Mg. Liu et al. [48] have also studied the *in vitro* degradation of Mg–Ca alloy in the presence of albumin. The corrosion and the formation of filiform induced by chloride are significantly inhibited due to the adsorption of albumin molecule. Strontium (Sr) is also a frequently used alloying element and has been known to promote the growth of osteoblast and prevent bone resorption. Bornapour et al. [49] have investigated the biocompatibility and corrosion of binary Mg–Sr alloys in the cast state with the Sr content 0.3–2.5 wt%. Mg–Sr alloys containing Sr < 1 wt% have a slower corrosion rate than pure Mg, while the addition of Sr > 1 wt% accelerates the corrosion rate. It is attributed to the formation of a HA Sr-substituted layer presenting at the interface between Mg–Sr alloy and the

corrosion products. Moreover, Zn is one of the most commonly used alloying element in Mg, which is known to be a good solid solution and precipitation strengthening agent in Mg alloys [50]. Rosalbino et al. [51] have found that the Mg–2Zn–0.2Mn alloy exhibited a fourfold increase in the polarization resistance than AZ91 alloy after 168 h exposure to Ringer's solution. Reviewing the literatures, most of the successful reports on *in vivo* application of Mg implants have investigated Mg alloys containing rare earth element (REE) even the long term biosafety of the REEs is still doubtful. Chang et al. [52] and Birbilis et al. [53] find that the reactivity of $Mg_{12}Nd$ is only a little more positive than that of pure Mg, thus the galvanic corrosion effect is negligible. Having the fine grains and $Mg_{12}Nd$ phases, the aged Mg– Nd–Zn–Zr alloy exhibits slow corrosion rate (~0.3 mm/yr) in SBF, which is even lower than the commercial AZ31 (~0.2 mm/yr) and WE43 (~0.25 mm/yr) [54]. Generally, higher amount of alloying element addition will deteriorate the corrosion of Mg alloys, except for Al [42,55-57].

Meanwhile, most alloying elements contribute to some extent to improve the alloy strength by grain refinement, solid solution strengthening, and precipitation strengthening. For example, binary Mg–8.5wt%Li and Mg–9wt%Li alloys were found to have extremely high elongation of 610% and 460%, respectively [58]. With Li content between 5.5–11 wt%, body-centered cubic (bcc) structure β phase of Li solid solution will co-exist with the hexagonal close packed (hcp) α phase of Mg. This dual phase structure will remarkably improve the ductility of Mg alloy. Also, Mg–Zn–Zr alloy system, including ZK30, ZK60, and ZK61, is mature commercial

wrought Mg alloys. Their yield and ultimate tensile strength increase with increasing Zn content.

However most of the Mg alloys are originally designed for industrial application and potentially contain toxic elements and are not suitable from the perspective of biosafety. For example, the biocompatibility of Al, the most common used alloying element, is poor. Al primarily accumulates in nervous system and implicates in the pathogenesis of Alzheimer's disease [59]. Zr, usually used as a grain refiner, has been found to be closely associated with liver cancer, lung cancer, breast cancer and nasopharyngeal cancer [45]. When the plasma concentration of Li exceeds 2 mmol/L, reduced kidney function and neurotoxicity is observed. [59] In addition, severe hepatotoxicity has been detected after the administration of Ce, Pr and Y [60]. As a result, great effort has been moved beyond commercial alloys and towards new designed Mg alloys using biocompatible or low toxic alloying element.

Another strategy to slow down the degradation of Mg alloys is purification. Song [45] found that commercial purity Mg (0.02 wt.% Fe, < 0.002 wt.% Cu and < 0.002 wt% Ni) exhibited 26 mL/(cm^2 ·d) of hydrogen evolution rate in Hank's solution. Purification did remarkably bring down the degradation rate to 0.008 mL/(cm^2 ·d) for high purity Mg (~0.0045 wt% Fe, < 0.002 wt% Cu and < 0.002 wt% Ni). Since Mg is a constituent of human body, Mg by itself is considered to be a well-accepted implant. Hence, without the concern of alloying element releasing, high purity Mg seems to be attractive for medical applications.

2.3.2. Surface coating

Surface coating is generally preferred as it shows better performance in decreasing the degradation rate of Mg and improving its bioactivity. Ideally, corrosion would be slowed to allow the mechanical integrity of the metal to remain intact during tissue healing. This would minimize hydrogen evolution, which has been observed as a potential dangerous corrosion by-product for Mg alloys. The slowly wear away of coatings is expected to allow the degradation controlling of substrate [61]. A large choice of techniques and coating materials are another attractiveness of surface coating, including the chemical conversion, alkali heat treatment, anodic and micro arc oxidation, electrodeposition, and sol–gel methods. As a coating materials, most of the studies focus their attention on ceramic, in particular calcium phosphate group, and polymer, considering their good biocompatibility and solubility/degradability [42,61,62].

- **Calcium phosphate based coating**

Calcium phosphate based ceramics have many appealing qualities for use as biomaterials since they are not toxic, rather biocompatible. [63-67] They have a similar chemical composition and architecture to those of the mineral component of bones and teeth, resulting in better recognition as a part of human body, not a foreign material. In consequence, calcium phosphate based ceramics are often used as bone substitute, integrating into living tissues and actively remodeling healthy bones. [32]

Under the circumstances, calcium phosphate coatings are of special interest for surface modification of Mg used as orthopedic materials in terms of corrosion protection and bioactivity.

Calcium phosphate based ceramic coatings have already shown great potential for biomedical application. One of the most common, but bio-mimicking methods to produce calcium phosphate coating is simple chemical immersion techniques. Zhang et al. [67] have prepared the bonelike HA coatings by immersing pure Mg into three times concentrated SBF for 24 h at 42°C. The slower corrosion rate is observed for the thicker HA coatings group obtained by longer immersion time in SBF. Yang et al. [68] have reported the preparation of HA coating by 48 h immersion in supersaturated calcification solution (SCS) containing $Ca(NO)_3$, NaH_2PO_4, and $NaHCO_3$ at 37°C, followed by 2 h heat treatment at 300 °C. After 15 d immersion in SBF, the reduction of Ca and P content in coating is observed and only edges of the Mg substrate reveals corrosion.

Micro-arc oxidation (MAO) is a combination of an electrochemical oxidation with a high-voltage spark treatment performed in electrolyte and thus the calcium and phosphorus in electrolyte can be incorporated into the resulting coatings. Srinivasan et al. [69] have produced coatings on AM50 alloys using the $Ca(OH)_2$ and Na_3PO_4 electrolytes with different mass ratios. All the three coatings are found to be constituted with MgO and $Mg_3(PO_4)_2$ and the phase composition is influenced by the phosphate ion concentration and conductivity of the electrolyte.

Ravazi et al [70] have employed another technique to modify the surface of Mg and the benefits of HA. A fluoridated HA (FHA) coating was applied on a micro-arc oxidized AZ91 implant sample by electrophoretic deposition (EPD) which has been broadly used in the biomedical field. The results of the *in vivo* tests revealed a significant enhancement in the biocompatibility of FHA/MAO coated implant compared to the uncoated one. The amount of weight loss and Mg ion release in blood plasma decreased from 30 ppm to 17 ppm for bare AZ91 and coated one, respectively. Moreover, new bone was formed around the coated implant and less inflammation was observed, making the FHA/MAO coated implant a suitable candidate for future clinical orthopedic applications. There is few data about the bonding strength between the EPD coatings and the Mg substrates, which is important for practical use. Wang et al. [71] suggest a pulse electrodeposition process using positive and reverse currents. A Ca deficient HA coating is obtained which slows down the substrate corrosion and improves bone response [72]. Moreover, this technique is reported to significantly improve the bonding strength between coating and substrate to (41.8±2.7) MPa [71].

- **Polymer coating**

Polymers appear as other promising candidates to functionalize biomaterial surfaces because of the infinite diversity of the chemical and physical properties they can offer. They already have been used as biomaterials with a wide range of

functions such as contact lenses (hydrogels), catheters (silicone), breast implants (silicone), bone screws (poly-lactic acid), etc. [73] Researchers have therefore focused their attention on polymer coatings so that their benefits could be effectively utilized, including biocompatibility, elasticity, biodegradability, etc. Also additional services can be expected, by employing their ability to function with organic biomolecules and deliver drugs. Moreover, the degradable polymer based coatings, such as polycaprolactone (PCL), poly(L-lactic acid) (PLLA), and poly(DL-lactide-co-glycolide) (PLGA), are assumed to provide the protection of the Mg substrate in the early stage and gradually degrade with time [42]. Thus various polymer based coatings have been applied to improve the corrosion resistance of Mg substrate.

Dip coating is the simplest method to apply polymer coatings on metals. Diez et al. [74] have prepared a HA/PLLA coating on WE43 alloy with a coating thickness of 3 μm of HA and 3 μm of PLLA. From the literature, the dual coating layer provided good protection to the underlying WE43 from corrosion regardless of deformation. Gu et al. [75] have applied the chitosan coating on Mg–Ca alloy and found that the quality of coatings depends on the molecular weight of the chitosan and the number of coating cycles.

Alternatively, Xu et al. [76,77] have prepared the uniform and non-porous PCL and PLLA coatings on Mg substrate using spin coating technique. The results showed that the PLLA coating revealed an amorphous nature, providing better protection and bonding to Mg substrate than the semi-crystallized PCL coating. Xu

et al. [76,77] also found that the coatings prepared by the low molecular weight polymers exhibited faster corrosion than those prepared by the high molecular weight polymers.

Additionally, Wong et al. [78] spray the PCL solution on the AZ91 alloy layer by layer and the porous polymer membrane was obtained. The porosity of the PCL membrane was related to the PCL concentrations (2.5% and 3.33%) and thus influenced the corrosion behavior. The *in vitro* and *in vivo* corrosion tests indicated that the AZ91D with low porosity coatings exhibited slower corrosion rate than that with high porosity coatings.

Several techniques to apply calcium phosphate coatings and/or polymer coatings on Mg have been introduced. However, none of the surface coatings mentioned above has clearly eliminated the concerns regarding its applications in clinical area since biological environment in the body dynamically varies depending on the patient's conditions. Moreover, the coatings cannot alter the localized corrosion mechanism of Mg, and the susceptibility of Mg towards localized corrosion attack will increase once the coatings fail. Therefore, the durability and integrity of the coating are crucial for the lifetime of medical devices fabricated from Mg and need further investigations.

Chapter 3.

HA coating on Mg for orthopedic application

3.1. Introduction

Metallic materials including titanium alloys, stainless steels, and cobalt–chromium-based alloys continue to play an essential role in biomedical implant applications, particularly load-bearing applications, due to their outstanding mechanical properties.[17-19] However, the wear particles produced during service and/or release of toxic metallic ions from the alloys as a result of corrosion may cause health hazards, such as chronic inflammation.[20] The mechanical strength, fracture toughness, and elastic modulus are key characteristics of medical implants, and loss of the implant's functionality, notably through stress shielding effect, [23] may be a consequence of a mismatch in these properties between the implant material and the natural bone. In addition, current metallic biomaterials are commonly used in temporary fixtures, whose removal requires a secondary surgery after the tissue has sufficiently healed. [8] Therefore, biodegradable materials that can be resorbed in the body when the function of the implant is fulfilled have become a subject of intensive research. [5]

Mg and its alloys have long been considered as suitable materials for biomedical implants. A history of the development of this area can be found in Ref. [2]. In recent years, Mg and its alloys came to the fore again as promising materials for biodegradable implants owing to their advantageous properties profile. [6] First, Mg is one of the most abundant elements in the human body and an essential mineral in human metabolism, both facts suggesting that release of Mg ions would not be

harmful to the body but may rather promote bone tissue growth. [6] Second, the elastic modulus and the compressive strength of Mg are close to those of natural bone, so the risk of stress shielding is mitigated. Thus in many ways, biodegradable Mg implants would have an advantage over biodegradable polymers, ceramics or bioglasses owing to their mechanical characteristics being a better match to those of bone. Despite these prominent merits of Mg vis- à -vis other materials, its use in biomedical applications has been limited because of poor corrosion resistance of Mg in aqueous solutions, [3,4], particularly solutions containing chloride ions, [41] such as body fluids. When Mg-based implants are exposed to a biological environment, they lose their functionality by deterioration of their mechanical performance before the bone tissue is fully restored. Furthermore, by-products of profuse Mg dissolution, including hydrogen bubbles and hydroxide ions, can be hazardous to the host tissue, inducing alkaline poisoning and tissue necrosis. [9]

Many methods have been tried to suppress or reduce the excessively rapid corrosion of Mg, including alloying [3,4,9,40,41,44-47] and surface modification. [79-84] Recently, it was also reported that a particular form of surface modification, namely surface grain refinement, leads to a reduction of corrosion rate of Mg alloys. [85,86] Surface modification with protective coatings was suggested to be a potent method for controlling the rate of Mg degradation. [63-65,67,87-91] The coating layer can act as a corrosion barrier between the corrosive medium and the metal substrate to prevent their interaction, without affecting the intrinsic properties of the metal substrate.

Excellent biocompatibility is also achieved by coating Mg with a bioactive material,[63-67] such as HA (HA; $Ca_{10}(PO_4)_6(OH)_2$).[92-96] HA provided great bioactivity and improved the bonding between the substrate and the natural bone.

In the present study, pure Mg samples were treated in an aqueous solution containing calcium and phosphate sources in order to coat the samples with an HA layer, thereby reducing their biocorrosion rate and enhancing the biocompatibility and bone response. Owing to the ionic conductivity of the aqueous solution, this kind of treatment can be applied for Mg parts of any shape and form, even for complex, three-dimensional (3D) shapes. The corrosion properties of Mg samples with and without an HA coating layer were investigated by measuring the amounts of hydrogen gas and hydroxide ions that were released in the SBF. The biological response of the samples was evaluated by *in vitro* cell tests using MC3T3-E1 preosteoblast cells to observe cell attachment, viability, and differentiation. In addition, animal tests were performed to assess *in vivo* behavior (e.g., biodegradation and bone response) of Mg bone implants, as well as their *in vivo* mechanical stability.

3.2. Experimental procedure

Sample preparation and coating procedure

High purity (99.99%) Mg plates, 20 mm × 20 mm × 2 mm and 10 mm × 10 mm × 2 mm in size, were prepared. The specimens were polished mechanically by up to 1200 grit SiC paper, cleaned ultrasonically with ethanol and air dried. For HA coating, a treatment solution was prepared based on the procedure reported by Hiromoto et al. [93] The solution was produced with 0.05 M ethylenediaminetetraacetic acid calcium disodium salt hydrate (Ca-EDTA)/0.05 M potassium dihydrogenphosphate (KH_2PO_4). The pH of the solution was adjusted to 8.9 with sodium hydroxide (NaOH). The Mg samples were immersed in the heated treatment solution at 363K and then held at this temperature for 2 h. The coated samples were rinsed with distilled water and dried in air.

Microstructure, chemical composition and crystalline structure characterizations

The surface morphologies of the bare Mg and HA coated Mg specimens were observed by scanning electron microscopy (SEM, JSM-5600; JEOL, Japan). The cross-sectional morphologies of the coated samples were analyzed by field-emission scanning electron microscopy (FE-SEM, JSM-6330F; JEOL). The chemical composition of the HA coating layer was characterized by energy-

dispersive spectrometer (EDS) attached to the SEM. The crystalline structure of the HA coating layer was examined by X-ray diffraction (XRD, D8-Advance; Bruker Co., Germany).

Adhesion strength test

The adhesion strength between the HA coating layer and the substrate was determined using an adhesion tester (RB302 single-column type; R&B, Korea). The HA coated Mg samples, where a pre-epoxy coated stud was attached, were heated to 150 °C for 1 h in an oven. After a sample was fixed to the tester jig, the stud was pulled off vertically until the coating layer failed. The adhesion strength was calculated using the failure area and the maximum pulling force that was recorded.

***In vitro* corrosion tests**

The HA coated samples were soaked in SBF with ion concentrations nearly equal to those of human blood plasma (i.e., 142 mM Na^+, 5 mM K^+, 2.5 mM Ca^{2+}, 1.5 mM Mg^{2+}, 147.8 mM Cl^-, 4.2 mM HCO_3^-, 1 mM HPO_4^{2-}, 0.5 mM SO_4^{2-}) for up to 7 days to evaluate their surface corrosion properties. [97] Each sample was immersed in 80 mL of SBF adjusted to pH 7.4 at 37 ℃ with an exposed area of 2 cm^2. At each immersion time point, the solution pH and the volume of hydrogen gas were recorded. The pH of the immersion solution was monitored every 12 h using a pH

meter (sp-701; Suntex, Taiwan). The Mg concentration for each immersion period was analyzed by inductively coupled plasma atomic-emission spectrometry (Optima-4300DV; PerkinElmer, Welleslev, MA). The corrosion products formed on the bare Mg and HA coated Mg samples were characterized using FE-SEM, EDS, and XRD. In addition, potentiodynamic tests were performed using a potentiostat/galvanostat (Model 273; EG&G Princeton Applied Research) in the SBF.

***In vitro* biocompatibility tests**

For the *in vitro* cell tests, the samples (bare Mg and HA coated Mg) were sterilized under ultraviolet irradiation on a clean bench. For comparison, Thermanox® and HA pellets were used as the positive controls. A pre-osteoblast cell line, MC3T3-E1 (ATCC, CRL-2593), was used to assess the cell response to the specimen surfaces. The pre-incubated cells were seeded on specimens at densities of 1.0×10^4 cells/cm^2, 1.25×10^4 cells/cm^2 and 0.25×10^4 cells/cm^2 to evaluate the cell attachment, viability, and differentiation behavior, respectively. Alpha-minimum essential medium (α-MEM, Welgene Co., Ltd., Korea) with the addition of 5% fetal bovine serum (FBS) and 1% penicillin-streptomycin was used as the cell culture medium and the cells were cultured in a humidified incubator in air atmosphere containing 5% CO_2 at 37 ℃.

Cell morphology observations

After culturing for 24 h, the attached cells were observed by scanning electron microscopy (SEM, JSM-5600, JEOL, Japan) and confocal laser scanning microscopy (CLSM, LSM 510 NLO, Germany). Prior to the SEM observations, the samples were fixed with 2.5% glutaraldehyde for 10 min, dehydrated in graded ethanol (70, 90, 95, and 100% ethanol in sequence), immersed in hexamethyldisilazane for 10min, and dried in air. For the CLSM examination, the cultured cells were dyed with Alexa Fluor 546 phalloidin (Eugene) and ProLong Gold antifade reagent with DAPI (Eugene).

Cell viability and proliferation

Cell proliferation was determined after 5 days of culturing using a Cyquant cell proliferation assay kit (C7026 Invitrogen). Before measurements, the cells that adhered to the samples were detached and suspended in a fluorescent dye solution. The DNA level of the detached cells was measured using a multiple plate reader (Victor3, PerkinElmer, USA) at 480/535 nm wavelength. The measured florescence values were converted to the DNA content using a DNA standard curve. In this assay kit, the DNA level was directly proportional to the number of living cells.

Alkaline phosphatase (ALP) activity assay

To evaluate cell differentiation, an alkaline phosphatase (ALP) activity test was performed using p-nitrophenyl phosphate (pNPP, Sigma-Aldrich, UK). During this test, pNPP was converted to p-nitrophenol (pNP) in the presence of ALP at a rate that was proportional to the ALP activity. The level of pNP production was determined by absorbance at 405 nm using a micro reader (Biorad, Model 550, USA). For the ALP activity test, 10mM β-GP and 50μg/mL ascorbic acid were added to the culture medium and measurements were performed after 14 days of culturing. HA pellets and a commercial culture plate (Thermanox®, NUNC, Rochester, NY) were also tested for comparison.

***In vivo* biocorrosion and mechanical stability tests**

The *in vivo* bio-corrosion behavior and mechanical stability of the bare Mg and HA coated Mg were evaluated by *in vivo* animal experiments using 60 healthy Sprague-Dawley rats (10 weeks old, average weight of approximately 370 g). All rats were anaesthetized through intramuscular injection of a combination of Xylazine HCl (10 mg/kg, Rompun, Bayer Korea, Korea) and Ketamine HCl (50 mg/kg, Ketalar, Yuhan, Korea), and 1:100,000 epinephrine was injected as the local anesthesia. The samples, which had proper geometry and dimensions for tensile tests (ASTM E 8/E 8M - 08), were inserted into bone-pericranium pouches after elevating

the musculo-periosteum above the calvaria. Then, the wounds were sutured in separate layers, and the animals postoperatively received a subcutaneous injection of gentamycin (5mg/kg) as an antibiotic prophylaxis.

After 2, 4, 6, 8, and 12 weeks of implantation, the rats were sacrificed to extract the specimens (bare Mg and HA coated Mg). To characterize the bio-corrosion behavior of both kinds of specimens, the changes in the morphology were examined by optical microscopy. To evaluate the mechanical stability of the bare Mg and HA coated Mg after *in vivo* exposure, tensile tests were conducted on specimens extracted from the bone-pericranium pouches. A universal testing machine (OUT-05D, Oriental TM Corp., Korea) operated at a cross-head speed of 1 mm/min was used.

In vivo biodegradation and bone response evaluations

In vivo animal experiments were performed on 13 healthy New Zealand white rabbits (12 weeks old, average weight of approximately 3.5 kg) for evaluating the *in vivo* biodegradation and bone response of the bare Mg and HA coated Mg. All rabbits were anaesthetized through intramuscular injection of a combination of Xylazine HCl (10mg/kg, Rompun, Bayer Korea, Korea) and Ketamine HCl (50mg/kg, Ketalar, Yuhan, Korea), and 1:100,000 epinephrine was injected as the local anesthesia. In this study, two types of screw samples (bare Mg and HA coated Mg), 2 mm in diameter and 7 mm in length, were used. Two screws of both types

were implanted into the left and right tibial defects, respectively, after pre-drilling holes on the tibial shafts using a hand-operated drill. Then, the wounds were sutured in separate layers, and the animals postoperatively received a subcutaneous injection of gentamycin (5 mg/kg) as an antibiotic prophylaxis.

After 6 or 12 weeks of healing, the rabbits were sacrificed to extract their bone defect regions. The harvested bone tissues were scanned using a micro-CT (Skyscan 1172 Micro-tomography System, Skyscan, Kontich, Belgium) with a 0.5 mm aluminum filter at a resolution of 7.04 μm, voltage of 74 kV and current of 133 mA to study the morphologies of the Mg samples and the bone tissues. Subsequently, 3D images were reconstructed and then observed to evaluate the implant morphology and the bone tissue in the cortical area. The volume of interest was defined by manual drawing of contours for each sample, and a specific threshold for image analysis was determined, which was kept constant for all evaluations.

For histological evaluation of the specimens, the extracted bone samples were fixed in a neutral 10% formaldehyde solution and embedded in resin. Non-decalcified thin ground sections were prepared and reduced to a thickness of ~30 μm. The microscopic images of the haematoxylin-eosin (H-E) stained sections were obtained using Axioskop microscopy (Olympus BX51, Olympus Inc., Japan). The newly formed bone along the screws was quantitatively assessed and the bone-to-implant contact (BIC) ratio was calculated from the images using a digital image analysis program (SPOT, Diagnostic Instruments Inc., MI, USA). The ratio was

defined within the confined area where the cortical bone was supposed to be.

Statistical analysis

All experiments were performed more than three times, and the experimental results were expressed as the mean value ± standard deviation (SD). The difference between the two groups (HA coated *vs*. bare Mg implants) was determined using a one-way analysis of variance (ANOVA) and $p < 0.05$ was considered a statistically significant difference.

3.3. Results

3.3.1. Microstructure and crystalline structure of HA coating layers

Figure 3.1 presents the morphology of the HA coated Mg surface and a cross-sectional view of the coating layer. The micrographs in Figure 3.1. (A–D) show the surface morphology at 5 minute intervals during the coating procedure. These images clearly indicate that numerous seed particles had formed within the first 5 min of the coating procedure, and the seeds grew vigorously to form the final "cauliflower" HA morphology seen in Figure 3.1. (D, E). The higher resolution Figure 3.1. (E) shows the morphology of the HA layer in greater detail, revealing that needle-shaped HA crystals with a diameter of 50–200 nm and a length of approximately 1.5 μm formed dispersed bundles. The cross-sectional image shows that the thickness of the HA layer was approximately 2 μm and the layer was composed of two distinct strata [Figure 3.1. (F)]. While the lower stratum was relatively dense and contiguous, the upper one exhibited bundles of needlelike crystals, as seen in the surface view. The surface coating layer was analyzed by XRD, as shown in Figure 3.2. Prior to the surface treatment, only Mg diffraction peaks were observed in Figure 3.2. (A) suggesting no other phases were present, while clear XRD peaks originating from HA were detected along with the Mg substrate peaks after treatment, compare Figure 3.2. (B). In particular, the relative intensity of the diffraction peak of the $(002)_{HA}$ plane at $2\theta = 26^{\circ}$ was higher than the intensities of the other crystallographic planes of HA.

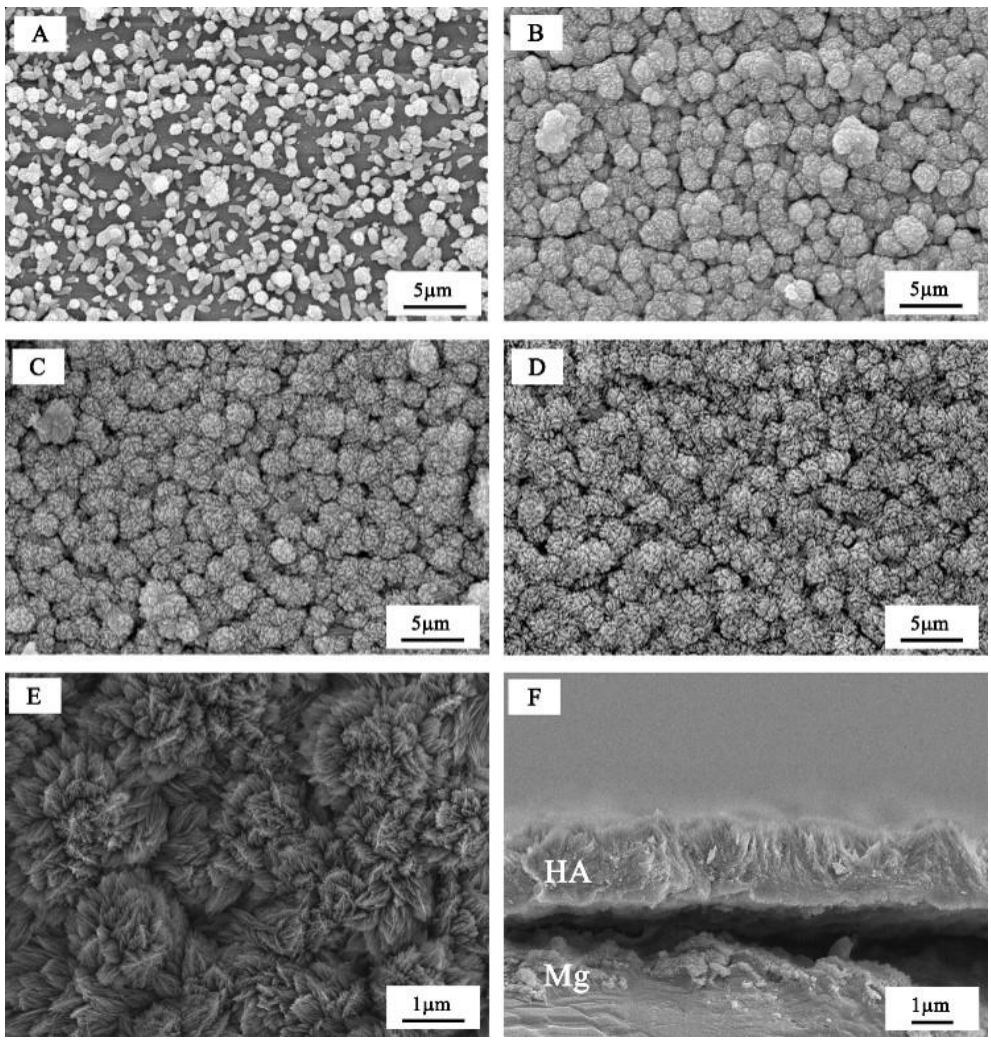

Figure 3.1. SEM images of the HA coated Mg treated for (A) 5 min, (B) 10 min, (C) 15 min, (D) 20 min, (E) 2 h, and (F) 2 h (through-thickness section).

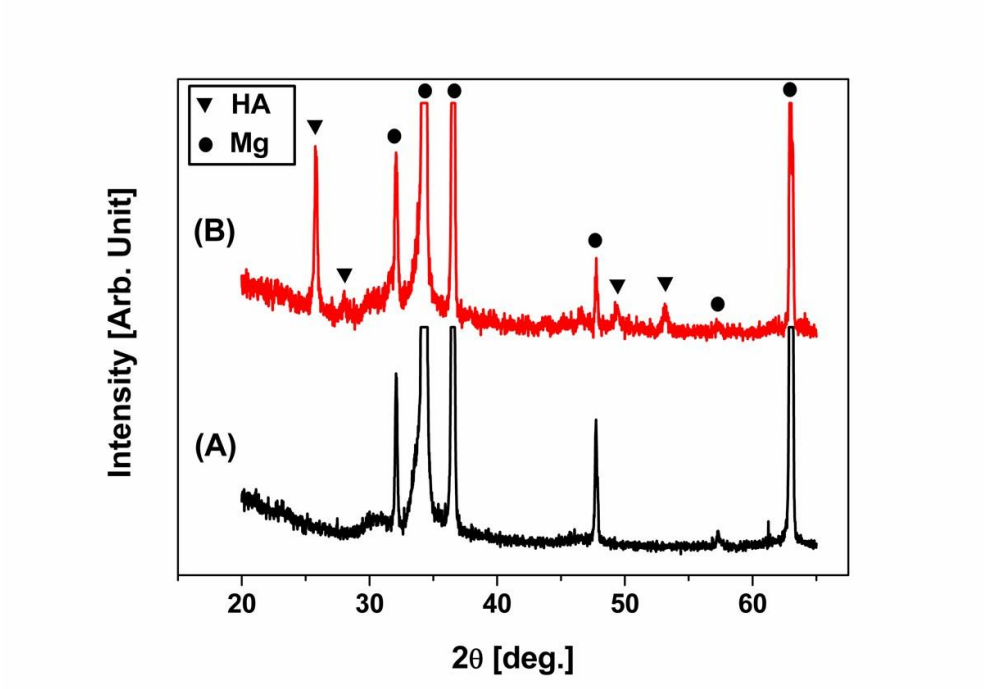

Figure 3.2. XRD patterns of (A) bare Mg and (B) HA coated Mg (●: Mg, ▼: HA).

3.3.2. Adhesion strength

The adhesion strength of coatings on Mg has rarely been reported. In this study, the adhesion strength of HA coating on Mg was measured using the pull-out test as shown in Figure 3.3. The HA coating layer, which was formed through a chemical reaction in an aqueous solution, exhibited a relatively high bonding strength of approximately 20 MPa, qualifying it as a protective coating with regard to strength of adhesion. [98] In addition, all of the specimens tested fractured at the interface between the HA coating layer and Mg substrate.

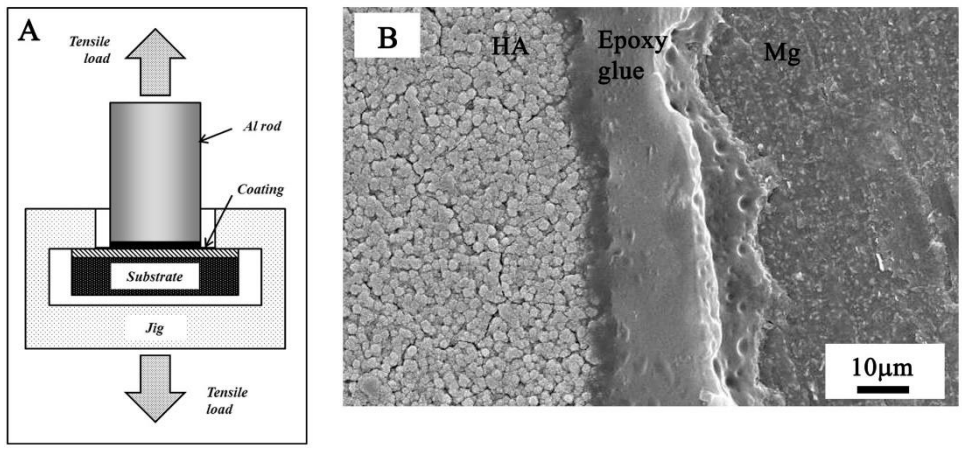

Figure 3.3. (A) Schematic diagram of testing method and (B) surface morphology after the adhesion strength test.

3.3.3. *In vitro* corrosion resistance

Immersion corrosion tests, in which the bare Mg and HA coated Mg samples were soaked in an SBF solution, were conducted to estimate their surface corrosion properties. For each immersion, the pH variation and evolved hydrogen volume were measured, as shown in Figure 3.4. (A, B). The change in the pH value of the solution with HA coated samples was considerably lower than that of the untreated samples for immersion times up to 120 h. Furthermore, the hydrogen evolving from the samples with a protective HA coating exhibited a similar trend to the pH change; that is, a much smaller amount of hydrogen was evolved from the samples with an HA coating than from the bare Mg samples. The retarded production of by-products on the treated specimen provides clear evidence that HA acted as a protective layer enhancing the corrosion resistance of Mg quite substantially. The surface morphologies of the bare Mg and HA coated Mg samples after 5 days of immersion in the SBF are shown in Figure 3.5. (A, B). The bare Mg sample was severely corroded and cracked, suggesting its poor corrosion resistance [Figure 3.5. (A)]. On the other hand, the HA coated Mg sample showed a negligible change in surface morphology even after 5 days of immersion in the SBF [Figure 3.5. (B)]. This finding suggests that the HA coating layer could significantly enhance the corrosion resistance of Mg *in vitro*. The crystalline structures of the corrosion products formed on the bare Mg and HA coated Mg samples after 5 days of immersion in the SBF were characterized by XRD, as shown in Figure 3.6. (A, B). The bare Mg sample showed additional strong peaks corresponding to the $Mg(OH)_2$

[Figure 3.6. (A)], implying that the corrosion layer would be mainly comprised of $Mg(OH)_2$ or $Mg(OH)_2 \cdot nH_2O$. However, the HA coated Mg sample showed relatively low intensities of the peaks corresponding to the $Mg(OH)_2$ [Figure 3.6. (B)]. This finding suggests that the corrosion of Mg could be significantly retarded via the formation of a protective HA coating layer. The corrosion resistances of the bare Mg and HA coated Mg samples were determined by electrochemical polarization tests in the SBF, as shown in Figure 3.7. (A, B). The corrosion potential (E_{corr}), corrosion current density (I_{corr}), and polarization resistance (R_P) are summarized in Table 3.1. The HA coated Mg sample showed much lower I_{corr} and higher R_P than the bare Mg, while E_{corr} was shifted in the positive direction. This finding indicates that the corrosion resistance of Mg was significantly improved by HA coating.

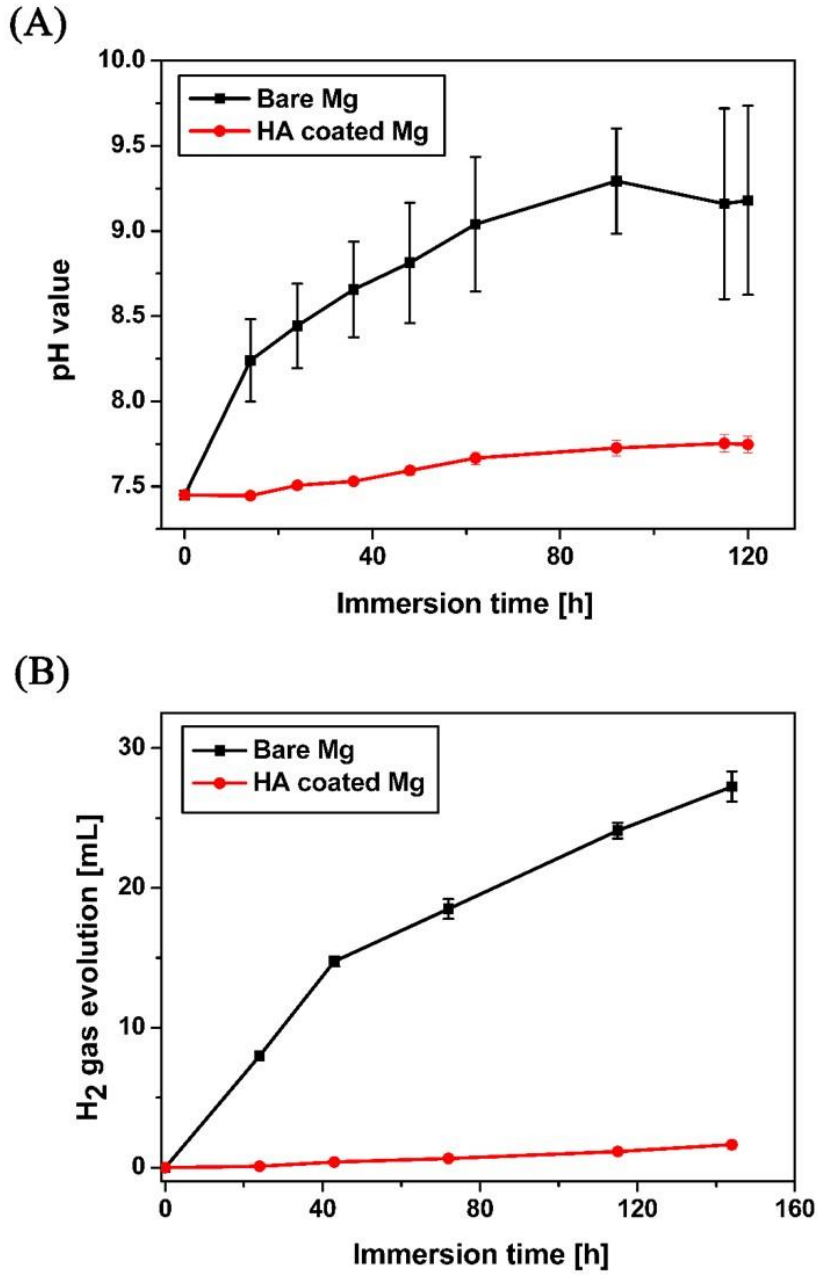

Figure 3.4. (A) Variation of pH and (B) hydrogen gas evolution in the SBF for bare and HA coated Mg.

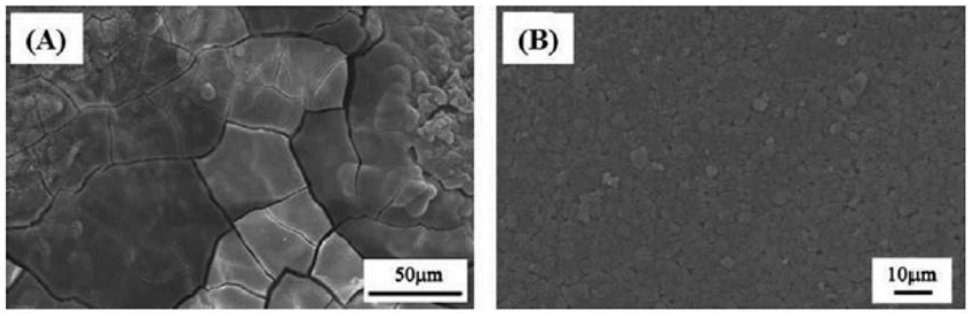

Figure 3.5. SEM images of (A) the bare Mg and (B) HA coated Mg samples after 5 days of immersion in the SBF, showing their surface morphology.

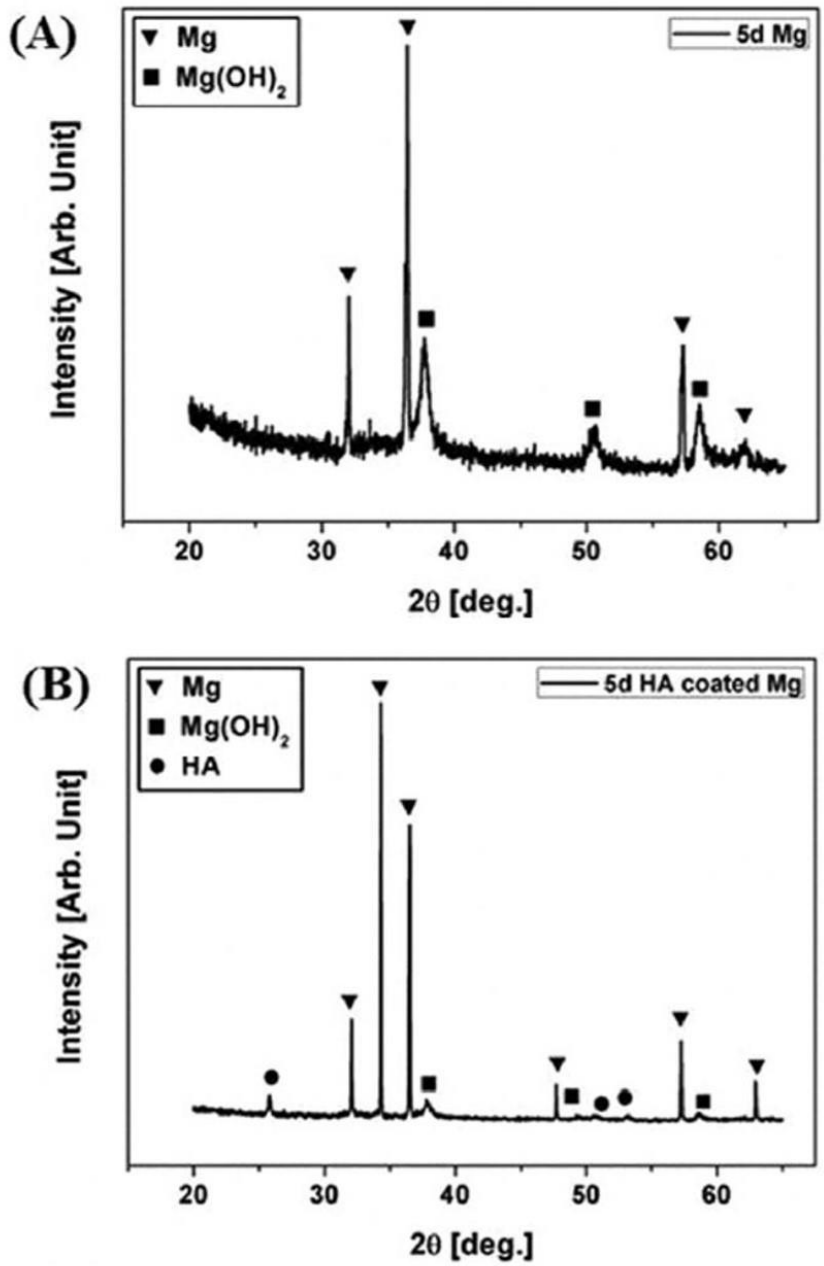

Figure 3.6. XRD patterns of (A) the bare Mg and (B) HA coated Mg samples after 5 days of immersion in the SBF (▼: Mg, ●: HA, and ■: $Mg(OH)_2$).

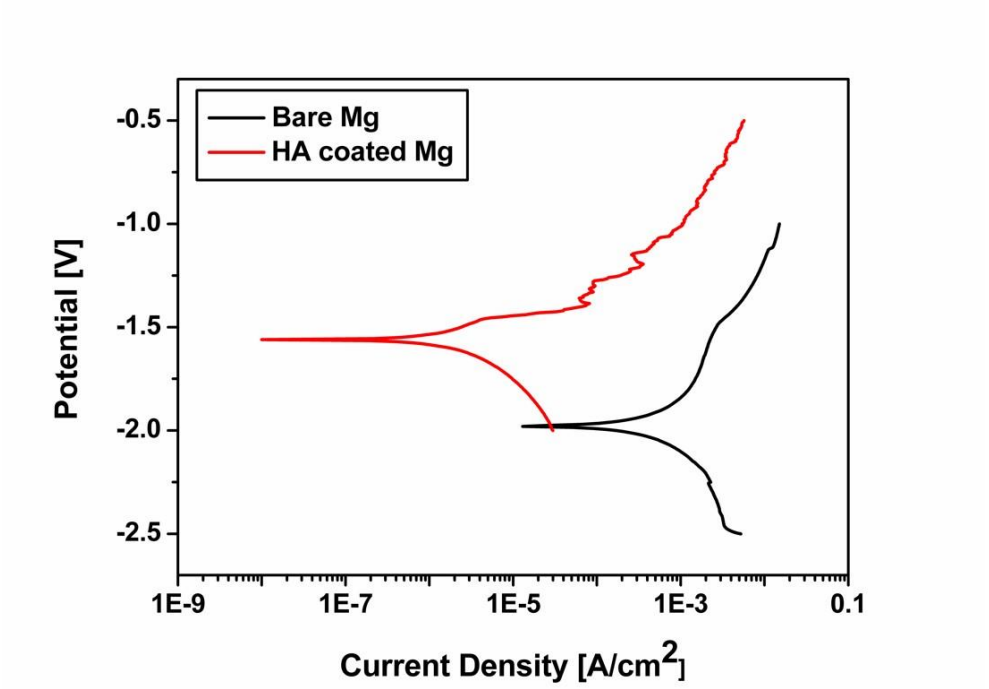

Figure 3.7. Potentiodynamic polarization curves of (A) the bare Mg and (B) HA coated Mg samples in the SBF.

Table 3.1. Corrosion potential (E_{corr}), corrosion current density (I_{corr}), and polarization resistance (R_p) of bare Mg and HA coated Mg samples in the SBF.

	E_{corr} (V SCE)	I_{corr} ($\mu A/cm^2$)	R_P ($k\Omega \cdot cm^2$)
Bare Mg	-1.98	6831	0.13
HA coated Mg	-1.56	3.062	23.4

3.3.4. *In vitro* cell responses

In vitro cell tests were performed using MC3T3-E1 preosteoblast cells to evaluate the biological properties of bare Mg and HA coated Mg, including the cell attachment, proliferation, and differentiation. Figure 3.8 shows the morphology of the preosteoblast cells that were cultured for 1 day on the samples of bare Mg and Mg with an HA layer, obtained by using SEM in Figure 3.8. (A, B), and CLSM in Figure 3.8. (C, D). Only a few cells with a spherical shape were attached to the surface of the bare Mg specimen, as shown in Figure 3.8. (A). By contrast, in the case of the coated specimen, more cells were attached to the HA surface and spread well with an active cytoskeletal extension, as shown in Figure 3.8. (B). These results were confirmed by the CLSM images in Figure 3.8. (C, D), which demonstrated that thriving cells with multiple filopodia were attached to the HA coating layer [Figure 3.8. (D)], whereas only a small number of cells were detected on the bare Mg specimen [Figure 3.8. (C)].

In Figure 3.9, cell proliferation was evaluated by DNA quantification after 5 days of culturing. To evaluate the effect of the HA layer on cell proliferation in greater detail, HA and Thermanox® were included as the positive controls in addition to bare Mg. The DNA content from the bare samples was close to zero, whereas that from the HA coated samples showed a considerably higher levels, close to those associated with HA and Thermanox®, which are widely known as biocompatible

materials. [99-102]

The morphologies of the preosteoblast cells after 5 days of culturing on the bare Mg and HA coated Mg samples are shown in Figure 3.10. (A, B). The bare Mg sample showed no noticeable cells attached on its cracked surface [Figure 3.10. (A)], which was presumably due to the fast corrosion of Mg. On the other hand, the HA coated Mg sample showed that cells were attached and spread well with an active cytoskeletal extension [Figure 3.10. (B)], suggesting its good biocompatibility *in vitro*.

To evaluate the differentiation of cells on the surfaces of the two kinds of specimens, ALP activities were also measured, as shown in Figure 3.11. After 14 days of culturing, the cells cultured on Mg with an HA layer exhibited ALP activity similar to that of Thermanox® and slightly lower than that of HA. However, it should be noted that the ALP activity of bare Mg could not be measured because of the fast corrosion of Mg *in vitro*, which would not allow the active proliferation and differentiation of cells. The entirety of the above biocompatibility data are a clear demonstration that coating Mg with HA gives rise to a noticeable improvement of cell of response.

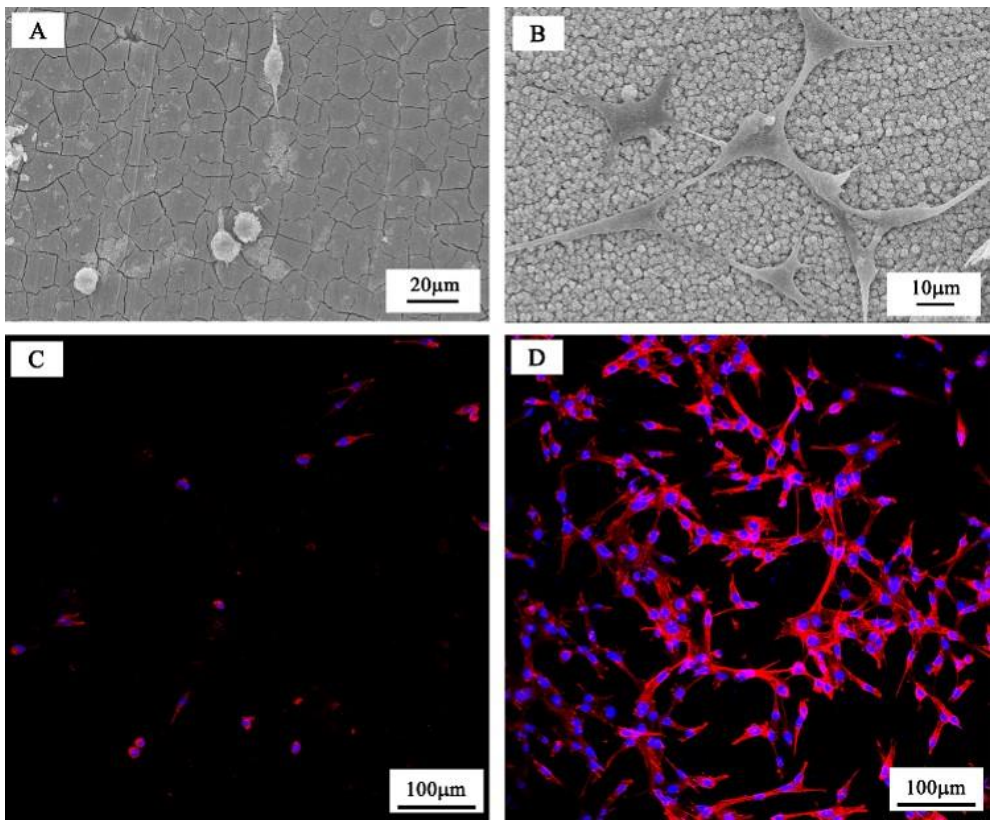

Figure 3.8. SEM (A and B) and CLSM (C and D) images of the MC3T3-E1 cells that were cultured on bare Mg (A and C) and HA coated Mg (B and D).

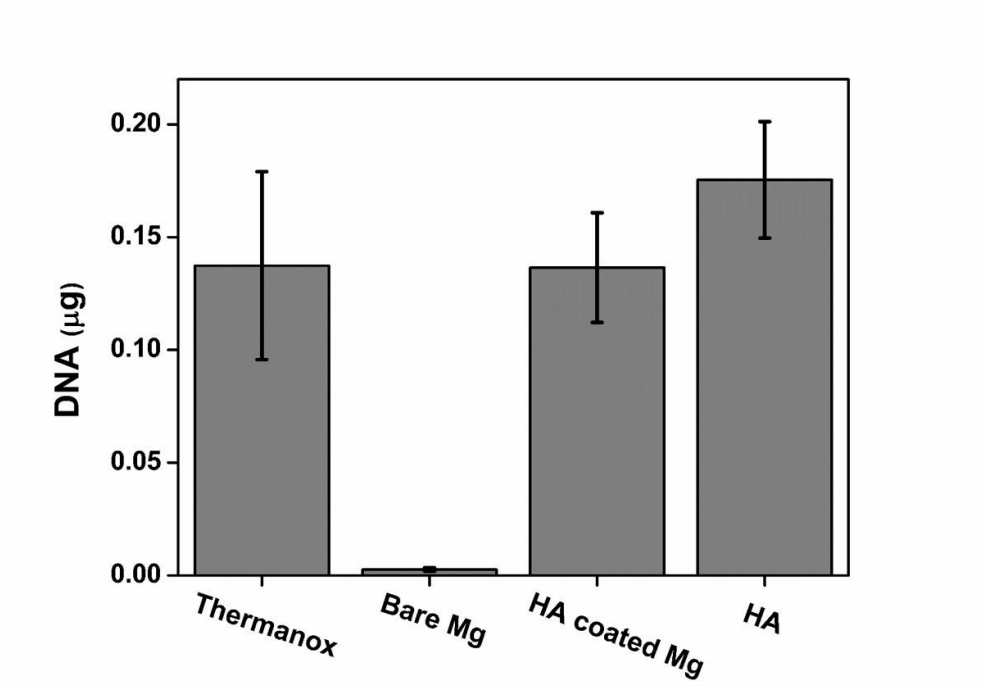

Figure 3.9. DNA levels of the MC3T3-E1 cells that were cultured for 5 days.

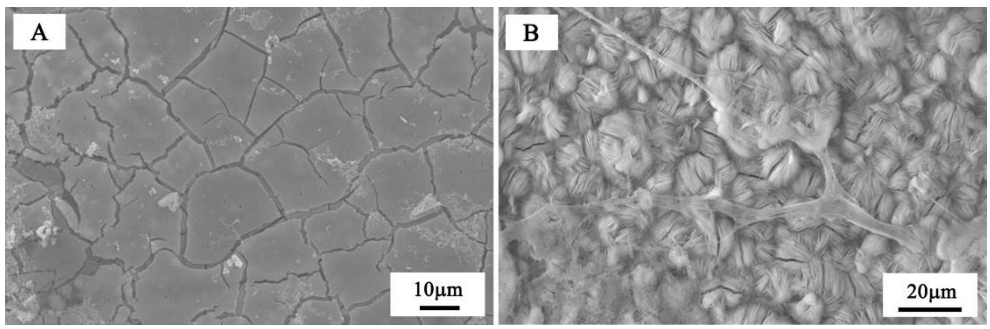

Figure 3.10. SEM images of the MC3T3-E1 cells on (A) the bare Mg and (B) HA coated Mg samples after 5 days of culturing.

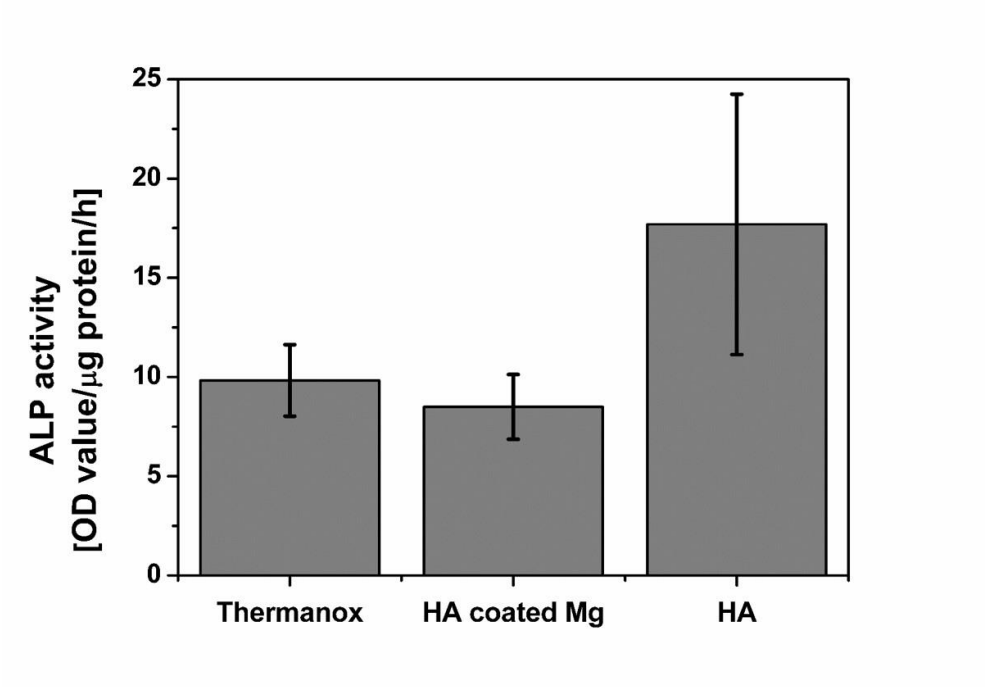

Figure 3.11. ALP activity levels of the MC3T3-E1 cells that were cultured for 14 days.

3.3.5. *In vivo* biocorrosion and mechanical stability

In order to evaluate the *in vivo* biocorrosion behavior and mechanical stability of the HA coated Mg, the specimens with the shape and dimensions for tensile tests were inserted into bone-pericranium pouches on calvaria, as shown in Figure 3.12. For comparison purpose, the bare Mg was also tested. The optical images of the bare Mg and HA coated specimens after 2, 4, 6, 8, and 12 weeks of implantation are shown in Figure 3.13. The bare Mg specimen degraded severely already after 2 weeks of implantation, suggesting its extensive biocorrosion. This biocorrosion became more severe with increasing implantation period. By contrast, the HA coated specimens showed much slower biocorrosion behavior. This preliminary study suggests that HA coating can effectively mitigate the excessively rapid biocorrosion behavior of Mg implants.

The surface morphologies of the bare Mg and HA coated Mg samples 2, 4, 6, 8, and 12 weeks of implantation were characterized by SEM. Even after 2 weeks of implantation, the bare Mg sample showed rough and cracked surfaces, suggesting its extensive corrosion *in vivo* [Figure 3.14. (A)]. This *in vivo* biocorrosion became more severe with increasing the implantation period up to 12 weeks [Figure 3.14. (B)]. On the other hand, the surface morphology of the HA coated Mg sample did not change much even after 12 weeks of implantation [Figure 3.14. (C)]. In addition, no other crystalline phases, except Mg and HA, were observed by XRD (data not shown here). This finding suggests that the HA coated Mg implants can degrade

more slowly than the bare Mg when used for orthopedic applications.

Mechanical stability of the bare Mg and HA coated Mg specimens in the *in vivo* environment was evaluated by measuring their tensile strength after 2, 4, 6, 8, and 12 weeks of implantation, compare Figure 3.15. Similar to the biocorrosion behavior, the bare Mg exhibited a drastic reduction in tensile strength, for example, an approximately 50% reduction after only 4 weeks of implantation. HA coated Mg performed distinctly better exhibiting only a slight decrease in tensile strength even after the whole 12 week implantation period. This finding demonstrates that HA coated Mg can retain good mechanical stability when implanted.

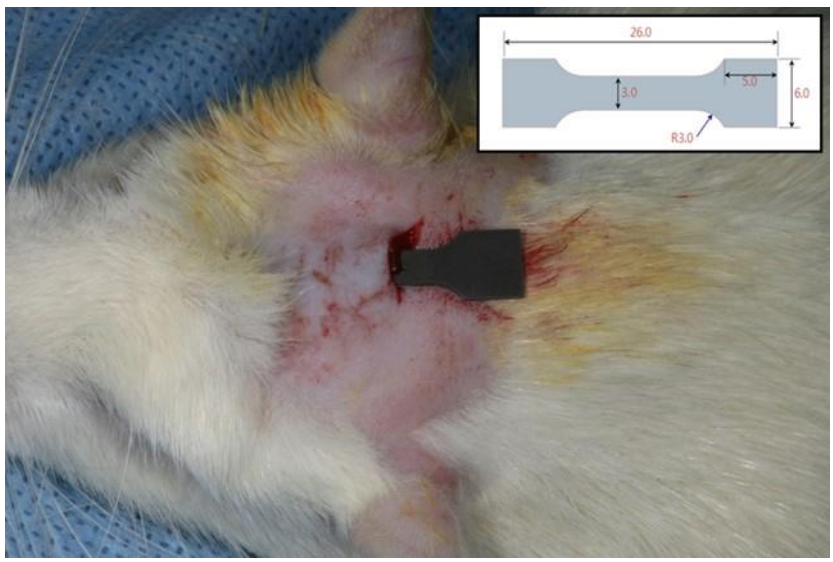

Figure 3.12. Optical images of the specimens that were implanted into rat bone-pericranium pouches. The inset shows the geometry and dimensions of the specimens for tensile tests.

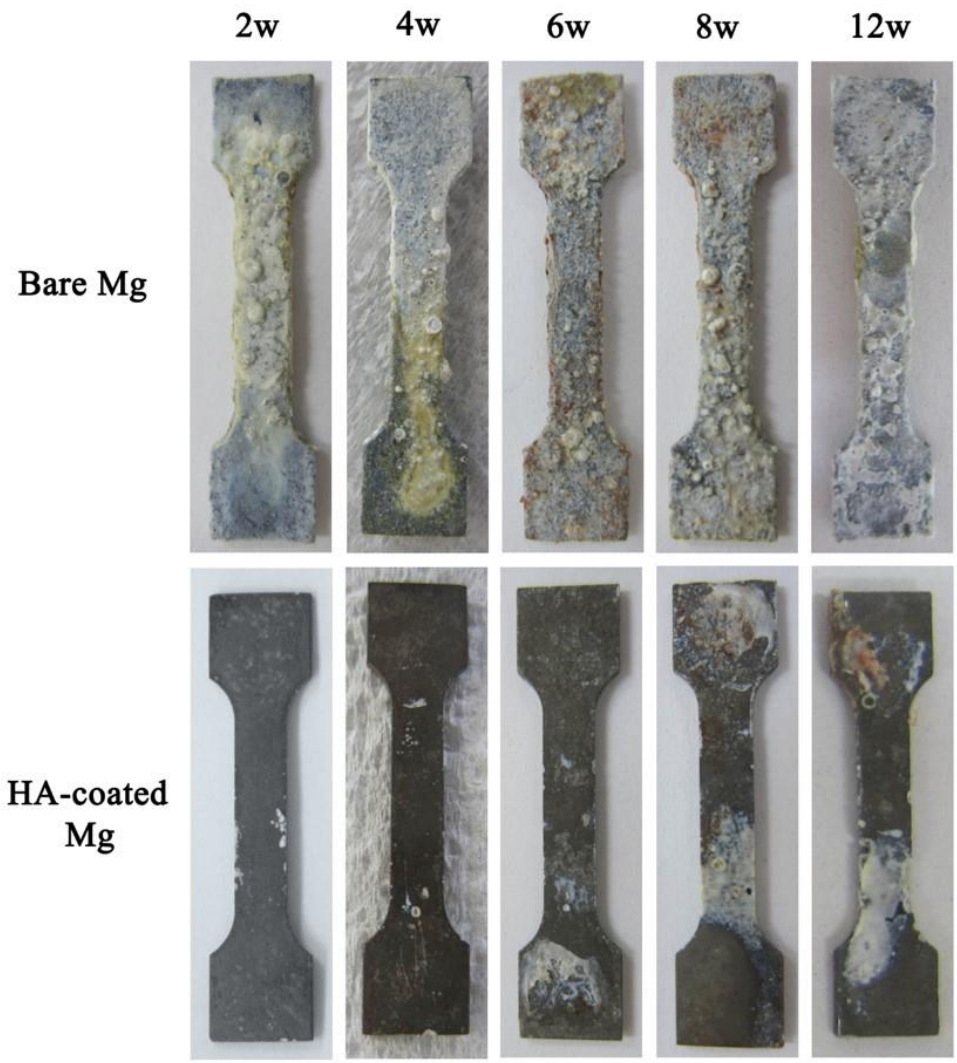

Figure 3.13. Optical images of the bare Mg and HA coated Mg specimens after 2, 4, 6, 8, and 12 weeks of implantation.

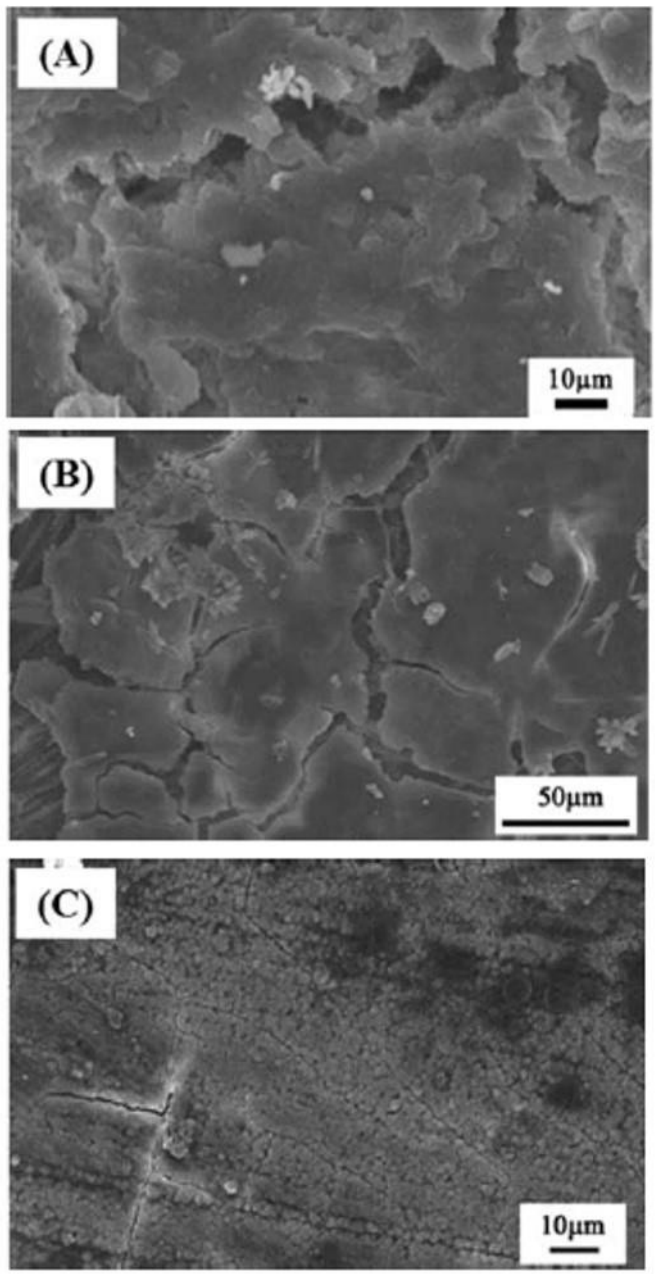

Figure 3.14. SEM images of the bare Mg (A and B) and HA coated Mg specimens (C) after 2 (A) and 12 (B and C) weeks of implantation.

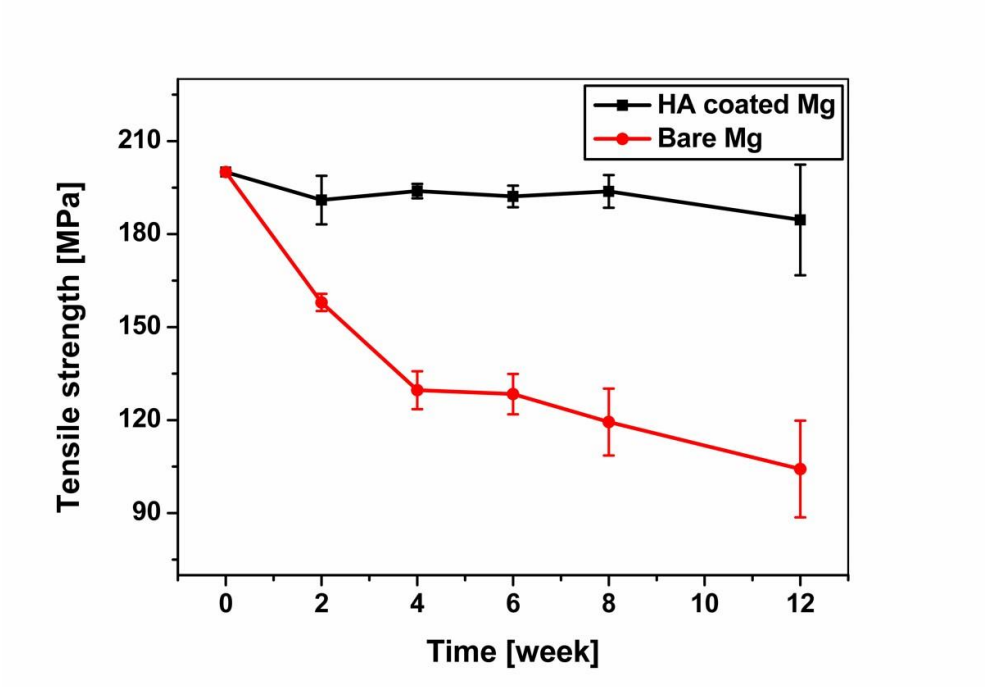

Figure 3.15. Ultimate tensile strength of the bare Mg and HA coated Mg specimens after 2, 4, 6, 8, and 12 weeks of implantation.

3.3.6. *In vivo* biodegradation and bone response

As a model of a real implant, screws machined from bare Mg and HA coated Mg were implanted into tibial defects in rabbits to closely evaluate their bone responses, as shown in Figure 3.16. After 6 and 12 weeks of healing, the surface morphologies and volume changes of the screws were examined by μ-CT analysis. As expected, the bare Mg and HA coated Mg screws exhibited very different degradation rates, as indicated by the changes in morphology shown in Figure 3.17. In the case of bare Mg, the thread of the screw was severely corroded already after 6 weeks of implantation, resulting in significantly reduced screw width in the cortical area. By contrast, the HA coated Mg screw showed that the shape of the implanted screw was mostly maintained and bone tissue integration was favorably promoted.

To quantify the amount of degradation, the volume of each screw was calculated. The degradation volume showed a trend consistent with the corrosion behavior, as illustrated in Figure 3.18. In the case of the HA coated samples, the initial screw volume decreased by 5.28% in the first 6 weeks, while in the case of the bare Mg samples, the initial screw volume dropped by 20% over the same period of time ($p<0.05$). Throughout the whole implantation time of 12 weeks, the volume of the HA coated screws was decreasing on average at a rate of approximately 0.29% per day. This is to be compared with the performance of the bare Mg screws which were losing volume at a rate of ~ 0.40% per day ($p<0.05$).

Biological interaction between the Mg implants (bare Mg and HA coated

Mg screws) and new bone was also observed after 6 and 12 weeks of implantation, as illustrated in Figure 3.19. Although newly formed bone tissue was observed around the implant surface for both bare Mg and HA coated Mg specimens, the HA coated ones showed more pronounced bone contact.

To quantify the bone responses to the implants, the BIC ratio for the thread in the cortical region was measured by using the SPOT image analysis program. After 6 weeks of healing, a statistically significant difference ($p<0.05$) of bone contact between the bare Mg and HA coated Mg samples was found, as depicted in Figure 3.20. The HA coated Mg screws exhibited considerably higher BIC ratios than the bare Mg screws. However, after 12 weeks of implantation, the average value of BIC ratios was just slightly higher for the HA coated Mg specimens than for the bare Mg ones, the difference being insignificant.

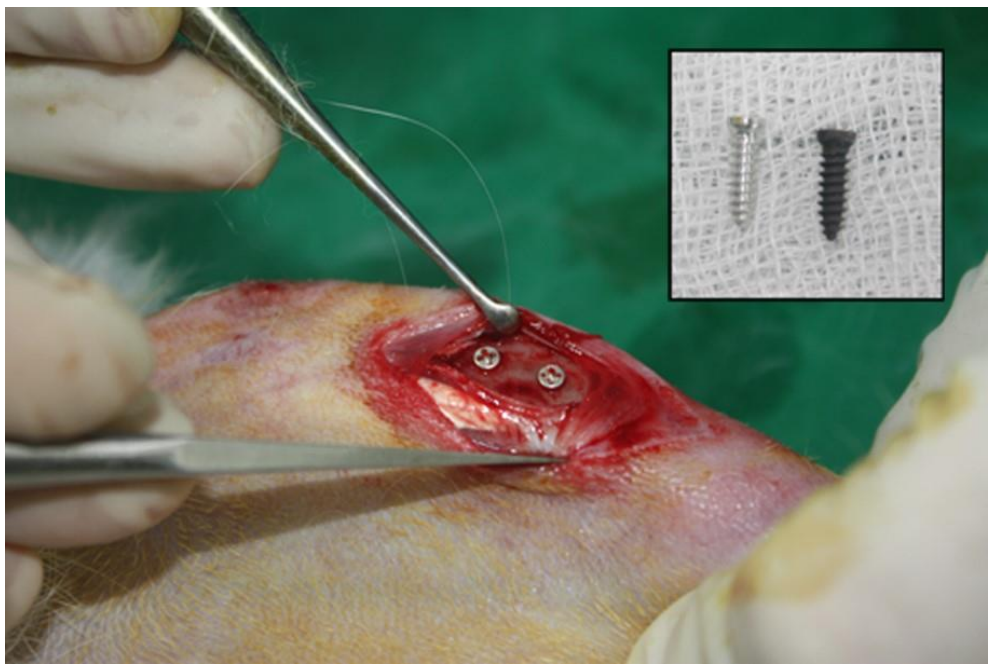

Figure 3.16. Optical images of the screw samples that were implanted into rabbit tibial shafts. The inset shows a bare and an HA coated Mg screw before the implantation.

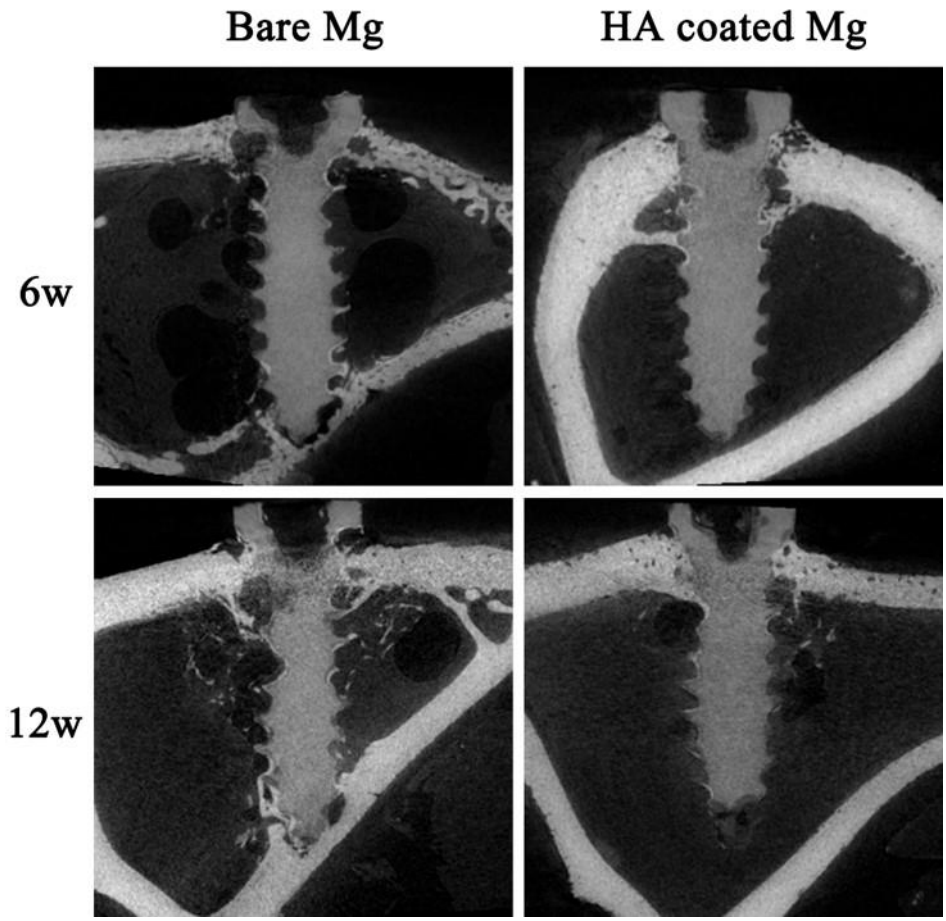

Figure 3.17. Reconstructed μ-CT images of the bare (left pictures) and HA coated Mg specimens (right pictures) after 6 weeks (upper images) and 12 weeks (lower images).

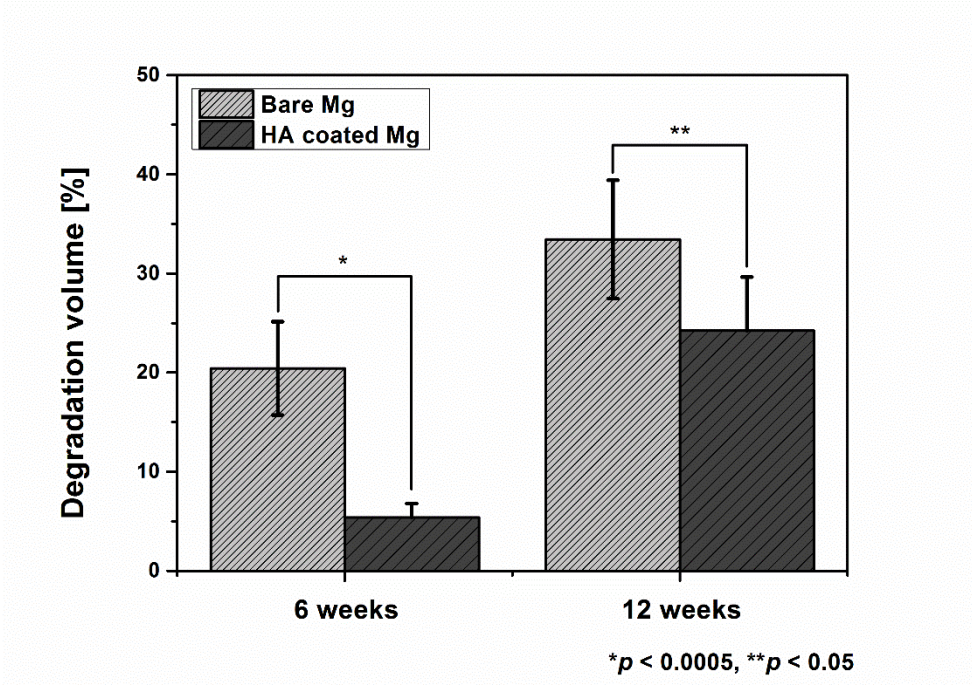

Figure 3.18. Degradation volumes of the bare and HA coated Mg specimens after 6 and 12 weeks of implantation.

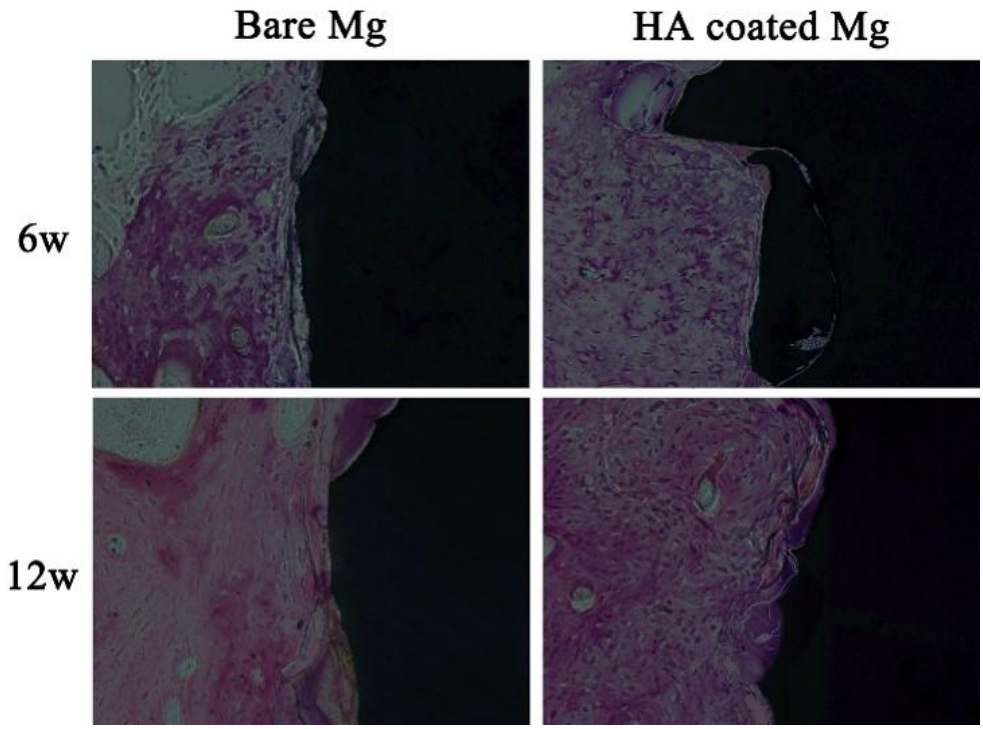

Figure 3.19. Histological images of the stained sections of the bare Mg (left pictures) and HA coated Mg (right pictures) after 6 and 12 weeks of implantation.

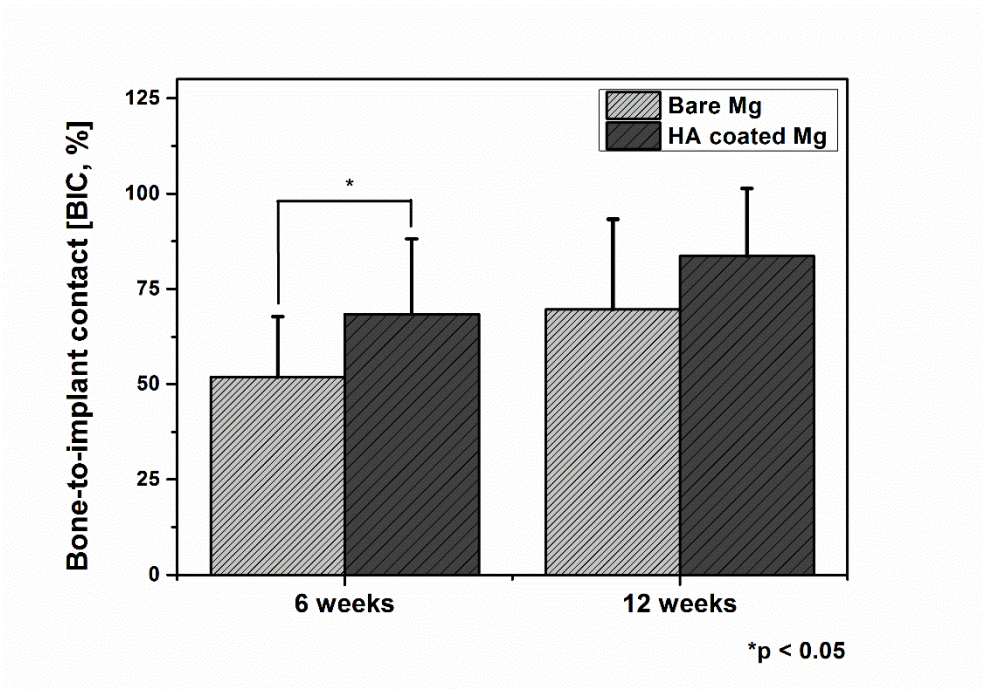

Figure 3.20. Bone-to-implant contact (BIC) ratios of the bare Mg and HA coated Mg in the cortical bone area after 6 and 12 weeks of implantation (*: $p<0.05$).

3.4. Discussion

In this work, the effect of coating with HA on the biocorrosion resistance, biocompatibility and bone response of pure Mg was studied by several techniques. Treatment of Mg specimens in an aqueous solution containing calcium and phosphate sources (Ca-EDTA/KH_2PO_4) following a recipe suggested in Ref. [93] was shown to result in a layer of HA about 2 μm thick, which consisted of two strata: a dense contiguous stratum near the Mg-HA interface and a less dense one with a "cauliflower"-like structure of bundles of needle-like HA crystals [Figure 3.1]. The treatment in an aqueous solution used is very simple, yet effective in producing a protective HA coating on a Mg substrate of arbitrary shape, including complex 3D ones, such as that of a screw. The adhesion strength of approximately 20 MPa achieved satisfies the requirements on deposition coatings for bioimplants. [98]

The two strata structure of the HA coating appears to be responsible for a favorable combination of properties: improved corrosion resistance and enhanced biocompatibility of potential Mg implants. The dense HA layer is believed to provide efficient protection of the Mg samples from contact with the corrosive medium, enhancing their corrosion resistance considerably. Indeed, the immersion tests in SBF returned the data showing that two different signatures of corrosion reactions—the amount of hydrogen evolved during corrosion and the variation of the pH value—were both significantly reduced through coating with HA, as shown in Figure 3.4. It

can be stated safely that the HA coating layer developed is effective in mitigating the harmful effects of Mg corrosion, such as alkalization and the evolution of hydrogen gas. [47]

A second aspect of the bioimplant-relevant effect of HA coating on Mg is the improvement of cell response achieved. Cytological *in vitro* tests demonstrated unequivocally that coating of Mg with HA promotes cell attachment, proliferation, and differentiation. In the first stage of attachment, the Mg substrate reacted vigorously with the culture medium, producing hydroxide ions and hydrogen gas. [8] Local alkalization and hydrogen bubbles, which the cells could not handle, produced a hazardous environment for the cells to attach. [87] Therefore, hardly any cells were detected on the bare Mg samples, and those that did attach appeared to be spherical without any filopodia. By contrast, numerous cells attached well to the surfaces of the HA coated Mg samples, having multiple filopodia and a relatively flattened and stretched shape, as shown in Figure 3.8. The good biocompatibility and favorable morphology of the HA coated samples provided a suitable interaction environment, simultaneously enlarging the bioactive surface area and releasing favorable signals. [103] The cells proliferated actively on the HA layer, whereas those on the bare Mg were almost dead during the testing period. As seen in Figure 3.9, the DNA level on the HA surface layer was nearly as high as on stand-alone HA pellets and Thermanox®, which are known to possess excellent biocompatibility. [99-102] The ALP activity indicated clearly that the surfaces of the HA coated samples facilitated cell

differentiation, Figure 3.11. Although an accurate comparison between the samples with and without the HA layer was not possible due to poor cell attachment and proliferation on the bare Mg samples, the HA coated samples showed a substantially higher level of ALP activity similar to that of Thermanox®. Furthermore, ALP activity of the HA coated Mg was similar to that of HA. In their entirety these results demonstrate that the HA coating significantly improved the *in vitro* cell response of Mg. This overall improvement of the cellular response is undoubtedly related to the rich morphology of the upper HA stratum facing the SBF. It is not clear at this stage, however, which features of the surface topography, including the diameter of the HA crystals and the length scale of the "cauliflower" pattern in which they cluster, are primarily responsible for the observed increase in cell response. As these factors may possibly be controlled through varying the parameters of the aqueous solution treatment, a detailed study into these effects would be of significant interest.

While the results of *in vitro* assays provide a convincing indication of the benefits of HA coating on Mg, the ultimate test of suitability of the proposed treatment on implants before clinical tests is an *in vivo* investigation. Indeed, it is not uncommon that the *in vivo* behavior of an implant does not live up to the expectations based on the *in vitro* response of the implant material. [104] Fortunately, the present results of the *in vivo* animal tests provide a clear demonstration of the positive effect of HA coating on the biocorrosion resistance and bone response of Mg and do support the *in vitro* results.

The HA coated Mg showed much slower biocorrosion behavior than that of the bare Mg (Figure 3.13), which was evaluated after implantation into bone-pericranium pouches on calvaria (Figure 3.12). This improved biocorrosion resistance allowed the tensile strength of the HA coated Mg to be well maintained even after 12 weeks of implantation (Figure 3.15). Furthermore, μ-CT images (Figure 3.17) clearly showed that severe *in vivo* biodegradation occurred in the bare Mg screws in that the implant diameter was reduced and the original thread degraded substantially during the implantation quite substantially. By contrast, HA coated Mg screws exhibited no significant morphological change, indicating that the coating layer effectively retarded *in vivo* biodegradation. Furthermore, the HA coated Mg implants showed good interaction with the surrounding tissues owing to the inhibition of the rapid degradation in the initial stages of implantation, as seen in the histological sections (Figure 3.19). The higher BIC ratio for the HA coated Mg specimens is a clear indication of enhanced bone response after implantation for 6 weeks (Figure 3.20). These results are in agreement with earlier studies where a bioactive HA coating layer was reported to promote bone-implant interaction and lead to a good contact with the bone. [105,106] We realize that it is not warranted that this favorable behavior in an animal test will be replicated in clinical surgery. However, the remarkable improvement of biocorrosion resistance, biocompatibility and bone response of Mg achieved in this work through coating with HA gives promise for greater acceptance of Mg implants in biomedical industry.

3.5. Conclusions

A protective HA layer was deposited onto a Mg substrate using a simple treatment in an aqueous solution. This treatment worked well both for flat laboratory specimens and more complex screw-shaped implants. The HA layer showed a substructure with a dense stratum at the interface with the Mg substrate and a top stratum formed by a population of HA crystals organized in a "cauliflower"-like bundled morphology. The dense, contiguous stratum exhibited sufficiently high adhesion strength complying with the standard requirements on adhesion of coatings for implant applications. Besides, it provided a protective barrier between the substrate and the corrosive medium to inhibit the corrosion of the Mg. Therefore, the undesirable excessive formation of corrosion by-products (e.g., hydrogen gas or hydroxide ions) in the SBF solution was mitigated. The rich morphology of the top HA stratum is believed to be responsible for the significant improvement of biological activity, including attachment, proliferation, and differentiation of the cells. Furthermore, the *in vivo* results supported the good biocorrosion protection, biocompatibility, and bone response of the HA coating in the initial stage of the healing period expected from the outcomes of the *in vitro* assays. These findings suggest that providing Mg with a protective HA coating by a simple treatment discussed is a promising avenue for introducing Mg implants in bone surgery.

Chapter 4.

Behavior of HA/PLLA patterned Mg under deformation

4.1. Introduction

Mg and its alloys have received great attention as a suitable material for biomedical application in accordance with the increasing demand for biodegradable materials in recent years. [5] Mg would achieve a complete dissolution as tissue heals, which prevents postoperative complications arising out of permanent implant such as foreign body response and secondary removal surgery. [8,25] Furthermore, its comparable elastic modulus to natural bone is advantageous over other metallic implants in terms of stress shielding effect. [23] Also, biodegradable Mg possesses higher potential for orthopedic application over biodegradable polymer or ceramic owing to its physical properties being a better match to those of bones. [1] Despite its beneficial characteristics, poor corrosion resistance of Mg under physiological conditions has restricted its active use in clinical applications, [1,3,4] particularly in environments containing chloride ion. [41] Large volume of hydrogen gas bubbles and local alkalization are the major phenomena of rapid degradation of Mg, leading to delayed recovery, even worse, necrosis of tissues. [9]

So far, various strategies to mitigate the aggressive degradation of Mg have been explored including alloying [3,4,9,40,41,44-47], heat processing, and surface modification [79-84]. Among them, surface treatment is known to be highly effective on modulating the corrosion rate without affecting the intrinsic properties of Mg. While achieving a controlled degradation behavior, it also provides additional function to Mg such as improved bioactivity. Calcium-phosphate based coatings,

such as HA and tri-calcium phosphate (TCP), enhance surface bioactivity due to their compositional similarity to natural bone, resulting in better bonding between the implant and the bone. [92-96] Furthermore bio-ceramic coatings are relatively stable in the physiological condition, offering reliable corrosion protection. However, once the implant undergoes various modes of deformation, ceramic coating easily cracks due to its intrinsic brittleness and consequently fails to protect Mg from corrosion, which is a major problem with ceramic coatings. [74] Biodegradable polymer coatings such as poly(L-lactide) (PLLA), poly(lactide-co-glycolide) (PLGA) and poly(ε-caprolactone) (PCL) are also vigorously investigated because these polymers are known to be biocompatible, flexible and capable of delivering antibiotics, growth factors, and genes. [42,73] In particular, their flexibility has widened the operation area, such as stent application which requires extreme deformation. However, weak adhesion strength between those polymers and Mg, causing delamination of the coating, contributes to insufficient corrosion protection compared to the ceramic coatings. [76] Composite coating layer made of the biodegradable polymer and ceramic is also studied to combine the advantages of the two, however, this coating is still not free from the adhesion issue because the adhesion of the composite coating is mainly dependent on the bonding strength between the polymer and Mg.

Surface patterning has recently gained great interest in biomedical applications due to its ability to modulate cell behavior. [107-114] Many studies have proved that ordered surface pattern, compared to flat or unordered rough surface, can directly have an influence on cell adhesion, spreading, migration, cytoskeleton

organization, proliferation, etc. [114] In particular, surface patterning made of biodegradable polymer and ceramic is expected to achieve synergetic properties while clearing the problems associated with single-phase coating discussed above. By arranging the bioactive ceramics in discontinuous pattern, severe crack propagation over the coating layer can be mitigated, resulting in better performance under the external deformation. Also, overall coating stability could be enhanced because bio-ceramics have relatively high adhesion strength to Mg and consequently the polymers obtains better durability to the deformation in terms of delamination.

Therefore, micro-patterned HA and PLLA coating has been introduced on pure Mg by the combination of photolithography and solution treatment containing calcium and phosphate sources. The objective of the study is to increase both coating stability and bioactivity under the tensile strain mode, where patterned HA improves corrosion resistance and bioactivity of the coating layer and PLLA tolerates the deformation of the Mg substrate. The corrosion resistance of the samples was investigated by measuring the amount of hydrogen gas released from the corrosion medium, SBF. Furthermore, the biological responses were assessed through *in vitro* cell tests using MC3T3-E1 pre-osteoblast cells to observe cell attachment and viability under the deformation.

4.2. Experimental procedure

Sample preparation and patterning procedure

High purity (99.99%) Mg plates, 10 mm × 10 mm × 2 mm in size, and dog-bone shape specimens were prepared. The specimens were polished mechanically by up to 4000 grit SiC paper, cleaned ultrasonically with ethanol and air dried. For HA/PLLA patterning, positive photoresist (AZ5214) was patterned by a photoaligner (Karl-Suss MA-6 Ⅱ). Photomask was precisely designed to have hole arrays with a 10 μm in diameter and 20 μm between the centers of the holes. After developing the photoresist pattern, HA coating was proceeded on the patterned substrate by the method as described in chapter 3. Briefly, Mg samples were treated in 0.05M Ca-EDTA/0.05M KH_2PO_4 aqueous solution. During the treatment, pH was adjusted to 8.9 with NaOH and the temperature of the solution was kept to 368K in an oven for 2 h. HA was only formed on the exposed part of Mg by photoresist patterning, then photoresist pattern was removed by acetone cleaning. As a final step, 5 wt% of PLLA in dichloromethane (DCM) was spin-coated on the HA patterned Mg, then heat-treated at 250℃ on hot plate to form a uniform polymeric layer between the HA rods. For comparison, HA coated and PLLA coated Mg were also prepared by the method as described above. Schematic diagram of the patterning procedure is illustrated in Figure 4.1.

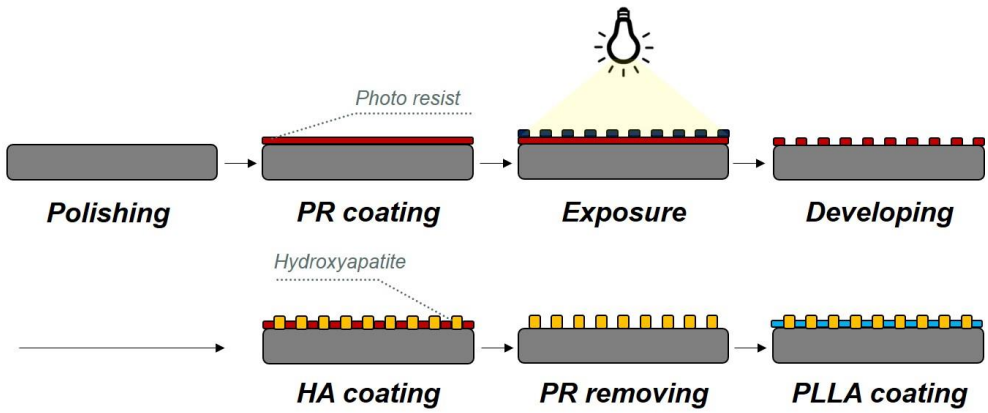

Figure 4.1. Schematic diagram of HA/PLLA patterning procedure.

Tensile deformation on the coating layer

Deformation was applied to the specimens by Instron 5582 tensile machine to reach 5% strain at a speed of 0.5 mm/min. This value was chosen in accordance with the strain to failure of the cortical bone, representing the maximum deformation that can be transferred to the implant. Moreover, no extensometer was used in order to not deteriorate the coated area of the samples during deformation. Then, the two sides of the dog bone shape specimen that were not subjected to deformation were covered with epoxy so that the only strained part of the sample was analyzed.

Microstructure, chemical composition and crystalline structure characterizations

The surface morphologies of the bare, HA coated, PLLA coated, and HA/PLLA patterned Mg specimens were observed by scanning electron microscopy (SEM, JSM-5600; JEOL, Japan). The cross-sectional morphologies of the patterned samples were analyzed by focused ion beam milling (FIB, AURIGA; Carl Zeiss, Germany). The chemical composition of the HA/PLLA patterned layer was characterized by energy-dispersive spectrometer (EDS) attached to the SEM. The crystalline structure of the HA/PLLA pattern was examined by X-ray diffraction (XRD, D8-Advance; Bruker Co., Germany).

In vitro corrosion tests

The bare, HA coated, PLLA coated, and HA/PLLA patterned Mg specimens were soaked in SBF with ion concentrations nearly equal to those of human blood plasma for up to 10 days to evaluate their surface corrosion properties. Each sample was immersed in 50 mL of SBF adjusted to pH 7.4 at 37 ^{o}C with an exposed area of 1 cm^2. At each immersion time point, the volume of hydrogen gas were recorded. Also, on day 3 and 9, the samples were extracted from the medium and analyzed to see how morphology of the coating layer changes as immersion time increases by SEM.

In vitro biocompatibility tests

For the *in vitro* cell tests, the samples (bare, HA coated, PLLA coated, and HA/PLLA patterned Mg) were sterilized under ultraviolet irradiation on a clean bench. A pre-osteoblast cell line, MC3T3-E1 (ATCC, CRL-2593), was used to assess the cell response to the specimen surfaces. The pre-incubated cells were seeded on specimens at densities of 5.0 x 10^3 cells/cm^2 and 2.5 x 10^3 cells/cm^2 to evaluate the cell attachment and proliferation respectively. Alpha-minimum essential medium (α-MEM, Welgene Co., Ltd., Korea) with the addition of 5% FBS and 1% penicillin-streptomycin was used as the cell culture medium and the cells were cultured in a humidified incubator in air atmosphere containing 5% CO_2 at 37^{o}C.

Cell morphology observations

After culturing for 1, 3, and 5 days, the attached cells were observed by scanning electron microscopy (SEM, JSM-5600, JEOL, Japan). Prior to the SEM observations, the samples were fixed with 2.5% glutaraldehyde for 10 min, dehydrated in graded ethanol (70, 95 and 100% ethanol in sequence), immersed in hexamethyldisilazane for 10min, and dried in air.

Cell viability and proliferation

Cell proliferation was determined after 3 and 5 days of culturing using a Cyquant cell proliferation assay kit (C7026 Invitrogen). Before measurements, the cells that adhered to the samples were detached and suspended in a fluorescent dye solution. The DNA level of the detached cells was measured using a multiple plate reader (Victor3, PerkinElmer, USA) at 480/535 nm wavelength. The measured florescence values were converted to the DNA content using a DNA standard curve. In this assay kit, the DNA level was directly proportional to the number of living cells.

Statistical analysis

All experiments were performed more than three times, and the experimental results were expressed as the mean value ± standard deviation (SD).

The difference between the four groups (bare, HA coated, PLLA coated, and HA/PLLA patterned Mg) was determined using a one-way analysis of variance (ANOVA) and $p < 0.05$ was considered a statistically significant difference.

4.3. Results

4.3.1. Microstructure and crystalline structure of HA/PLLA patterned layers

Figure 4.2 presents the surface morphology of HA/PLLA patterned Mg [Figure 4.2. (D)], and its tilted [Figure 4.2. (D)-1] and cross-sectional [Figure 4.2. (D)-2] view. For comparison, surface morphologies of bare, HA coated, and PLLA coated Mg were represented in Figure 4.2. (A, B, and C). HA micro-dots with a diameter of ~10 μm and a height of ~2 μm were uniformly fabricated with the interspacing distance of ~ 10 μm on the Mg surface and were well embedded in the PLLA matrix as shown in Figure 4.2. (D)-1. The cross-sectional image shows that the thickness of the HA layer was approximately 2 μm and the layer was composed of two distinct strata [Figure 4.2. (D)-2]. While the lower stratum was relatively dense and contiguous, the upper one exhibited bundles of needlelike crystals, as seen in the surface view. PLLA seemed to exist only between the HA micro-pillars, resulting in the exposure of HA pattern, not covering the whole surface. By the EDS analysis, clear calcium and phosphate signals were detected where HA pattern was formed as illustrated in Figure 4.3. Weak Mg signal was also measured between the HA rods, because the area was also covered with PLLA. The crystalline structure of the surface patterned layer was analyzed by XRD, as shown in Figure 4.4. Prior to the surface treatment, only Mg diffraction peaks were observed in Figure 4.4. (A), suggesting no other phases were present, while clear XRD peaks originating from HA were detected along with the Mg substrate peaks after treatment, in Figure 4.4.

(B, D). The HA peaks from the HA/PLLA pattern exactly match those found from the HA single coated Mg. In particular, the relative intensity of the diffraction peak of the $(002)_{HA}$ plane at $2\theta = 26^{\circ}$ was higher than the intensities of the other crystallographic planes of HA.

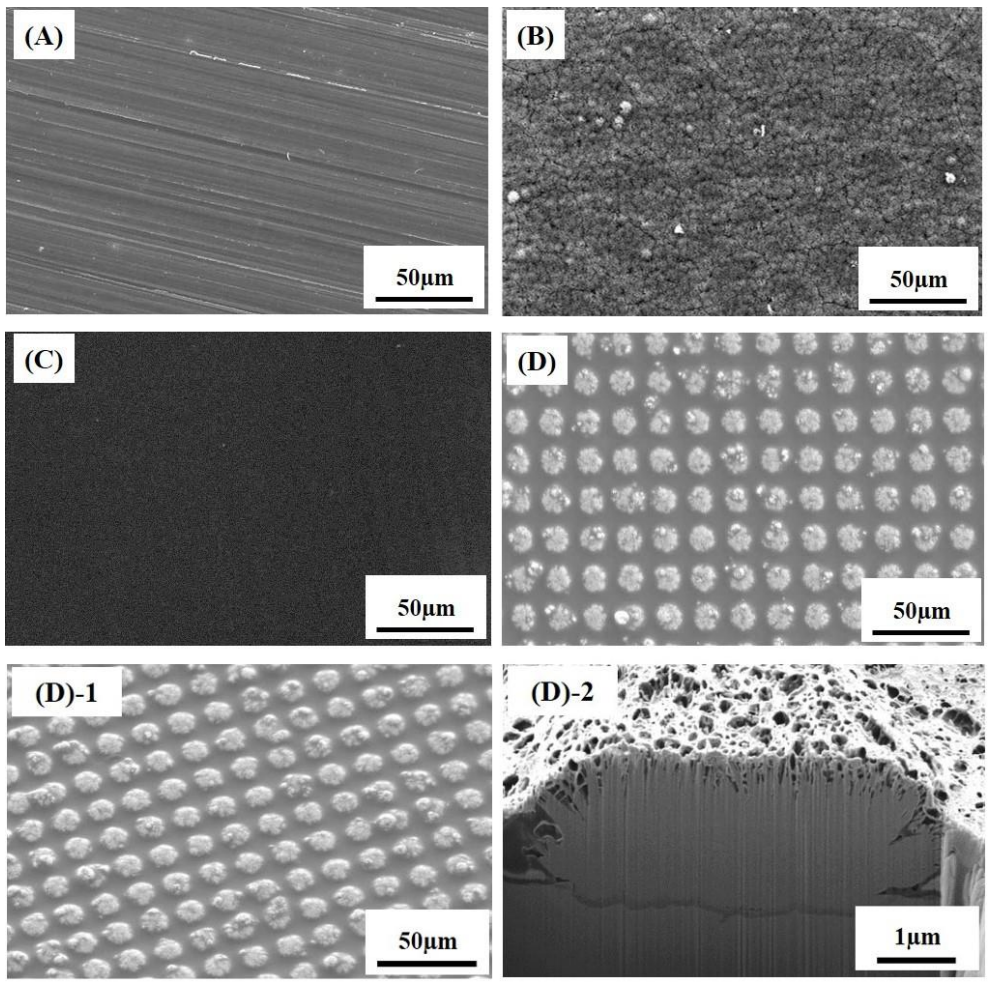

Figure 4.2. SEM images of (A) the bare Mg, (B) HA coated Mg, (C) PLLA coated Mg, and (D) HA/PLLA patterned Mg. ((D)-1 tilted and (D)-2 cross-sectional view of HA/PLLA patterned Mg)

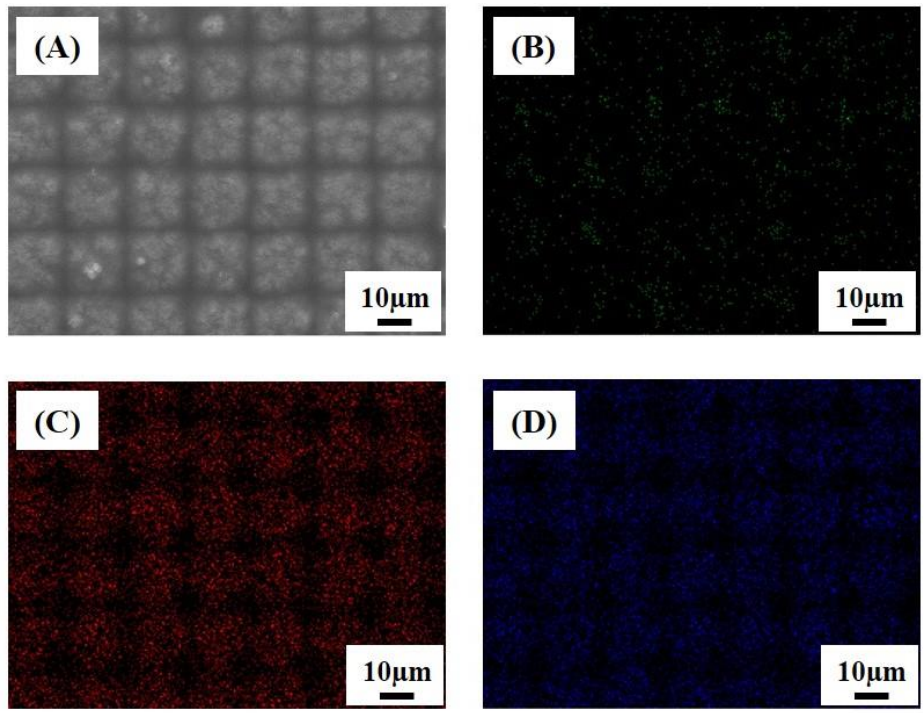

Figure 4.3. Atomic signals from the HA/PLLA patterned surface. [(B): Mg, (C): Ca, and (D): P]

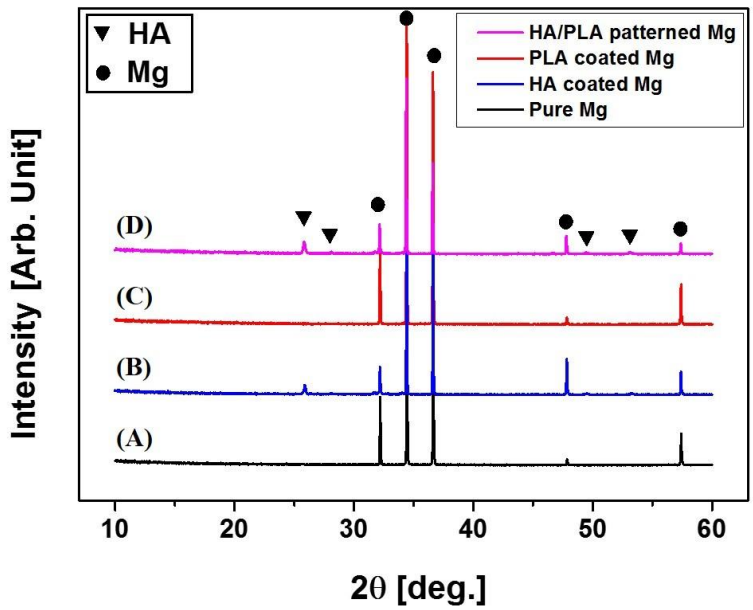

Figure 4.4. XRD patterns of (A) bare Mg, (B) HA coated Mg, (C) PLLA coated Mg, and (D) HA/PLLA patterned Mg (●: Mg, ▼: HA).

4.3.2. Microstructure after application of strain

In order to study the behavior of the patterned Mg in practical application, the specimens were deformed to a tensile strain of 5%. SEM images taken after application of strain are presented in Figure 5.5. While bare Mg did not show any apparent microstructural changes, the HA coating layer exhibited multiple cracks, with length of more than 50 μm. Some parts of the coating already detached from the substrate, exposing Mg to the outer environment. PLLA coated Mg also exhibited severe tearing and delamination all over the surface. Thus it is clear that HA and PLLA cannot sustain the protection to Mg when deformation is applied to the implant due to its brittle behavior and low adhesion strength, respectively. It is believed that lower levels of strain result in the same way of crack formation and damages in the coating layer. Observations of HA/PLLA patterned sample subjected to the strain did not reveal the presence of cracks or defects in the coating layer and seemed to maintain a quite good adhesion to the substrate.

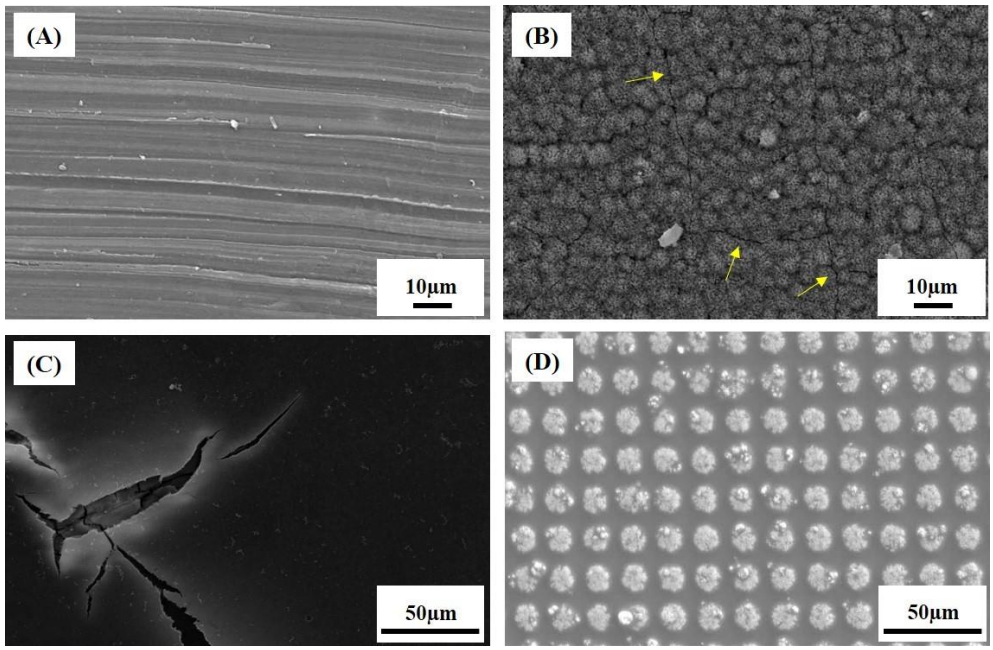

Figure 4.5. SEM images of (A) bare Mg, (B) HA coated Mg, (C) PLLA coated Mg, and (D) HA/PLLA patterned Mg under 5% of tensile deformation.

4.3.3. *In vitro* corrosion tests

Immersion corrosion tests, in which the bare, HA coated, PLLA coated, and HA/PLLA patterned Mg samples were soaked in an SBF solution, were conducted to estimate their surface corrosion properties under deformation. For each immersion, the evolved hydrogen gas volume was measured up to 10 days. The results are presented in Figure 4.6 where the hydrogen gas evolution as a function of immersion time measured for non-strained and strained specimens. Without deformation, the hydrogen gas evolving from the samples with a protective HA coating and HA/PLLA patterning was negligible compared to that of bare and PLLA coated Mg. Bare Mg released more than 40 mL of hydrogen gas within 10 days. Although no strain was applied to the PLLA coated sample, it can be seen that the amount of hydrogen gas evolution increased linearly, leading to about 25 mL of hydrogen gas formation. This result is attributed to the very low adhesion of polymers to metallic surfaces, previously mentioned, causing the exposure of Mg to the liquid solution and consequent corrosion. Once a 5% of tensile strain is applied to the samples, corrosion rate of HA coated and PLLA coated Mg increased dramatically. While HA coating provided good protection to Mg when strain was not applied, a fast and enormous hydrogen gas evolution was observed under deformation, suggesting the exposure of Mg to the SBF solution and its subsequent corrosion. This can be explained by the early contact of Mg with SBF due to the presence of cracks and delaminated areas, previously detected by SEM images in the strained ceramic layer before immersion. In the case of PLLA coated Mg, corrosion rate reached that of bare Mg,

producing almost same amount of hydrogen gas to bare Mg. It implies that PLLA coating layer no longer provided corrosion protection once strain is applied, and consequent delamination occurred. In the case of HA/PLLA patterned Mg, on the other hand, the hydrogen gas evolution was very similar to that of the non-strained sample, less than 3 mL up to 10 days in the SBF. Indeed, the best performance under tensile strain condition was achieved with the HA/PLLA patterned Mg that almost did not undergo corrosion. It is suggesting that HA/PLLA patterning provided stable corrosion protection to Mg whether there was an external strain or not.

During the immersion test in SBF, the specimens were taking out of the solution and their surface morphology was analyzed by SEM on day 3 and 9. Without any protection, the surface of bare Mg was severely corroded with the presence of corrosion pits and multiple cracks as shown in Figure 4.7. A fast degradation rate was observed since the sample started crumbling after few days, causing massive hydrogen gas formation in the solution. Similar surface morphology was observed on the bare sample subjected to 5% strain. In the case of HA coating [Figure 4.8. (A, B, and C)], no visible deterioration of the layer was observed up to 9 days. However, in the case of HA coating under tensile strain conditions [Figure 4.8. (D, E, and F)], the application of HA coating on the surface did not show much efficiency due to the brittle behavior of HA. Figure 4.8. (E and F) reveals the damaged HA coating layer after 3 and 9 days of immersion in SBF solution. As it can be seen, the coating layer was severely cracked and Mg was not protected in some areas of a size of hundreds of microns, explaining the increased hydrogen gas formation in the solution.

Moreover, the local exposure of Mg led to localized corrosion pits, sometimes very deep and able to reach the width of the specimen. In the same way, deposition of a PLLA layer on Mg did not provide protection to the sample. As illustrated in Figure 4.9. (A, B, and C), corroded Mg was found under the polymer layer that peeled off during immersion into the fluid. Much severe delamination was observed on the PLLA coated Mg under tensile deformation, exposing whole surface area underneath the coating layer [Figure 4.9. (D, E, and F). The surface morphology of HA/PLLA patterned Mg, non-strained and subjected to 5% strain, is displayed in Figure 4.10. As it can be seen, no cracks of the HA rods and no tearing of PLLA occurred, suggesting a good adhesion of HA/PLLA pattern, and no major degradation of the sample was detected.

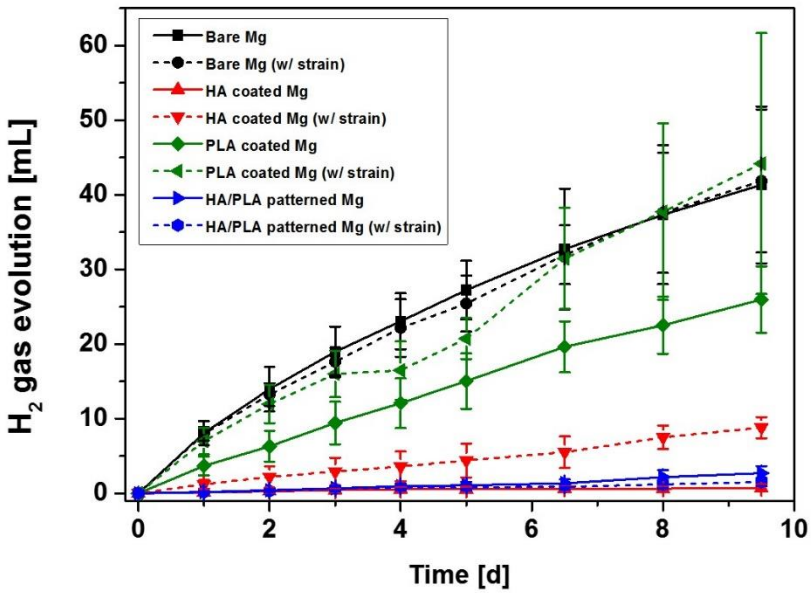

Figure 4.6. Hydrogen gas evolution in the SBF for bare Mg, HA coated Mg, PLLA coated Mg, and HA/PLLA coated Mg with and without 5% tensile strain.

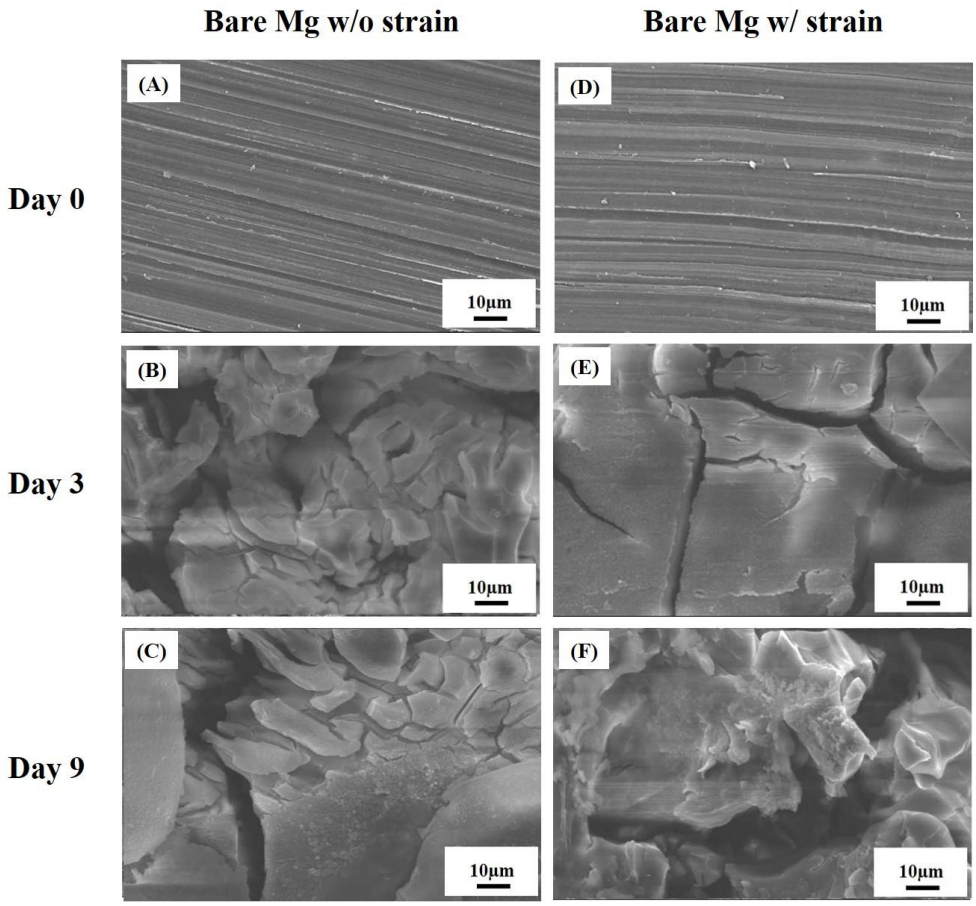

Figure 4.7. SEM images of unstrained (A, B, and C) and 5% strained (D, E, and F) bare Mg after 0 (A and D), 3 (B and E), and 9 (C and F) days of immersion in the SBF.

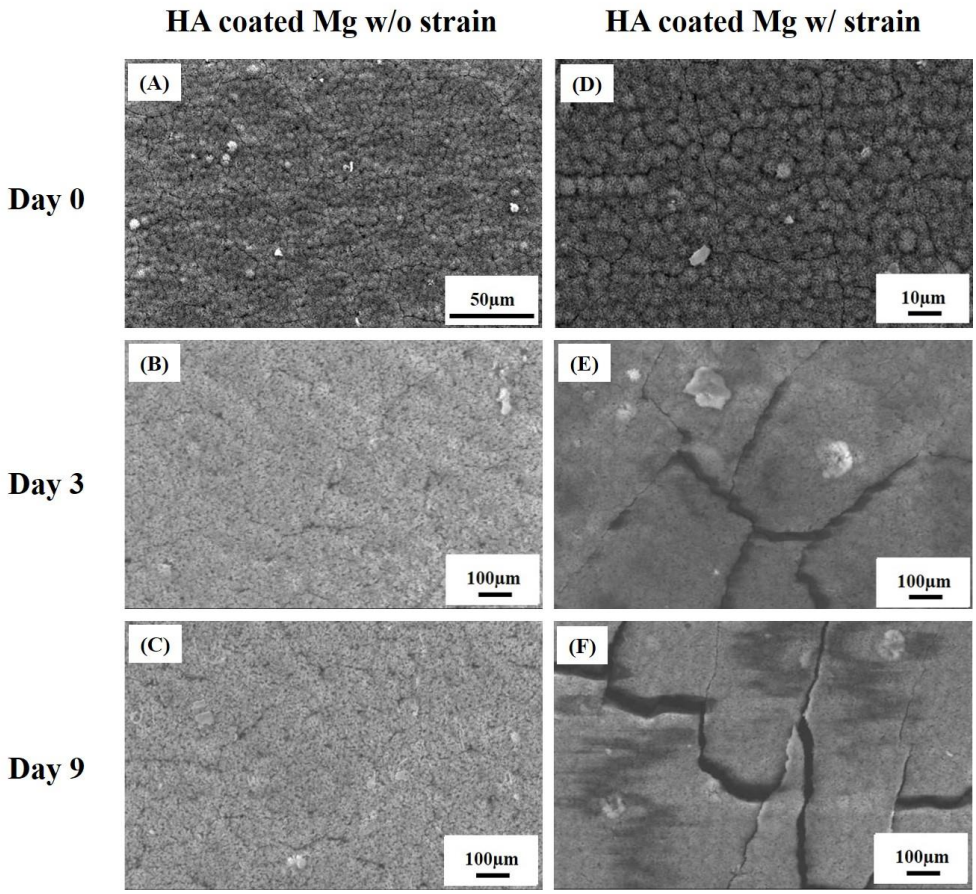

Figure 4.8. SEM images of unstrained (A, B, and C) and 5% strained (D, E, and F) HA coated Mg after 0 (A and D), 3 (B and E), and 9 (C and F) days of immersion in the SBF.

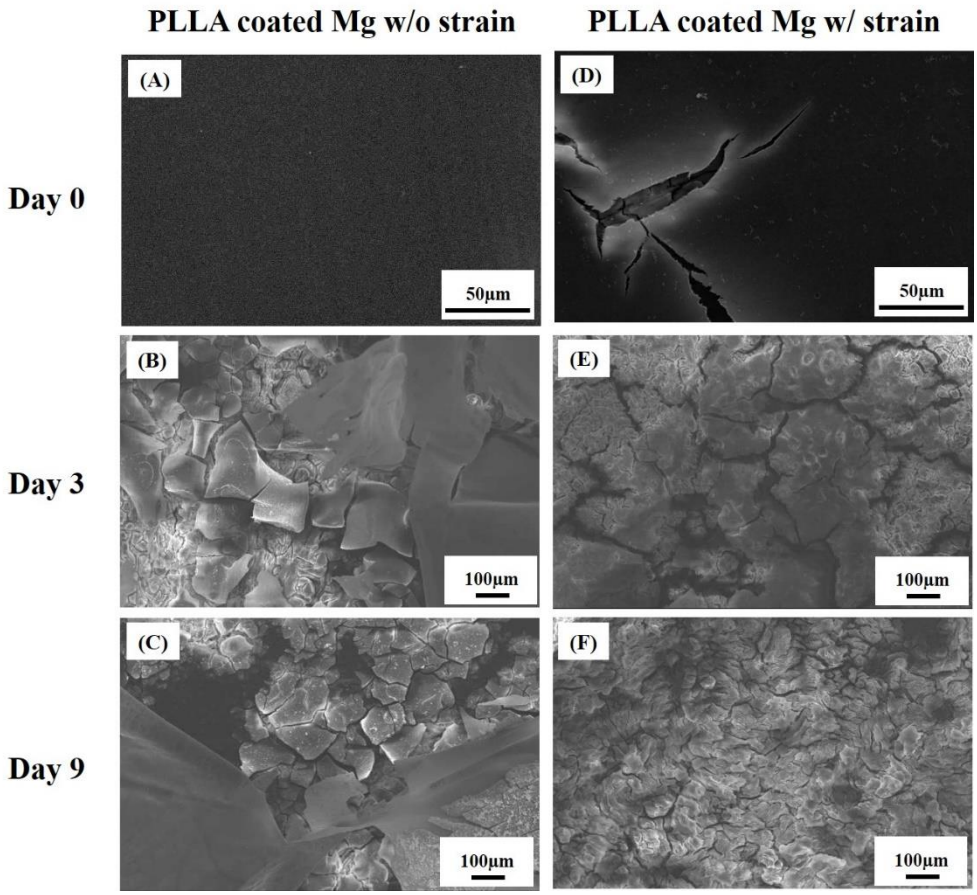

Figure 4.9. SEM images of unstrained (A, B, and C) and 5% strained (D, E, and F) PLLA coated Mg after 0 (A and D), 3 (B and E), and 9 (C and F) days of immersion in the SBF.

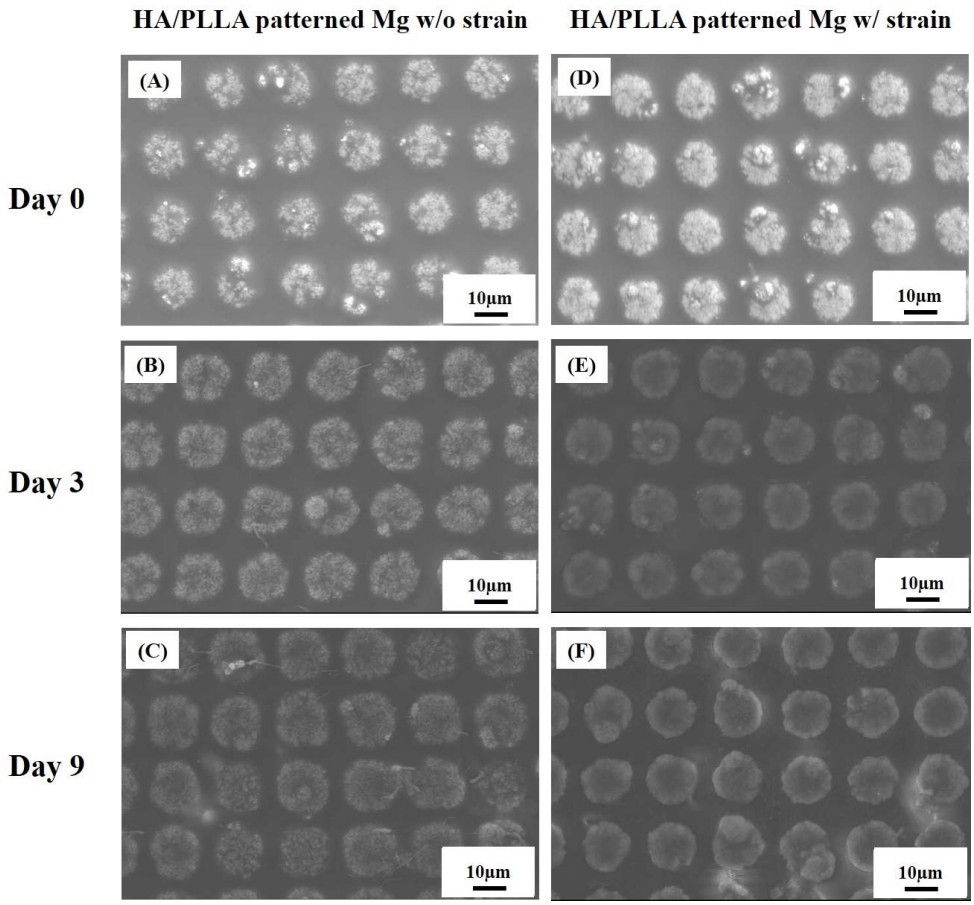

Figure 4.10. SEM images of unstrained (A, B, and C) and 5% strained (D, E, and F) HA/PLLA patterned Mg after 0 (A and D), 3 (B and E), and 9 (C and F) days of immersion in the SBF.

4.3.4. *In vitro* cell responses

In vitro cell tests were performed using MC3T3-E1 preosteoblast cells to evaluate the biological properties of bare, HA coated, PLLA coated, and HA/PLLA patterned specimens, including cells attachment and proliferation. SEM images of the MC3T3-E1 cells that were cultured for 1, 3, and 5 days on bare, HA coated, PLLA coated, and HA/PLLA patterned samples in the non-strained and strained conditions are shown in Figure 4.11, 4.12, 4.13 and 4.14. As it can be seen, only few cells were attached to the corroded surface of bare Mg, in both non-strained and strained conditions as shown in Figure 4.11. However, the cytocompatibility of bare Mg was greatly improved by coating its surface, with good cell responses on HA coated Mg (Figure 4.12), PLLA coated Mg (Figure 4.13) and HA/PLLA patterned Mg (Figure 4.14). Multiple cells attached on all coating layers and spread with an active cytoskeletal extension. From the SEM images, the three different kinds of coating seemed to show a good cytocompatibility and no conclusion can be drawn as for the best cell attachment conditions.

However, when a 5% strain was applied, a loss of biological response was observed with the HA coated Mg sample due to corroded state of the sample in the cell medium. Cracks, release of Mg ions in the medium, increase of pH, and subsequent release of hydrogen gas did not provide suitable environment to the cells, resulting in very small amount of cells attached to the calcium phosphate based layer. Moreover, the few cells found on the surface of the sample did not spread well, as

illustrated in Figure 4.12, suggesting a low affinity to the substrate. In the case of PLLA coated Mg, the cell response also decreased when tensile strain was applied to the sample. Fewer cells attached to the coating layer and their filopodia was not well spread but rather very close to the nuclei, as appearing in Figure 4.13. Coating layer was severely peeled off, exposing Mg to the medium and leading to the subsequent occurrence of corrosion. In contrast, HA/PLLA patterning exhibited minor damages over the immersion period into the medium, resulting in a good cell attachment with multiple cells observed on its surface as seen in Figure 4.14. The cells were well spread and maintained an active cytoskeletal-shape extension, like in the non-strained conditions. Figure 4.15 summarizes the biological circumstances of the each sample after 5 days of culturing. In the case of bare Mg, cells were barely observed on the both, unstrained and strained surface. On the other hand, significantly decreased amount of cells was observed in HA coated sample after the application of 5% strain. PLLA coated samples exhibited similar tendency with the HA coated Mg, while there was no noticeable difference between unstrained and strained HA/PLLA pattern.

In Figure 4.16, the cells proliferation was assessed by quantifying the DNA levels of the cells cultured for 3 and 5 days on bare Mg and coated Mg specimens. The DNA amount of untreated Mg was very low, close to 0.0024 μg and 0.0013 μg, in the non-strained and strained conditions on day 3, respectively. Even after 5 days of culturing, cells on the bare Mg did not well proliferate because of consistent corrosion in the cell medium. However, it can be seen that the ability of the cells to

proliferate was greatly improved when the Mg was coated, especially in the case of HA/PLLA patterning with DNA values reaching 0.006 μg on day 3 and 0.016 μg on day 5. Also, in the case of HA coating, DNA levels were reasonably similar to that of HA/PLLA patterning, in the amount of 0.006 μg and 0.017 μg on day 3 and 5 respectively. Cells on PLLA coated Mg also proliferated more than those on bare Mg did, exhibiting the levels of 0.005 μg on day 3 and 0.011 μg on day 5. However, the application of 5% strain led to a severe overall decrease of DNA levels, as a consequence of the loss of the biological response from the deformed samples, previously highlighted in the cell attachment tests. The most dramatic decrease of cell proliferation was observed for HA coated Mg as the DNA amount dropped from 0.006 μg to 0.0009 μg on day 3 and from 0.017 μg to 0.004 μg on day 5. In the case of PLLA coating, the loss was less pronounced, with DNA values decreasing from 0.005 μg to about 0.002 μg after 3 days of culturing and from 0.011 μg to 0.006 μg after 5 days of culturing. In the case of HA/PLLA patterning, the application of tensile strain did not severely affect the cell proliferation since the decrease of DNA values was limited, from 0.006 μg in the non-strained conditions to 0.004 μg in the strained conditions on day 3 and from 0.016 μg to 0.015 μg on day 5. Survival rate of the cells (Figure 4.17) on the HA/PLLA patterned Mg was more than 2 times higher than the rest of the conditions, about 65% on day 3 and 113% on day 5. In particular, HA coated Mg exhibited less than 25% of cell survival after applying tensile deformation.

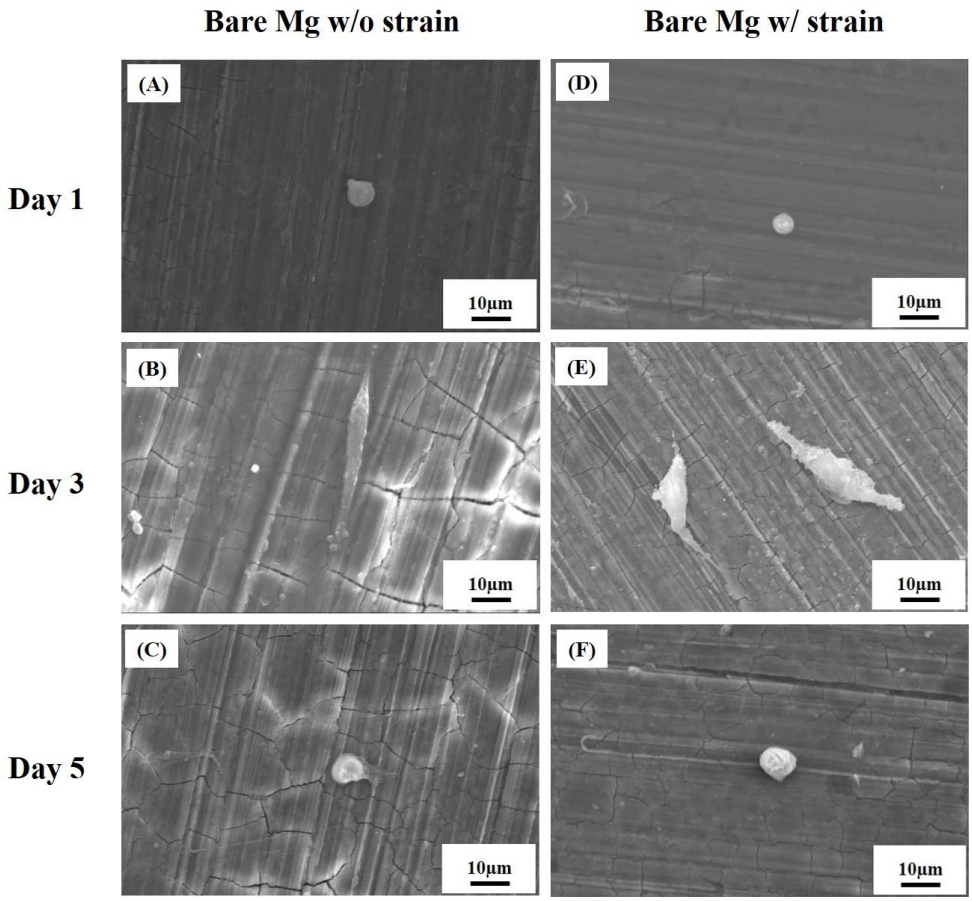

Figure 4.11. SEM images of the MC3T3-E1 cells on unstrained (A, B, and C) and 5% strained (D, E, and F) bare Mg after 1 (A and D), 3 (B and E), and 5 (C and F) days of culturing.

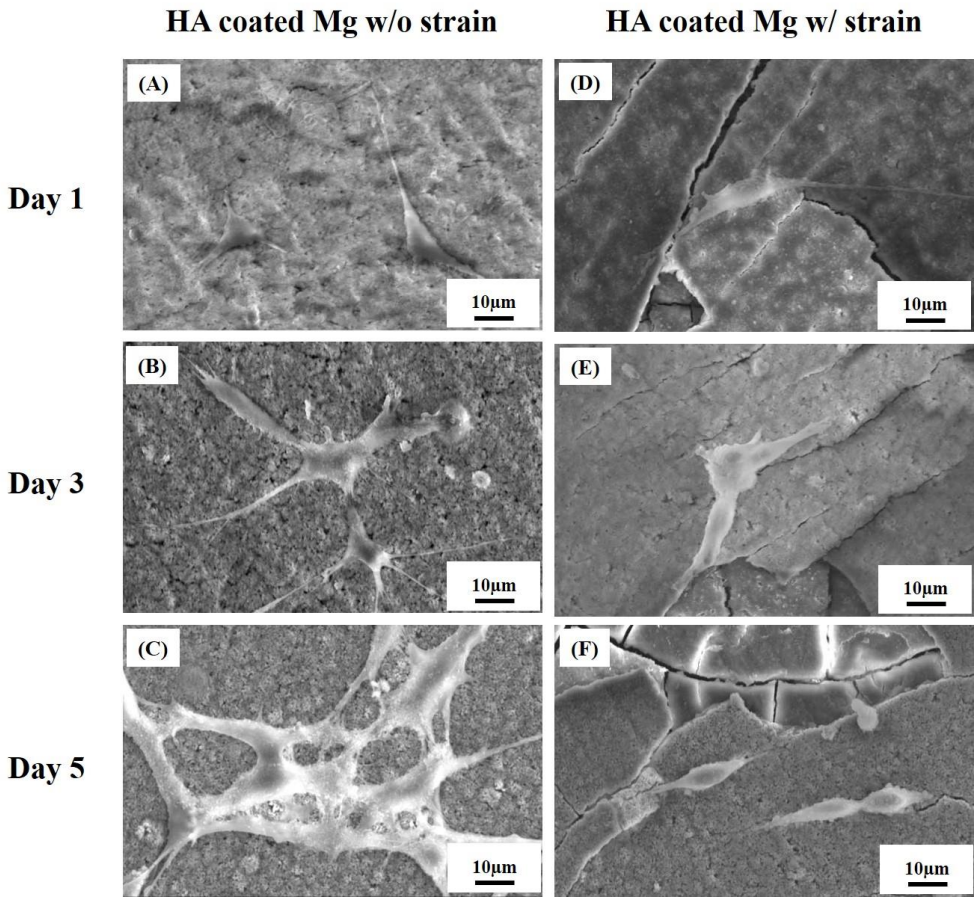

Figure 4.12. SEM images of the MC3T3-E1 cells on unstrained (A, B, and C) and 5% strained (D, E, and F) HA coated Mg after 1 (A and D), 3 (B and E), and 5 (C and F) days of culturing.

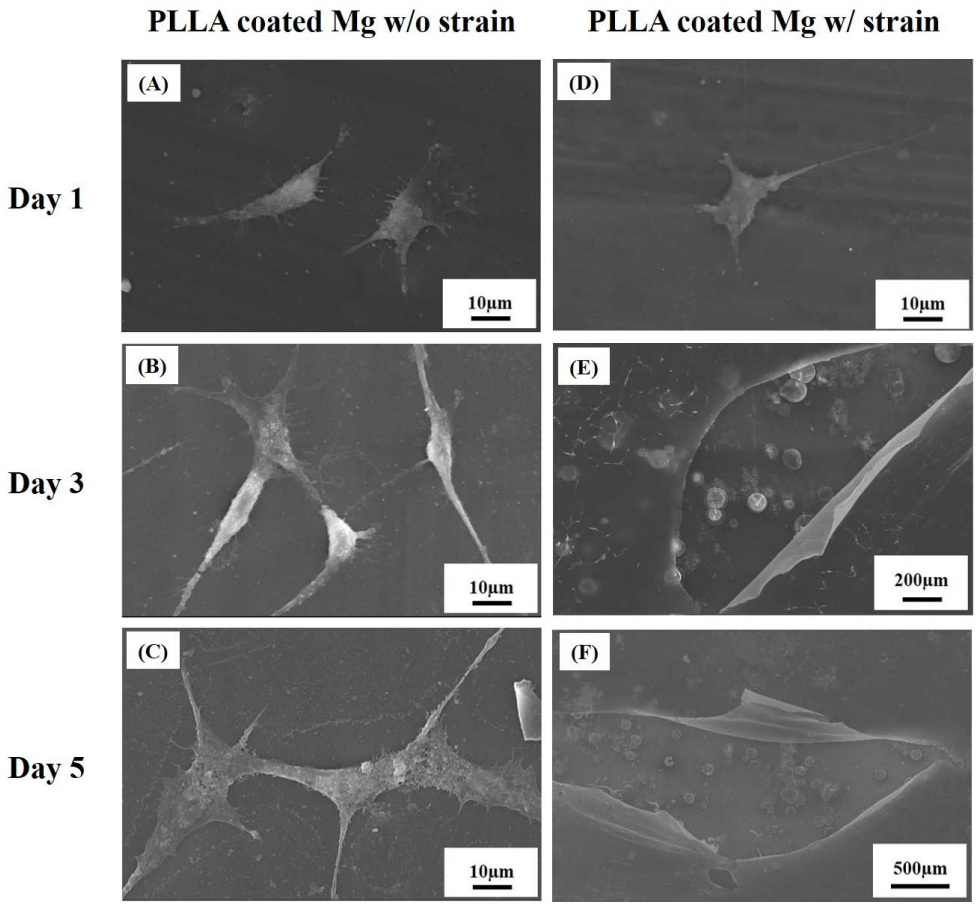

Figure 4.13. SEM images of the MC3T3-E1 cells on unstrained (A, B, and C) and 5% strained (D, E, and F) PLLA coated Mg after 1 (A and D), 3 (B and E), and 5 (C and F) days of culturing.

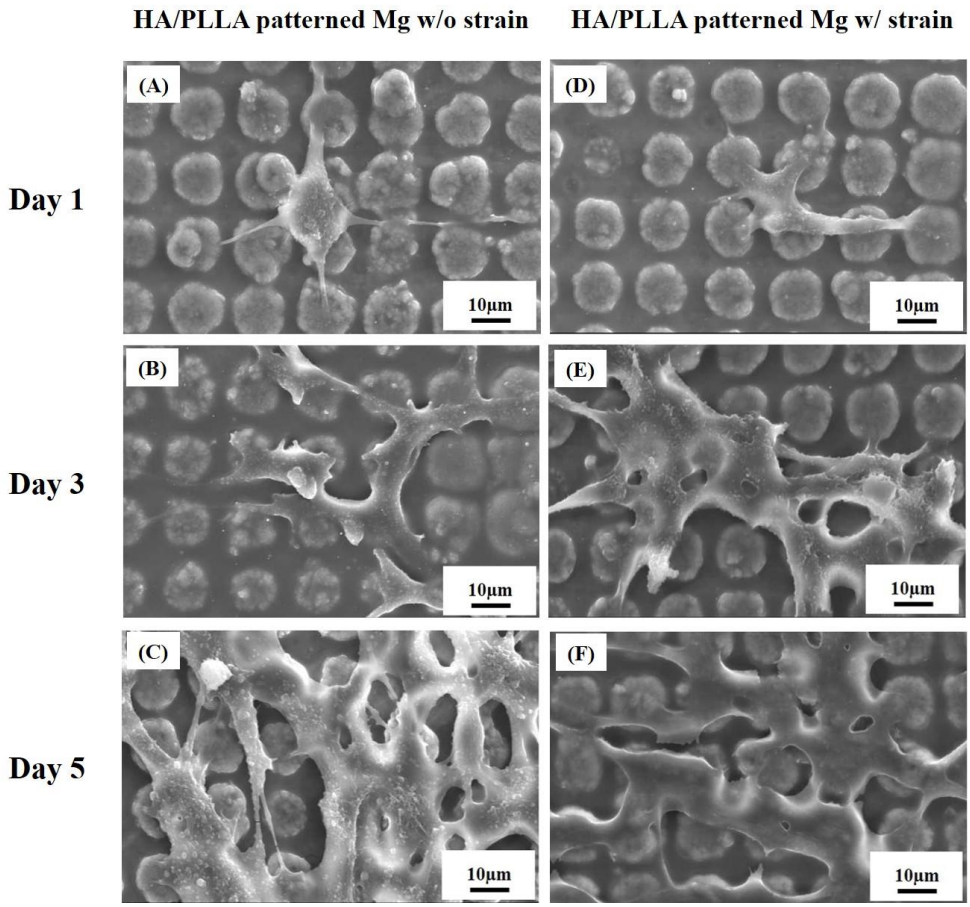

Figure 4.14. SEM images of the MC3T3-E1 cells on unstrained (A, B, and C) and 5% strained (D, E, and F) HA/PLLA patterned Mg after 1 (A and D), 3 (B and E), and 5 (C and F) days of culturing.

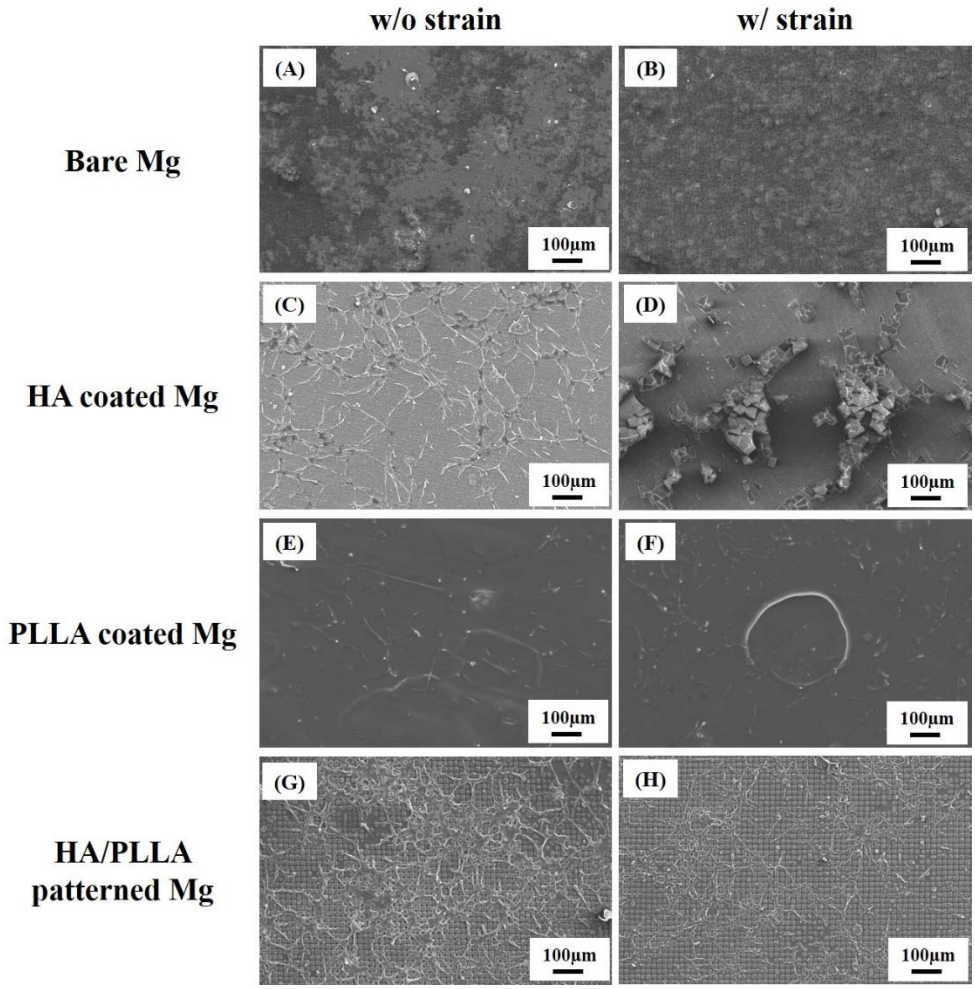

Figure 4.15. SEM images of the MC3T3-E1 cells on unstrained (A, C, E, and F) and 5% strained (B, D, F, and H) bare Mg (A and B), HA coated Mg (C and D), PLLA coated Mg (E and F), and HA/PLLA patterned Mg (G and H) after 5 days of culturing.

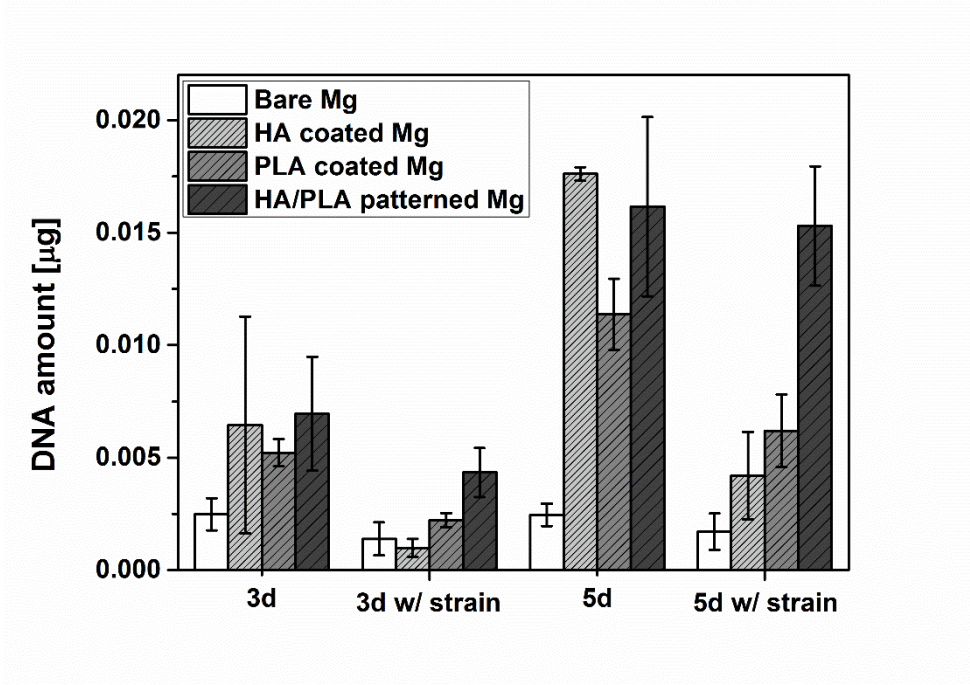

Figure 4.16. DNA levels of the MC3T3-E1 cells that were cultured for 3 and 5 days on bare Mg, HA coated Mg, PLLA coated Mg, and HA/PLLA patterned Mg, before and after application of 5% strain.

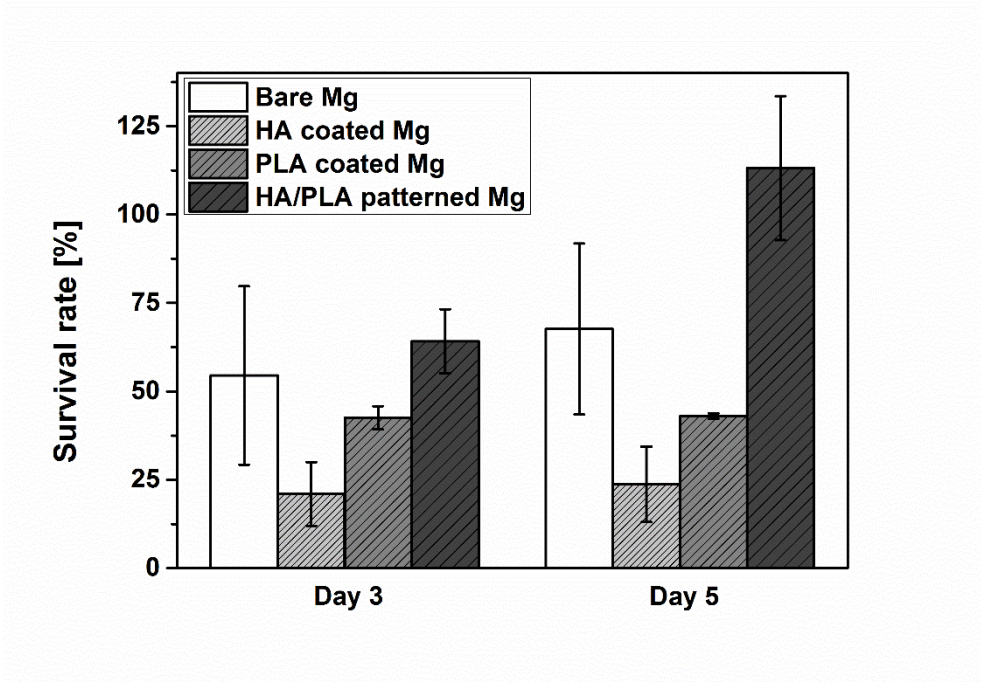

Figure 4.17. Survival rate calculated from the DNA levels of the MC3T3-E1 cells that were cultured for 3 and 5 days on bare Mg, HA coated Mg, PLLA coated Mg, and HA/PLLA patterned Mg, before and after application of 5% strain.

4.4. Discussion

In this work, we have investigated the effect of the HA/PLLA patterns on the corrosion resistance, biocompatibility and stability of the coating on Mg under deformation. As a first treatment, photoresist patterning enabled to selectively form HA on Mg surface, with the size of 10 μm in diameter and 20 μm between the centers of the HA dots. The pattern geometry directly follows the design of photomask, implying various type of patterns can be easily obtained by changing photomask as long as the treatment solution (Ca-EDTA/KH_2PO_4) can fill in the patterns and react with Mg. Even though HA was fabricated in a pattern geometry, its surface morphology and chemical composition were same with those of HA coating as produced in chapter 3, suggesting that similar level of adhesion strength is expected, approximately 20 MPa. As a following treatment, PLLA was spin-coated on HA pattern, with a suitable viscosity for the polymer to infiltrate well between the HA array. The exposure of HA pattern was easily achieved through the short-time (2 min) heat treatment at 250 ℃ for PLLA layer to flow down into the space between HA dots.

This HA/PLLA pattern structure appears to be responsible for a favorable combination of properties: improved corrosion resistance and enhanced biocompatibility of potential Mg implants under deformation. The HA pattern is believed to provide good bioactivity and support the PLLA layer from delamination

or tearing by being located regularly between the PLLA as a fixing pin. Also, discrete HA pattern is advantageous when it comes to crack generation, because the spacing between the rods hinders rapid crack propagation. Meanwhile, stably deposited PLLA layer provides efficient protection of the Mg samples from contact with the corrosive medium, enhancing their corrosion resistance considerably. At the same time, flexible polymeric layer can play a role as a bumper to alleviate the deformation on ceramic pattern when external strain is applied to the substrate.

Indeed, the immersion tests in the SBF returned the data showing that a signature of corrosion reaction—hydrogen gas evolution—was significantly reduced through patterning with HA and PLLA whether a tensile strain was applied or not, as shown in Figure 4.6. From the fact that the polymer was not detached from the structure, it can be assumed that HA pattern helped to improve the bonding strength between PLLA and Mg substrate. On the other hand, once tensile strain was applied, HA and PLLA single coatings experienced severe damages, such as cracks, delamination or peeling when immersed into the SBF. Therefore it can be safely stated that the HA/PLLA patterning layer developed is effective in mitigating the harmful effects of Mg corrosion, and more importantly it can maintain its mechanical integrity under the presence of 5% tensile strain.

A second aspect of the bioimplant-relevant effect of HA/PLLA on Mg is the improvement of cell responses. Better coating stability under tensile deformation, achieved through patterning, consequently accomplished the good biocompatibility

during *in vitro* cell tests. Cytological *in vitro* tests demonstrated unequivocally that patterning of Mg with HA and PLLA promotes cell attachment and proliferation. Cells attached well to the HA/PLLA pattern with a flattened shape and very good extension of filopodia, suggesting their good adhesion to the substrate. The good biocompatibility and favorable morphology of the HA/PLLA patterned samples provided a suitable interaction environment, simultaneously enlarging the bioactive surface area, and releasing favorable signals. Although HA single coating showed a similar bioactivity to HA/PLLA pattern in non-strained conditions, due to its similar composition with that of the bone, the application of deformation severely affected the cell response, as a consequence of the presence of cracks that did not provide suitable environment for the cells. In the same way, tearing or peeling of PLLA layer during the immersion into cell medium resulted in fewer attached cells and not a good extension of filopodia. Cell proliferation test confirmed these results as the highest DNA levels was obtained for HA/PLLA patterned samples subjected to deformation after 3 and 5 days culturing. Survival rate of the cells on the HA/PLLA patterned Mg was more than 2 times higher than the rest of the conditions, about 65% on day 3 and 113% on day 5. It is strongly believed that the suppressed corrosion of HA/PLLA patterned Mg, resulting from improved stability of the coating layer under deformation, assisted the cell's growth by providing favorable conditions to live. Therefore, the remarkable improvement of biocorrosion resistance and biocompatibility of Mg achieved in this work through HA/PLLA patterning gives promise for greater acceptance of Mg implants in flexible applications.

4.5. Conclusions

The micro-patterned HA/PLLA was successfully fabricated on Mg via sequential processes including photolithography patterning, selective HA formation and PLLA spin coating. The HA/PLLA patterned coating allows deformation of underneath Mg substrates without any surface cracks, maintaining the coating stability in the physiological environments. It is believed that this combination of a ceramic pattern and a flexible polymer layer has allowed the cancellation of the drawbacks associated with these two materials, namely a brittle behavior and a low bonding strength to the metal substrate. Indeed, HA/PLLA patterning provided a protective barrier between the substrate and the corrosive medium to inhibit the corrosion of the Mg. Therefore, the undesirable excessive formation of by-products of Mg corrosion (e.g., hydrogen gas or hydroxide ions) in the SBF solution was mitigated under 5% of tensile strain mode. Additionally, the HA micro-pillars of the hybrid coating likely promote cell affinity as a center of cell attachment. *In vitro* cell tests showed that HA/PLLA patterning sustained a good biocompatibility when Mg was subjected to deformation. These findings suggest that providing Mg with a HA/PLLA pattern is a promising avenue for introducing Mg implants in flexible applications.

Chapter 5.

HA patterning on PLLA to modulate cellular response

5.1. Introduction

Biodegradable materials that can be resorbed in the body have been intensively investigated since they eliminate the need of a secondary surgery after the function of the implant is fulfilled. [5,73] Among the biodegradable materials, poly(L-lactic) acid (PLLA) and its copolymer, e.g., poly(lactic-co-glycolic) acid (PLGA), are considered one of the most desirable polymers for fracture fixation, repair, and tissue engineering because they are approved for clinical use by FDA, and their mechanical strength is relatively high. [115] However, the degradation byproducts create an acidic environment which causes inflammatory or allergic responses. [116] Moreover, poor hydrophilicity, related to limited bioactivity [117,118], restricts their active use in clinical area, often requiring incorporation of bioactive ceramic, e.g., hydroxyapatite (HA).

So far, composites made of PLLA and bioactive ceramics such as HA have been extensively developed to improve its clinical performance. Incorporating HA particles into PLLA matrix not only neutralizes the degraded acidic monomers, also increases tissue compatibility due to the compositional similarity of HA to that of hard tissue. [119,120] However, the interface between PLLA matrix and HA particles often weaken the overall strength of the composite owing to the low affinity each other, which limits its application in load-bearing area. [117,121,122] Surface coating is another approach to increase bioactivity without altering mechanical characteristics of PLLA matrix. Depending on the coating material, various functions such as

improved biocompatibility or antibacterial property can be also achieved. However, a critical problem of the surface coating is a risk of delamination, resulting from low bonding strength between PLLA substrate and coating layer. Moreover it has been rarely reported to apply ceramic coating layer on polymer matrix because polymer matrix generally has more flexibility than ceramic coating layer.

In the last decade, surface patterning has gained great interest in biomedical applications due to its ability to modulate cell behavior. [107-114] Many studies have proved that ordered surface pattern, compared to flat or unordered rough surface, can directly have an influence on cell adhesion, spreading, migration, cytoskeleton organization, proliferation, etc. [114] The important aspect of the surface patterning is that it only affect the surface-dependent properties, such as hydrophilicity and cellular responses, while not disturbing the matrix-dependent factors, such as mechanical strength and degradation mechanism. It implies that surface patterning with bioactive material on PLLA could effectively modulate its biological responses and the flexible nature of the polymer could be maintained without any deterioration of the mechanical properties, such as increased stiffness or decreased strength.

Therefore, micro-patterned HA has been introduced on pure PLLA by the combination of photolithography, Mg deposition and solution treatment containing calcium and phosphate sources. The objective of the present work is to control bioactivity of pure PLLA by varying the geometry of HA patterns, while the PLLA matrix continues to exhibit its own mechanical characteristics. High volume of HA

micro-pattern is exposed on the surface to increase the bioactivity, which is hard to be achieved through simple powder blending. Since the patterns are almost embedded in the matrix, they have better bonding to the PLLA, resulting in low risk of delamination during operation. The microstructure of the HA patterned PLLA was investigated, and its mechanical properties were examined by tensile strength test. Furthermore, the in vitro biocompatibility of HA patterned PLLA sample was also evaluated in terms of attachment and proliferation of pre-osteoblast MC3T3- E1 cells.

5.2. Experimental procedure

Preparation of pure PLLA and HA powder mixed PLLA composite

Pure PLLA granules (P9001, Pure Eco, Korea) were put in a rigid die with a diameter of 12 mm and compressed at 190 ℃ under a uniaxial load of ~ 22 MPa for 10 min. For HA powder mixed PLLA composite, PLLA/HA mixture with 20 vol% of HA content was prepared by mechanically blending PLLA and HA powders via shear mixing at 190 ℃ for 30 min. The resultant PLLA/HA mixture followed same procedure as applied on pure PLLA rod fabrication. The produced samples were polished up to 2000 grit of SiC paper and ultrasonically cleaned in ethanol and distilled water in sequence.

Preparation of HA patterned PLLA production

Positive photoresist (AZ5214) was patterned on silicon wafer by a photoaligner (Karl-Suss MA-6 Ⅱ). Photomask was precisely designed to have hole-arrays with a 10, 20, and 50 μm in diameter and 20, 16, 32, and 80 μm between the centers of the holes. The geometric parameters of the patterns were listed in Table 5.1. After developing the photoresist pattern, Mg deposition was proceeded on the photoresist patterned surface by e-beam evaporator (EVACO-EB800R, DR Vacuum Inc., Korea). The commercially pure grade Mg plate was prepared as a target material,

grinded with 400 grit SiC abrasive paper and then cleaned ultrasonically in ethanol. The Mg layer was deposited onto the surface at an approximate rate of 1 nm/s to obtain a thickness of 1 μm. During the deposition process, the substrate holder was rotated at 5 rpm to achieve a uniform thickness. Then, photoresist layer was lifted off in acetone to leave only Mg pattern on wafer. This Mg array was converted to HA through the solution treatment as described in chapter 3 and 4. Next, 5 wt% of PLLA in DCM was spin-coated on HA patterned wafer to form a uniform polymeric layer between the HA rods, then dried in a 37 ℃ oven over night. Finally, HA/PLLA pattern on wafer was transferred to pure PLLA rod by melting the interface between pattern and rod at 250 ℃ hot plate. Schematic diagram of the patterning procedure is illustrated in Figure 5.1.

Table 5.1. Geometric parameters of HA patterns.

	Diameter of HA rod (μm)	Interspacing between the rods (μm)	HA content on the surface (%)
Pattern 1	10	10	20
Pattern 2	10	6	30
Pattern 3	20	12	30
Pattern 4	50	30	30

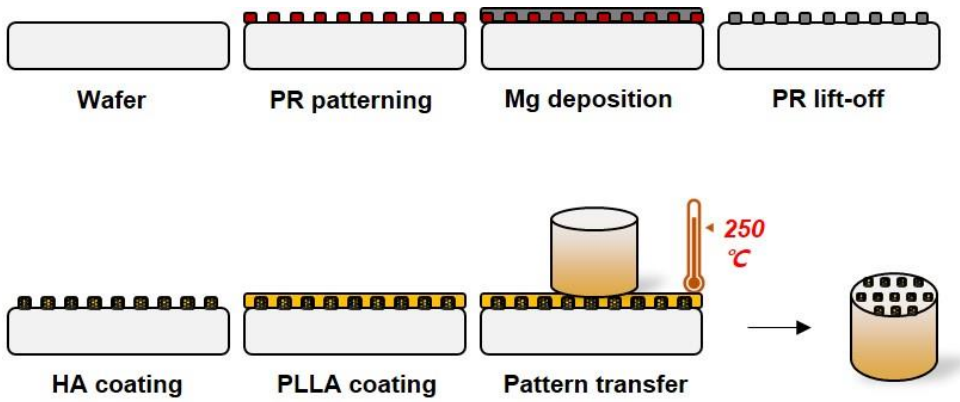

Figure 5.1. Schematic diagram of HA patterning procedure.

Microstructure and chemical composition

The surface morphologies of the pure, HA powder mixed, and HA patterned PLLA specimens were observed by scanning electron microscopy (SEM, JSM-5600; JEOL, Japan). The chemical composition of the HA patterned layer was characterized by energy-dispersive spectrometer (EDS) attached to the SEM.

Testing of mechanical properties

To evaluate the mechanical properties of pure, HA powder mixed, and HA patterned PLLA, tensile strength tests were conducted in accordance with ASTM 638. Specimens with a thickness of 1.5 mm and a gauge length of 8 mm were elongated uniaxially at a constant cross-head speed of 1 mm/min. The stress and strain responses of the specimens were monitored throughout the tensile strength tests. Five specimens were tested to obtain sufficient statistics of the measurements.

Testing of wettability

Contact angle tests were performed to investigate the wettability and hydrophobicity of the prepared samples. Static water contact angles were measured using a sessile drop method by a goniometer (PHX300, S.E.O, Suwon, Korea) at ambient temperature. The water droplet of 15 μL volume was used in the measurements. More than five measurements on different locations were conducted

for each sample.

In vitro biocompatibility tests

For the *in vitro* cell tests, the samples (pure, HA powder mixed and HA patterned PLLA) were sterilized under ultraviolet irradiation on a clean bench. A pre-osteoblast cell line, MC3T3-E1 (ATCC, CRL-2593), was used to assess the cell response to the specimen surfaces. The pre-incubated cells were seeded on specimens at densities of 5.0×10^3 cells/cm^2 and 2.5×10^3 cells/cm^2 to evaluate the cell attachment and proliferation respectively. Alpha-minimum essential medium (α-MEM, Welgene Co., Ltd., Korea) with the addition of 5% fetal bovine serum (FBS) and 1% penicillin-streptomycin was used as the cell culture medium and the cells were cultured in a humidified incubator in air atmosphere containing 5% CO_2 at 37 ^oC.

Cell morphology observation

After culturing for 24 hours, the attached cells were observed by scanning electron microscopy (SEM, JSM-5600, JEOL, Japan). Prior to the SEM observations, the samples were fixed with 2.5% glutaraldehyde for 10 min, dehydrated in graded ethanol (70, 95 and 100% ethanol in sequence), immersed in hexamethyldisilazane for 10min and dried in air.

Cell viability and proliferation

Cell proliferation was determined after 3 and 5 days of culturing using a Cyquant cell proliferation assay kit (C7026 Invitrogen). Before measurements, the cells that adhered to the samples were detached and suspended in a fluorescent dye solution. The DNA level of the detached cells was measured using a multiple Plate reader (Victor3, PerkinElmer, USA) at 480/535 nm wavelength. The measured florescence values were converted to the DNA content using a DNA standard curve. In this assay kit, the DNA level was directly proportional to the number of living cells.

Statistical analysis

All experiments were performed more than three times, and the experimental results were expressed as the mean value ± standard deviation (SD). The difference between the three groups (bare, HA powder mixed and HA patterned PLLA) was determined using a one-way analysis of variance (ANOVA) and $p < 0.05$ was considered a statistically significant difference.

5.3. Result

5.3.1. Comparing HA powder mixed PLLA with HA patterned PLLA

5.3.1.1. Microstructure of HA patterned PLLA

Figure 5.2 presents the surface morphology of pure, HA powder mixed and HA patterned PLLA. HA micro-dots with a diameter of ~ 10 μm were uniformly fabricated with the interspacing distance of ~ 10 μm on the PLLA surface and were well embedded in the PLLA matrix as shown in Figure 5.2. (C). HA powder was also well dispersed in the PLLA with the variation of the particle size from 1 to more than 50 μm, implying that the agglomeration of HA powders was unavoidable as illustrated in Figure 5.2. (B). There was no noticeable large defects, such as voids or cracks, in all conditions, suggesting that compression molding at 190 ℃ was well performed to produce the samples.

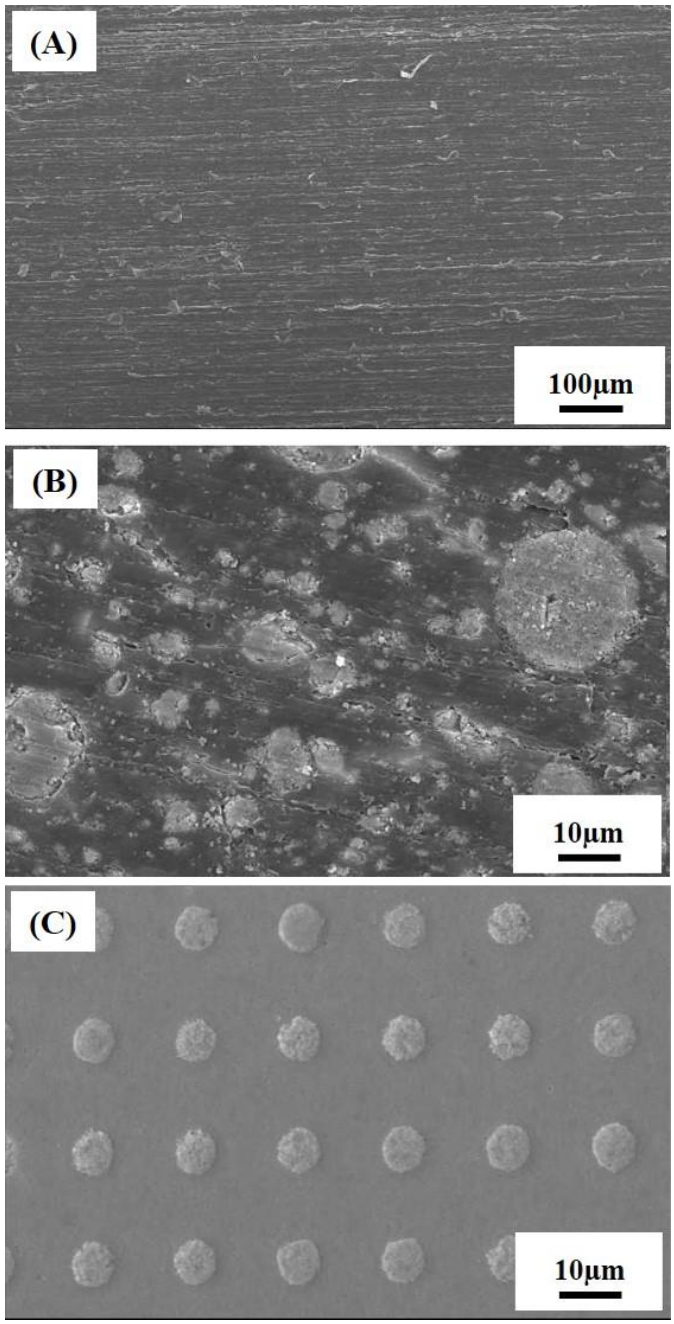

Figure 5.2. SEM images of (A) pure PLLA, (B) HA powder mixed PLLA, and (C) HA patterned PLLA.

5.3.1.2. Mechanical properties

For evaluating HA patterning effect on mechanical characteristics, their mechanical properties were examined by tensile strength tests. Figure 5.3 and Figure 5.4 present stiffness and tensile strength of the pure, HA powder mixed and HA patterned PLLA specimens, respectively. Since the ceramic HA powder was mixed to PLLA matrix, the stiffness of the composite increased significantly and tensile strength decreased because of the low affinity between HA powder and PLLA matrix as discussed before: from 3.65 GPa to 5.31 GPa in stiffness and from 53.4 MPa to 30.48 MPa in tensile strength. In the case of HA patterned PLLA, however, slight decrease of both stiffness and tensile strength was observed. Theoretically, since HA pattern only exists on the surface, it cannot alter the mechanical properties of pure PLLA. However, when we transfer the HA pattern from the wafer to PLLA, samples were exposed to the heat for melting the interface between them, causing polymer denaturation and consequent strength weakening. It should be noted that these values compare favorably to the tensile strength (~50 MPa) and stiffness (3-20 GPa) of natural cortical bone in transverse loading.

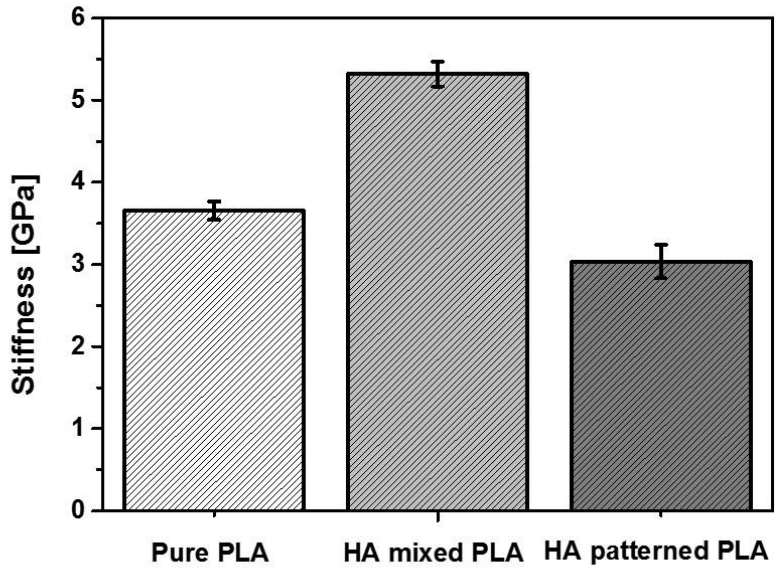

Figure 5.3. Stiffness of pure PLLA, HA powder mixed PLLA and HA patterned PLLA.

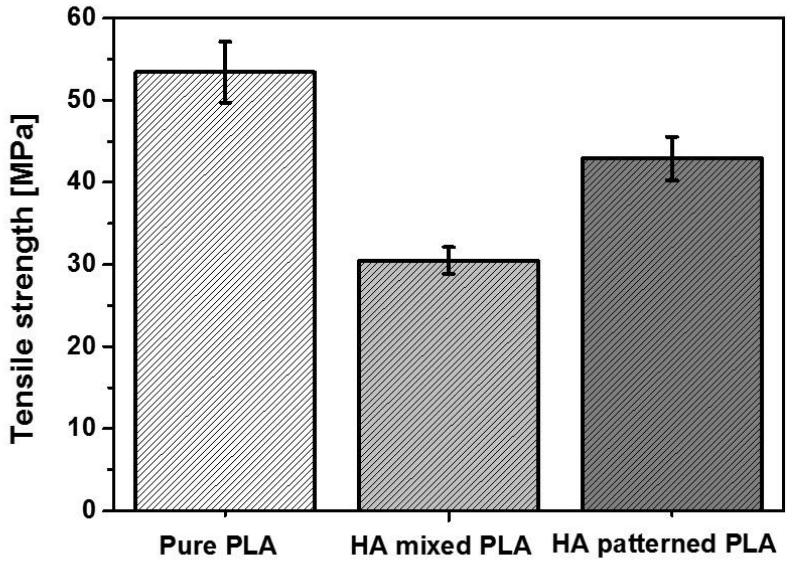

Figure 5.4. Tensile strength of pure PLLA, HA powder mixed PLLA and HA patterned PLLA.

5.3.1.3. Wettability

Contact angle test was performed to evaluate hydrophilicity of the prepared samples. Since the surface of all conditions were flat due to the pattern transfer method using high temperature, it can be assumed that only chemical composition of the surface can affect hydrophilicity of the specimens. As reported in many literatures, pure PLLA showed hydrophobic property, displaying about 80˚ in contact angle with static water. In the case of HA powder mixed PLLA, slightly lower level of wetting angle was observed compared to pure PLLA, around 74˚ even though hydrophilic HA powder was dispersed over the surface. On the other hand, dramatic decrease in contact angle was detected on HA patterned surface, exhibiting the value of around 20˚. Periodically arranged HA dots made a significant influence on wettability of PLLA matrix.

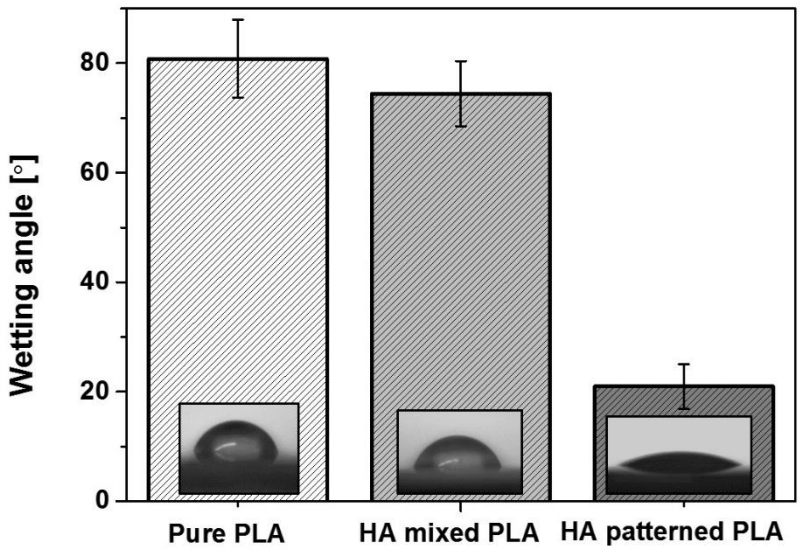

Figure 5.5. Wetting angle of pure PLLA, HA powder mixed PLLA, and HA patterned PLLA.

5.3.1.4. *In vitro* cell responses

The *in vitro* biocompatibility of the pure, HA powder mixed and HA patterned PLLA was examined using *in vitro* cell tests. Figure 5.6 shows the representative SEM images of the specimens after 1 day of MC3T3-E1 cell culturing. Generally, none of the samples showed any signs of cytotoxicity. However, for pure PLLA, cells with a relatively round shape that poorly adhered to and spread onto its surface were observed [Figure 5.6. (A)]. By contrast, cells showed filopodia extensions and flattened morphology on the surfaces of the HA powder mixed and HA patterned PLLA [Figure 5.6. (B and C)]. The degree of cell proliferation on the pure, HA powder mixed and HA patterned PLLA after 3 and 5 days of cell culturing was examined using a DNA assay, as shown in Figure 5.7. The HA involved specimens showed significantly larger absorbance values ($p < 0.05$) than that of the pure PLLA after 5 days of culturing. These findings suggest that the samples containing HA can significantly facilitate the attachment and proliferation of MC3T3-E1 cells *in vitro*, which would be expected to provide enhanced osseointegration ability *in vivo*.

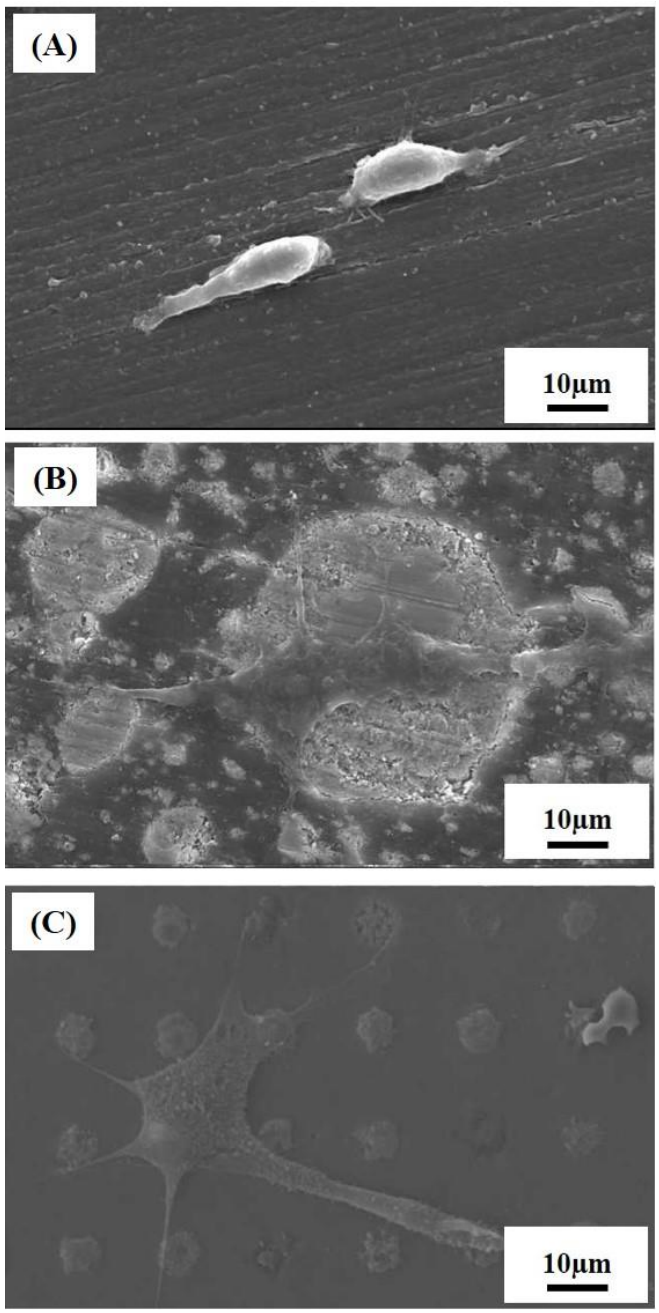

Figure 5.6. SEM images of the MC3T3-E1 cells on (A) pure PLLA, (B) HA powder mixed PLLA, and (C) HA patterned PLLA.

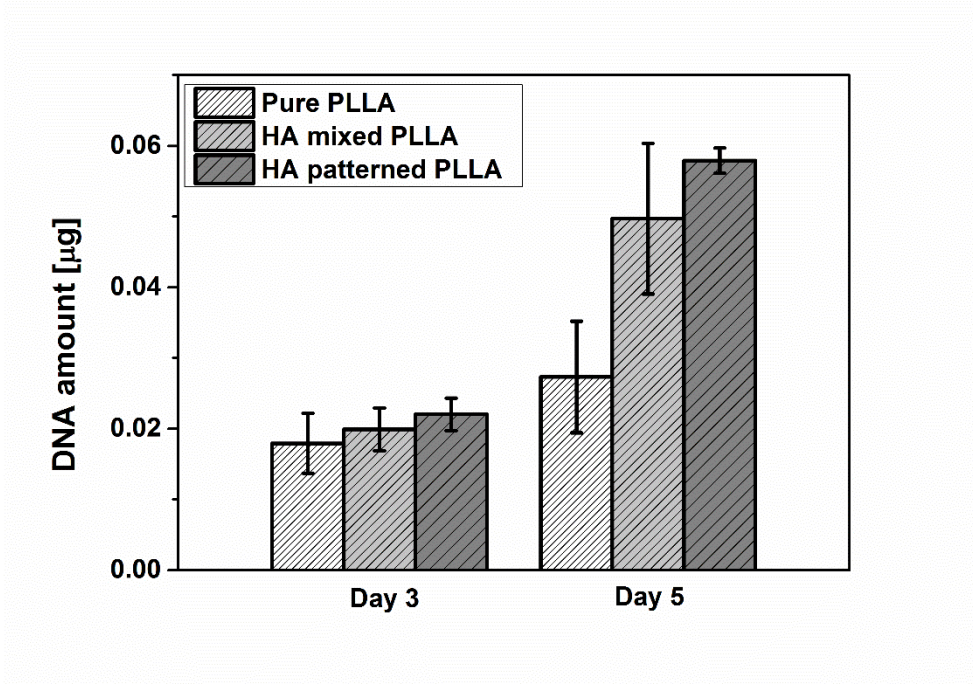

Figure 5.7. DNA levels of the MC3T3-E1 cells that were cultured for 3 and 5 days on pure PLLA, HA powder mixed PLLA, and HA patterned PLLA.

5.3.2. Various HA patterns on PLLA

5.3.2.1. Microstructure of various HA patterns

Figure 5.8 presents the surface morphology of various HA patterns on PLLA. HA micro-dots with a diameter of 10 to 50 μm were uniformly fabricated with the interspacing distance of 6 to 30 μm on the PLLA surface and were well embedded in the PLLA matrix as shown in Figure 5.8. Total surface coverage of HA was 20% for pattern 1 and 30 % for the rest of the conditions. Patterns possessed a clear round shape of HA arrays which came from the design of photomask. There was no noticeable large defects, such as voids or cracks, in all conditions, implying that pattern transfer procedure was well performed.

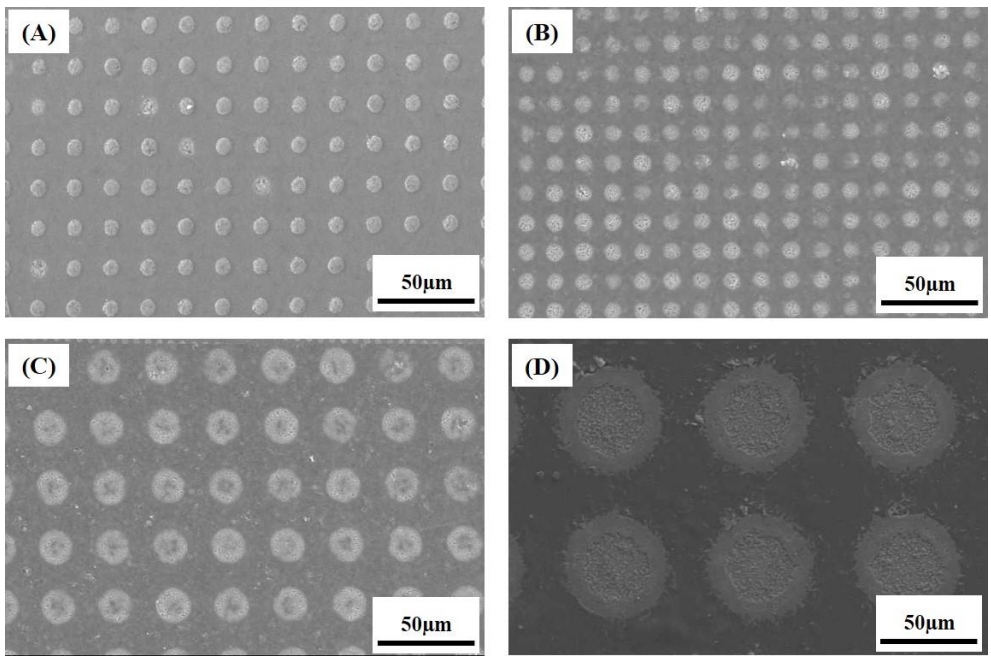

Figure 5.8. SEM images of (A) pattern 1, (B) pattern 2, (C) pattern 3, and (D) pattern 4.

5.3.2.2. Wettability

Contact angle test was performed to evaluate hydrophilicity of the prepared samples. Since the surface of all conditions was flat due to the pattern transfer method using high temperature, it can be assumed that only the geometry of HA patterns can affect hydrophilicity of the specimens. As mentioned in the previous result of the wetting angle (as shown in Figure 5.5, pattern 1 was used for comparison in that section), HA patterning dramatically increased its wettability (21.0˚) compared to pure HA (80.8˚) or HA powder mixed PLLA (74.4˚). Similar results were also observed for pattern 2 and 3, exhibiting the contact angle of 24.1˚ and 22.3˚, respectively. Enlarged size of HA dots from 10 to 20 μm, or increased content of HA on the surface from 20 to 30 % didn't noticeably affect the wettability of the samples. However, in the case of pattern 4, having 30 % of HA coverage with the size of 50 μm HA rods, wetting angle was sharply increased up to 70.0˚, regarded as having hydrophobic surface.

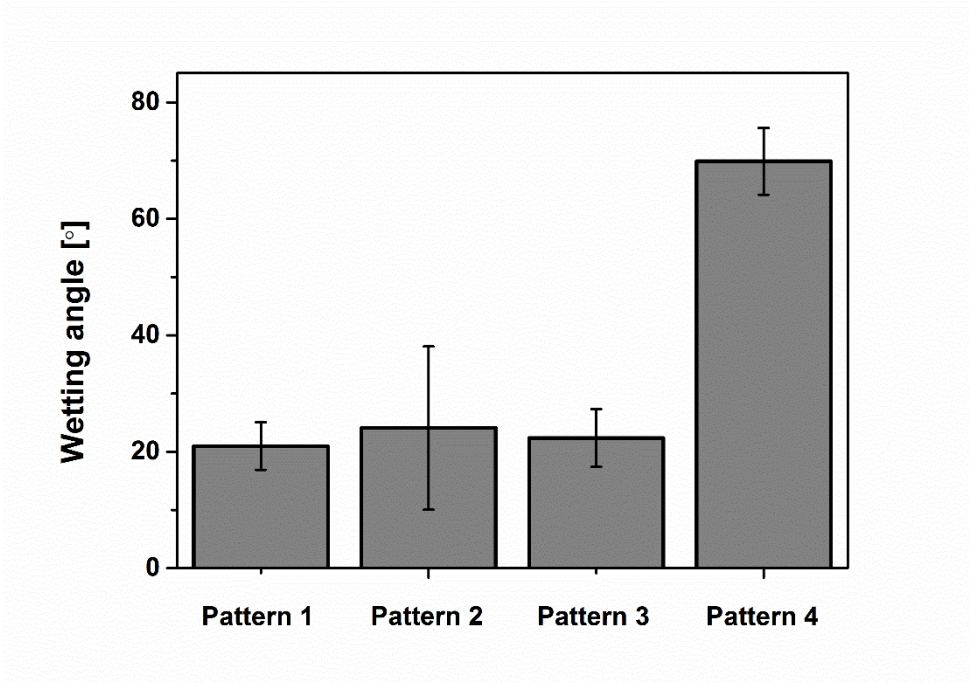

Figure 5.9. Wetting angle of pattern 1, pattern 2, pattern 3, and pattern 4.

5.3.2.3. *In vitro* cell response

The *in vitro* biocompatibility of the various HA patterns on PLLA was examined using *in vitro* cell tests. Figure 5.10 shows the representative SEM images of the specimens after 1 day of MC3T3-E1 cell culturing. Generally, none of the samples showed any signs of cytotoxicity, showing favorably stretched cells with active cytoskeletal extension. It implies that HA patterning on relatively bio-inert PLLA significantly improved cell affinity. However, in the case of pattern 4, which had a poor hydrophilicity as proved in the wettability test, it was observed that the cells preferentially adhered to and spread on the HA pattern part, suggesting that HA pattern part may provide more biocompatible surface for the initial cell attachment. The degree of cell proliferation on various HA patterns after 3 and 5 days of cell culturing was examined using a DNA assay, as shown in Figure 5.11. Cells from all conditions favorably proliferated with more than twice increment in DNA level from day 3 to 5. In particular, pattern 1, having 20 % of HA content with the dot size of 10 μm, showed the best performance in proliferation at day 5 (0.057 μg) while pattern 4 displayed the lowest level of DNA amount over the whole testing period (0.009 μg at day 3 and 0.037 μg on day 5). These findings suggest that HA patterns can effectively modulate the attachment and proliferation of MC3T3-E1 cells *in vitro* depending on the pattern geometry.

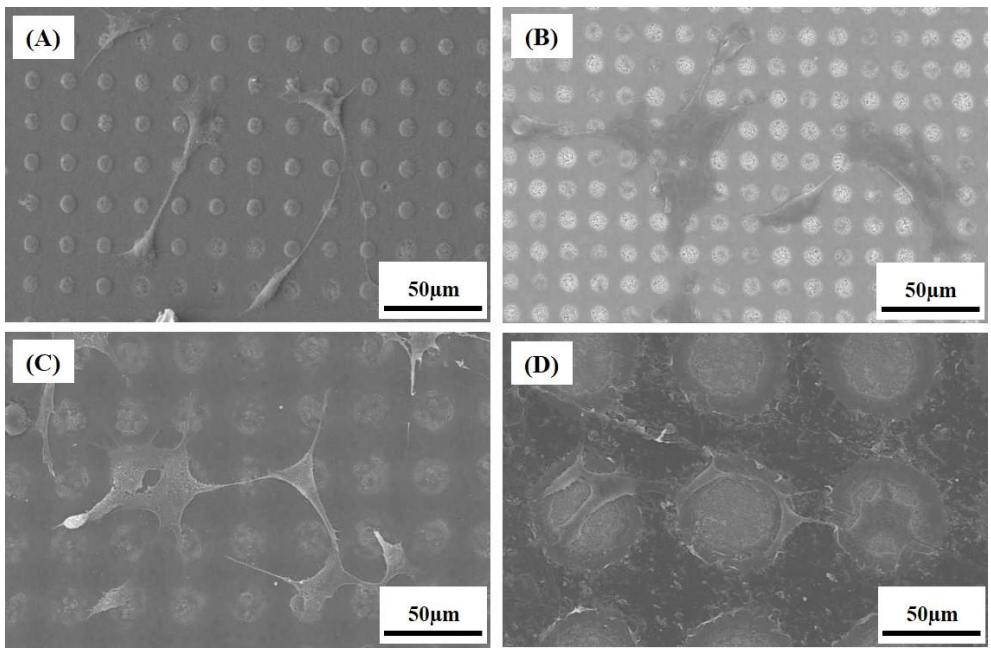

Figure 5.10. SEM images of the MC3T3-E1 cells on (A) pattern 1, (B) pattern 2, (C) pattern 3, and (D) pattern 4.

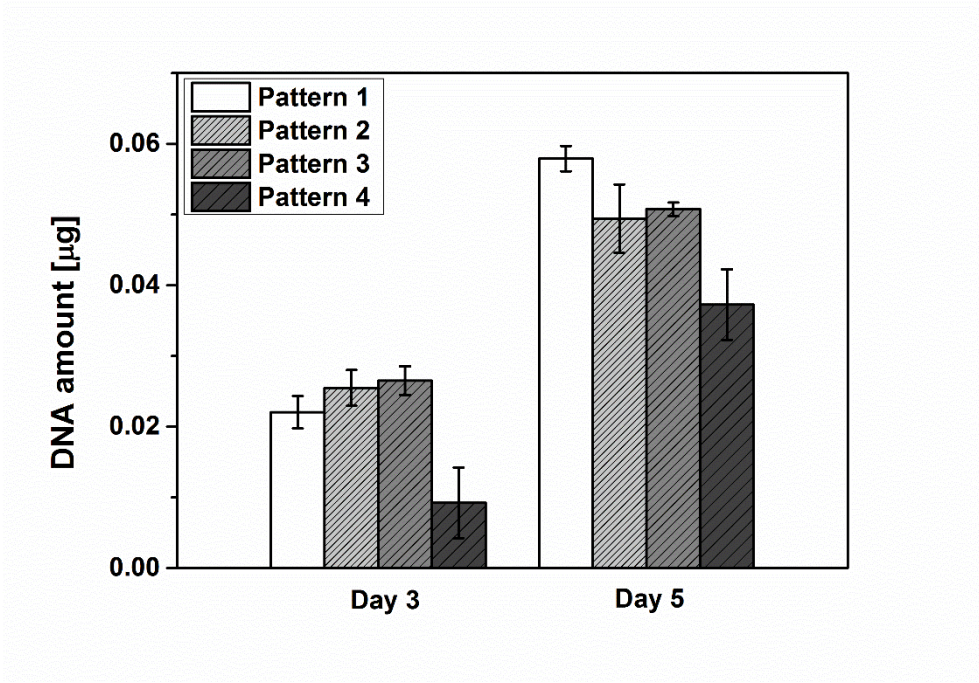

Figure 5.11. DNA levels of the MC3T3-E1 cells that were cultured for 3 and 5 days on (A) pattern 1, (B) pattern 2, (C) pattern 3, and (D) pattern 4.

5.4. Discussion

In this work, we have investigated the effect of the HA patterns on the mechanical properties and biocompatibility of PLLA. As a first treatment, photoresist patterning enabled to selectively form Mg pattern, and the consequent HA pattern on wafer, with the size of 10 to 50 μm in diameter and 16 to 80 μm between the centers of the HA dots. During the solution treatment to fabricate HA pattern, existing Mg dots were all consumed, providing basic environment around the substrate, in particular where Mg patterns were. In consequence, converted HA patterns were barely attached to wafer due to the absence of Mg, causing lack of adhesion strength to the substrate. Therefore, the pattern could be easily transferred to PLLA rod as shown in Figure 5.2. (C) and Figure 5.8. By coating of PLLA on HA patterned wafer prior to the transfer procedure, HA dots were well embedded in PLLA layer without any noticeably voids or cracks. During the transfer procedure, heating the samples could not be avoided to melt the interface and perfectly connect them. From the literatures, heating of PLLA causes the molecular weight reduction, proportional to mechanical strength. Even though PLLA was exposed to heat only for 10 to 20 sec, mechanical strength of the HA patterned PLLA was slightly decreased, from 3.65 GPa to 3.04 GPa and from 53.4 MPa to 43.0 MPa in stiffness and tensile strength, respectively. However, it should be noted that the changes in mechanical properties of HA patterned PLLA were considered not critical since those values are still matched to the tensile strength (~50 MPa) and stiffness (3-20 GPa)

of natural cortical bone in transverse loading. Meanwhile, in the case of HA powder mixed PLLA, the mechanical properties were seriously deteriorated, showing the results of increased stiffness (5.31 GPa) while decreased tensile strength (30.48 MPa). It is typically reported disadvantage of ceramic-polymer composite system when their affinity to each other were not matched well.

Wettability of the samples was analyzed since many literatures reported that hydrophilicity is a basis for rapidly measuring relative biocompatibility in terms of water affinity. Samples were polished to eliminate possible interference of roughness difference among specimens, rather only focus on the difference in surface distribution of HA particles. Wetting angles of HA powder mixed PLLA and HA patterned PLLA were contrastingly different, 74.4˚ for HA powder mixed PLLA and 22.3˚ for HA patterned PLLA. What makes the result interesting is that the exposed area of HA in both conditions was fixed to 20%, implying the periodic arrangement of HA particles made a significant influence on increased hydrophilicity of the specimens. Also, this result can be linked to the wetting angle difference of various patterns. Even though pattern 2, 3, and 4 had a same HA content (30 %) on the PLLA surface, the wetting angle of pattern 4 was considerably higher than other conditions. With the size point of view, the radius of the water droplet used for wettability test was approximately 700 μm while contacting area is much smaller than that value. It implies that HA arrays with a size of 10 to 20 μm and a spacing of 6 to 12 μm could be considered as a continuous HA layer, having favorable water affinity. However,

if the size of HA particles exceeds more than 50 μm (the pattern 4) or varies from 1 to more than 50 μm (the HA powder mixed PLLA), water may preferentially contact to the hydrophilic area on the substrate, resulting in increased wettability as shown in Figure 5.5 and 5.9.

Cell affinity difference between the HA patterns might be explained in the same way. Typical MC3T3-E1 cells are tens of micron in their lateral dimensions, much smaller than the size of the water droplet, suggesting that cells might react to the surface composition more sensitively. With the point of view, the HA pattern 4, 50 μm in size and 30 μm in spacing, was easily distinguished from the less bioactive PLLA matrix, leading to preferential attachment of cells on the HA pattern part. Consequently, the limited HA coverage on the PLLA matrix (30 %) might retard the proliferation of the adhered cells in the case of the pattern 4. These findings suggest that fabricating HA patterns on the surface of PLLA can effectively modulate cell affinity, including cell attachment and proliferation, depending on the geometry of the patterns, while favorable mechanical properties of PLLA can be maintained.

5.5. Conclusions

HA micro-patterned PLLA was successfully developed through the photo-lithography technique in conjunction with Mg deposition and the selective HA formation process on patterned wafer, varying the rod size and interspacing distances of HA micro pillars. The patterning was only applied on the surface, therefore, it enabled to modify surface-dependent properties, such as wettability and biocompatibility, while matrix-dependent property, such as mechanical strength and stiffness, can be maintained. Indeed, the patterned surface with HA exhibited low wetting angle and good cellular responses as compared to pure PLLA, implying cell affinity could be effectively modulated by HA patterning. Also, the mechanical properties of HA patterned PLLA, including tensile strength and stiffness, were retained, still matched to those of natural cortical bone, while HA powder mixed PLLA showed a significant deterioration in mechanical properties, distinctively increased stiffness and decreased tensile strength. Additionally, the possibility of controlling the cell affinity by changing the geometry of HA patterns was confirmed through the wettability and cellular responses test. The specimens having smaller HA size with smaller interspacing possessed better hydrophilicity and improved cell attachment and proliferation. These findings indicate that the HA patterns could significantly modulate *in vitro* biocompatibility of PLLA polymer, not disturbing polymer's intrinsic mechanical properties. With the help of this favorable combination of the properties, the HA patterned PLLA can potentially be used for

biodegradable implants.

Chapter 6.

Conclusions

6.1. Conclusions

The work presented in this thesis was aimed at developing a Mg-based implant that fulfills the two main requirements necessary to the development of such biodegradable devices, namely a low corrosion rate and a good biocompatibility.

Firstly, by introducing HA coating on pure Mg, its mitigated degradation rate and enhanced biocompatibility *in vitro* and *in vivo* were reviewed in chapter 3. Compared to the conventional methods of coating HA, such as aerosol deposition or spraying, the procedure, solution treatment containing calcium and phosphate sources, can be applied for Mg parts of any shape and form, even for complex, three-dimensional (3D) shapes, owing to the ionic conductivity of the aqueous solution. Indeed, screws of complex shape were successfully coated and used in the *in vivo* animal tests. Also, high adhesion strength between HA and Mg was achieved because the precipitates directly used the hydroxide ions, coming from the Mg degradation, to form HA beads. Besides, it provided a protective barrier between the substrate and the corrosive medium to inhibit the corrosion of the Mg. Therefore, the undesirable excessive formation of by-products from Mg corrosion (e.g., hydrogen gas or hydroxide ions) in the SBF solution was mitigated. Furthermore, the *in vitro* cell test showed that the HA coating was responsible for the significant improvement of biological activity, including attachment, proliferation and differentiation of the cells. The *in vivo* results also supported the good biocorrosion protection, biocompatibility and bone response of the HA coating in the initial stage of the

healing period expected from the outcomes of the *in vitro* assays.

Even though the corrosion resistance and biocompatibility of Mg was significantly improved through the HA coating as mentioned in chapter 3, a limited feasibility was noticed for the real clinical field due to a possible crack propagation from the HA layer when the implant undergoes deformation. Therefore chapter 4 aimed to develop a coating, allowing deformation of underneath Mg substrates without any surface cracks, maintaining the coating stability in the physiological environments. The micro-patterned HA/PLLA was successfully canceled the drawbacks associated with these two materials, namely a brittle behavior of HA and a low bonding strength of PLLA to the metal substrate. Indeed, HA/PLLA patterning provided a protective barrier between the substrate and the corrosive medium to inhibit the corrosion of the Mg under 5% of tensile deformation. Additionally, the HA micro-pillars of the hybrid coating likely promote cell affinity as a center of cell attachment. *In vitro* cell tests showed that HA/PLLA patterning sustained a good biocompatibility when Mg was subjected to deformation.

The rest of the study focused on the application of the HA pattern produced in chapter 4. Among the several candidates, PLLA was selected for HA patterning to modulate its cellular responses effectively. HA micro-patterned PLLA was successfully developed through the photo-lithography technique in conjunction with Mg deposition and the selective HA formation process on patterned wafer, varying the rod size and interspacing distances of HA micro pillars. The patterned surface

with HA exhibited low wetting angle and good cellular responses as compared to pure PLLA, and cellular responses varied depending on the geometry of HA patterns, implying cell affinity could be effectively modulated by HA patterning. Also, the mechanical properties of HA patterned PLLA, including tensile strength and stiffness, were retained, still matched to those of natural cortical bone, while HA powder mixed PLLA showed a significant deterioration.

This study suggests that the degradation and cellular responses of Mg can be effectively modified through HA coating and HA/PLLA patterning. Depending on the specific applications of the implant, different strategies could be employed, HA continuous coating for a strong corrosion protection and bioactivity, HA/PLLA patterning for increased coating stability under deformation, and HA patterning for modulating the bioactivity of PLLA. Therefore, the study highlighted a promising avenue for introducing Mg to a new generation of biodegradable implant.

6.2. Future work

In the thesis, patterning technique has been introduced to improve coating stability under deformation as well as corrosion resistance and biocompatibility of Mg. However, some open questions still remains and further investigations are needed. Here, we are suggesting the possible future directions of research and investigations.

In chapter 4, patterning composed of HA and PLLA considerably improves the coating stability under 5% tensile deformation. Unlike HA or PLLA single phase coating, HA/PLLA patterning having enhanced integrity under the strain effectively mitigated the surface corrosion of Mg, providing favorable environment for cells to live. We succeeded to prove a positive influence of the patterning on coating stability under deformation, however, its own effect on biological response is still unclear. Many studies have proved that ordered surface pattern, compared to flat or unordered rough surface, can directly have an influence on cell adhesion, spreading, migration, cytoskeleton organization, proliferation, etc. [107-114] Therefore its ability to modulate cell behavior would be an interesting research area and needed to be investigated. With the technique developed through the thesis, various design of patterns can be easily obtained to demonstrate the biological effects of different pattern geometry. As shown in Figure 6.1, several models, including straight and curved lines and letters of '#' and 'working', were simply fabricated, implying that pattern geometry could be easily modulated for specific purposes.

Regarding the work presented in chapter 5, HA patterns well fabricated on Si wafer, then transferred to the PLLA rod with the short-time heat treatment. During the procedure, we could see the possibility of making free-standing HA/PLLA film from the wafer. Once the thickness of the HA/PLLA layer reaches to some level, approximately tens of micrometer, the film can be peeled off from the wafer without tearing as shown in Figure 6.2. (A). Interestingly, the free-standing HA/PLLA film could be applied not only on the flat substrate, but on 3D curved surface. Figure 6.2. (B) shows the preliminary trial of HA/PLLA film on the Mg screw. So far, photolithography technique has been known to be only applicable to 2D flat surface, however, the film we developed clearly brightened its feasibility on 3D field.

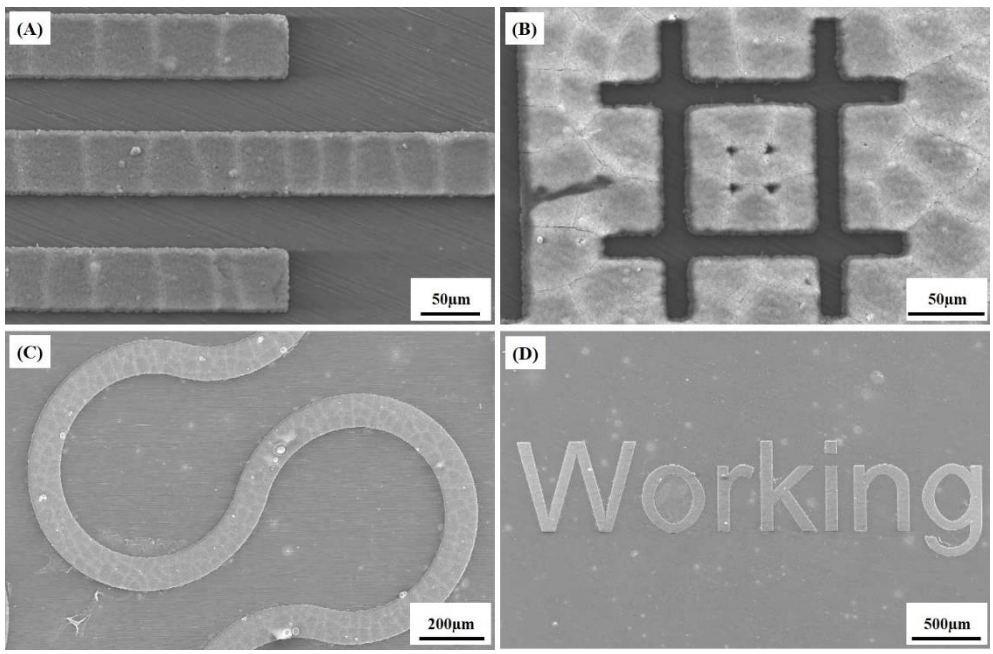

Figure 6.1. SEM images of different shapes of HA patterns.

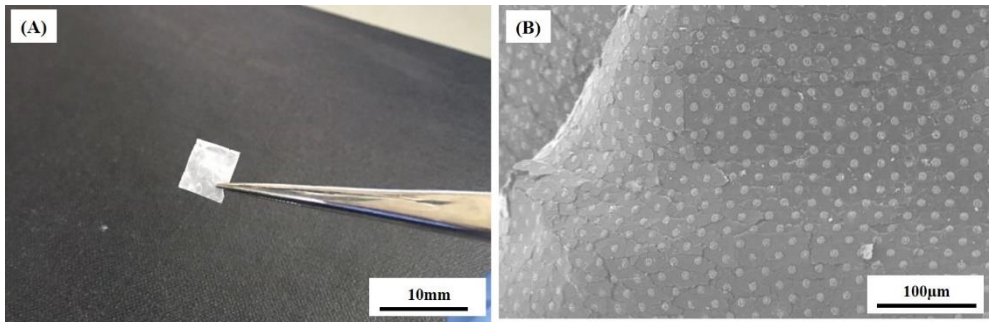

Figure 6.2. Optical mage of (A) HA/PLLA film and SEM image of (B) HA/PLLA patterns on curved surface.

References

1 Gu, X. N., Li, S. S., Li, X. M. & Fan, Y. B. Magnesium based degradable biomaterials: A review. *Front Mater Sci* **8**, 200-218 (2014).

2 Witte, F. The history of biodegradable magnesium implants: A review. *Acta Biomater* **6**, 1680-1692 (2010).

3 Witte, F. *et al.* In vitro and in vivo corrosion measurements of magnesium alloys. *Biomaterials* **27**, 1013-1018 (2006).

4 Witte, F. *et al.* In vivo corrosion of four magnesium alloys and the associated bone response. *Biomaterials* **26**, 3557-3563 (2005).

5 Nair, L. S. & Laurencin, C. T. Biodegradable polymers as biomaterials. *Prog Polym Sci* **32**, 762-798 (2007).

6 Zreiqat, H. *et al.* Mechanisms of magnesium-stimulated adhesion of osteoblastic cells to commonly used orthopaedic implants. *J Biomed Mater Res* **62**, 175-184 (2002).

7 Barbara A Bowman, R. M. R. Present Knowledge in Nutrition. 9th. *International Life Sciences Institute* **1**, 1-526 (2006).

8 Staiger, M. P., Pietak, A. M., Huadmai, J. & Dias, G. Magnesium and its alloys as orthopedic biomaterials: A review. *Biomaterials* **27**, 1728-1734 (2006).

9 Remennik, S., Bartsch, I., Willbold, E., Witte, F. & Shechtman, D. New, fast corroding high ductility Mg-Bi-Ca and Mg-Bi-Si alloys, with no clinically observable gas formation in bone implants. *Mater Sci Eng B-Adv* **176**, 1653-1659 (2011).

10 Erdmann, N. *et al.* Biomechanical testing and degradation analysis of MgCa0.8 alloy screws: A comparative in vivo study in rabbits. *Acta Biomater* **7**, 1421-1428 (2011).

11 Gu, X. N., Xie, X. H., Li, N., Zheng, Y. F. & Qin, L. In vitro and in vivo studies on a Mg-Sr binary alloy system developed as a new kind of biodegradable metal. *Acta Biomater* **8**, 2360-2374 (2012).

12 Tan, L. L. *et al.* Loss of mechanical properties in vivo and bone-implant interface strength of AZ31B magnesium alloy screws with Si-containing

coating. *Acta Biomater* **10**, 2333-2340 (2014).

13 Patrik Schmutz, N.-C. Q.-V., Isabel Gerber. Metallic Medical Implants: Electrochemical Characterization of Corrosion Processes. *The Electrochemical Society Interface* **Summer**, 35-40 (2008).

14 Dalury, D. F., Gonzales, R. A. & Adams, M. J. Minimum 5-Year Results in 96 Consecutive Hips Treated With a Tapered Titanium Stem System. *J Arthroplasty* **25**, 104-107 (2010).

15 Leventhal, G. S. Titanium, a Metal for Surgery. *J Bone Joint Surg Am* **33-A**, 473-474 (1951).

16 Marx, R. *et al.* Silicate Coating of Cemented Titanium-Based Shafts in Hip Prosthetics Reduces High Aseptic Loosening. *Z Orthop Unfallchir* **147**, 175-182 (2009).

17 Bordji, K. *et al.* Evaluation of the effect of three surface treatments on the biocompatibility of 316L stainless steel using human differentiated cells. *Biomaterials* **17**, 491-500 (1996).

18 Long, M. & Rack, H. J. Titanium alloys in total joint replacement - a materials science perspective. *Biomaterials* **19**, 1621-1639 (1998).

19 Reclaru, L., Lerf, R., Eschler, P. Y., Blatter, A. & Meyer, J. M. Pitting, crevice and galvanic corrosion of REX stainless-steel/CoCr orthopedic implant material. *Biomaterials* **23**, 3479-3485 (2002).

20 Ferrari, F. *et al.* Metal-Ion Release from Titanium and Tin-Coated Implants in Rat Bone. *Nucl Instrum Meth B* **79**, 421-423 (1993).

21 Ryan, G., Pandit, A. & Apatsidis, D. P. Fabrication methods of porous metals for use in orthopaedic applications. *Biomaterials* **27**, 2651-2670 (2006).

22 Chan, A. W. & Moliterno, D. J. In-stent restenosis: Update on intracoronary radiotherapy. *Clev Clin J Med* **68**, 796-803 (2001).

23 Nagels, J., Stokdijk, M. & Rozing, P. M. Stress shielding and bone resorption in shoulder arthroplasty. *J Shoulder Elb Surg* **12**, 35-39 (2003).

24 Levesque, J., Hermawan, H., Dube, D. & Mantovani, D. Design of a pseudo-physiological test bench specific to the development of biodegradable metallic biomaterials. *Acta Biomater* **4**, 284-295 (2008).

25 Hanawa, T. Metal ion release from metal implants. *Mat Sci Eng C-Bio S* **24**, 745-752 (2004).

26 Mani, G., Feldman, M. D., Patel, D. & Agrawal, C. M. Coronary stents: A materials perspective. *Biomaterials* **28**, 1689-1710 (2007).

27 vanderGiessen, W. J. *et al.* Marked inflammatory sequelae to implantation of biodegradable and nonbiodegradable polymers in porcine coronary arteries. *Circulation* **94**, 1690-1697 (1996).

28 Tamai, H. *et al.* Initial and 6-month results of biodegradable poly-l-lactic acid coronary stents in humans. *Circulation* **102**, 399-404 (2000).

29 Song, G. L. & Atrens, A. Understanding magnesium corrosion - A framework for improved alloy performance. *Adv Eng Mater* **5**, 837-858 (2003).

30 Kirkland, N. T. Magnesium biomaterials: past, present and future. *Corros Eng Sci Techn* **47**, 322-328 (2012).

31 A. Hruby, N. M. M. chapter 36 Magnesium and Metaboliv Syndrome: The Rold of Magnesium in Health and Disease. *Elsevier* (2012).

32 Dorozhkin, S. V. Calcium orthophosphate coatings on magnesium and its biodegradable alloys. *Acta Biomater* **10**, 2919-2934 (2014).

33 Kim, S. M. *et al.* Hydroxyapatite-coated magnesium implants with improved in vitro and in vivo biocorrosion, biocompatibility, and bone response. *J Biomed Mater Res A* **102**, 429-441 (2014).

34 Berat Barıs BULDUM, A. S., Iskender OZKUL. INVESTIGATION OF MAGNESIUM ALLOYS MACHINABILITY. *INTERNATIONAL JOURNAL OF ELECTRONICS; MECHANICAL and MECHATRONICS Engineering Applications of Artificial Intelligence* **2**, 261-268.

35 McBride, E. D. Absorbable metal in bone surgery - A further report on the use of magnesium alloys. *J Amer Med Assoc* **111**, 2464-2466 (1938).

36 McCord, C. P. Chemical gas gangrene from metallic magnesium. *Industrial Medicine* **11**, 71-79 (1942).

37 Zhang, E. L., Yin, D. S., Xu, L. P., Yang, L. & Yang, K. Microstructure, mechanical and corrosion properties and biocompatibility of Mg-Zn-Mn

alloys for biomedical application. *Mat Sci Eng C-Bio S* **29**, 987-993 (2009).

38 Kraus, T. *et al.* Magnesium alloys for temporary implants in osteosynthesis: In vivo studies of their degradation and interaction with bone. *Acta Biomater* **8**, 1230-1238 (2012).

39 Yang, J. X. *et al.* Modification of degradation behavior of magnesium alloy by IBAD coating of calcium phosphate. *Surf Coat Tech* **202**, 5733-5736 (2008).

40 Li, Z. J., Gu, X. N., Lou, S. Q. & Zheng, Y. F. The development of binary Mg-Ca alloys for use as biodegradable materials within bone. *Biomaterials* **29**, 1329-1344 (2008).

41 Xu, L. P., Yu, G. N., Zhang, E., Pan, F. & Yang, K. In vivo corrosion behavior of Mg-Mn-Zn alloy for bone implant application. *J Biomed Mater Res A* **83A**, 703-711 (2007).

42 Zheng, Y. F., Gu, X. N. & Witte, F. Biodegradable metals. *Mat Sci Eng R* **77**, 1-34 (2014).

43 A, S. B. Corrosion resistancce of magnesium alloy. In: Cramer DS, Covino B S, eds. *ASM Handbook: Corrosion Fundamentals, Testing and Protection. UK: ASM International* **13A** (2003).

44 Hanzi, A. C., Sologubenko, A. S. & Uggowitzer, P. J. Design strategy for new biodegradable Mg-Y-Zn alloys for medical applications. *Int J Mater Res* **100**, 1127-1136 (2009).

45 Song, G. L. Control of biodegradation of biocompatable magnesium alloys. *Corros Sci* **49**, 1696-1701 (2007).

46 Xin, Y., Hu, T. & Chu, P. K. In vitro studies of biomedical magnesium alloys in a simulated physiological environment: A review. *Acta Biomater* **7**, 1452-1459 (2011).

47 Zeng, R. C., Dietzel, W., Witte, F., Hort, N. & Blawert, C. Progress and challenge for magnesium alloys as biomaterials. *Adv Eng Mater* **10**, B3-B14 (2008).

48 Liu, C. L. *et al.* In vitro corrosion degradation behaviour of Mg-Ca alloy in the presence of albumin. *Corros Sci* **52**, 3341-3347 (2010).

49 Bornapour, M., Muja, N., Shum-Tim, P., Cerruti, M. & Pekguleryuz, M. Biocompatibility and biodegradability of Mg-Sr alloys: The formation of Sr-substituted hydroxyapatite. *Acta Biomater* **9**, 5319-5330 (2013).

50 Orlov, D., Ralston, K. D., Birbilis, N. & Estrin, Y. Enhanced corrosion resistance of Mg alloy ZK60 after processing by integrated extrusion and equal channel angular pressing. *Acta Mater* **59**, 6176-6186 (2011).

51 Rosalbino, F., De Negri, S., Saccone, A., Angelini, E. & Delfino, S. Bio-corrosion characterization of Mg-Zn-X (X = Ca, Mn, Si) alloys for biomedical applications. *J Mater Sci-Mater M* **21**, 1091-1098 (2010).

52 Chang, J. W., Fu, P. H., Guo, X. W., Peng, L. M. & Ding, W. J. The effects of heat treatment and zirconium on the corrosion behaviour of Mg-3Nd-0.2Zn-0.4Zr (wt.%) alloy. *Corros Sci* **49**, 2612-2627 (2007).

53 Birbilis, N., Easton, M. A., Sudholz, A. D., Zhu, S. M. & Gibson, M. A. On the corrosion of binary magnesium-rare earth alloys. *Corros Sci* **51**, 683-689 (2009).

54 Zhang, X. B., Yuan, G. Y., Mao, L., Niu, J. L. & Ding, W. J. Biocorrosion properties of as-extruded Mg-Nd-Zn-Zr alloy compared with commercial AZ31 and WE43 alloys. *Mater Lett* **66**, 209-211 (2012).

55 Atrens, A., Liu, M. & Abidin, N. I. Z. Corrosion mechanism applicable to biodegradable magnesium implants. *Mater Sci Eng B-Adv* **176**, 1609-1636 (2011).

56 Witte, F. *et al.* Degradable biomaterials based on magnesium corrosion. *Curr Opin Solid St M* **12**, 63-72 (2008).

57 Zeng, R. C., Sun, L., Zheng, Y. F., Cui, H. Z. & Han, E. H. Corrosion and characterisation of dual phase Mg-Li-Ca alloy in Hank's solution: The influence of microstructural features. *Corros Sci* **79**, 69-82 (2014).

58 Chang, T. C., Wang, J. Y., Chu, C. L. & Lee, S. Mechanical properties and microstructures of various Mg-Li alloys. *Mater Lett* **60**, 3272-3276 (2006).

59 H., S. Metal ions in biological system. *New York: Marcel Dekker Inc.* (1986).

60 Nakamura, Y., Tsumura, Y., Tonogai, Y., Shibata, T. & Ito, Y. Differences in behavior among the chlorides of seven rare earth elements administered

intravenously to rats. *Fund Appl Toxicol* **37**, 106-116 (1997).

61 Hornberger, H., Virtanen, S. & Boccaccini, A. R. Biomedical coatings on magnesium alloys - A review. *Acta Biomater* **8**, 2442-2455 (2012).

62 Shadanbaz, S. & Dias, G. J. Calcium phosphate coatings on magnesium alloys for biomedical applications: A review. *Acta Biomater* **8**, 20-30 (2012).

63 Geng, F., Tan, L. L., Jin, X. X., Yang, J. Y. & Yang, K. The preparation, cytocompatibility, and in vitro biodegradation study of pure beta-TCP on magnesium. *J Mater Sci-Mater M* **20**, 1149-1157 (2009).

64 Gray-Munro, J. E., Seguin, C. & Strong, M. Influence of surface modification on the in vitro corrosion rate of magnesium alloy AZ31. *J Biomed Mater Res A* **91A**, 221-230 (2009).

65 Wen, C. L. *et al.* Characterization and degradation behavior of AZ31 alloy surface modified by bone-like hydroxyapatite for implant applications. *Appl Surf Sci* **255**, 6433-6438 (2009).

66 Xu, L. P. *et al.* In vitro and in vivo evaluation of the surface bioactivity of a calcium phosphate coated magnesium alloy. *Biomaterials* **30**, 1512-1523 (2009).

67 Zhang, Y. J., Zhang, G. Z. & Wei, M. Controlling the Biodegradation Rate of Magnesium Using Biomimetic Apatite Coating. *J Biomed Mater Res B* **89B**, 408-414 (2009).

68 Yang, J. X. *et al.* Characterization and Degradation Study of Calcium Phosphate Coating on Magnesium Alloy Bone Implant In Vitro. *Ieee T Plasma Sci* **37**, 1161-1168 (2009).

69 Srinivasan, P. B., Liang, J., Blawert, C., Stormer, M. & Dietzel, W. Characterization of calcium containing plasma electrolytic oxidation coatings on AM50 magnesium alloy. *Appl Surf Sci* **256**, 4017-4022 (2010).

70 Razavi, M., Fathi, M., Savabi, O., Vashaee, D. & Tayebi, L. In vivo assessments of bioabsorbable AZ91 magnesium implants coated with nanostructured fluoridated hydroxyapatite by MAO/EPD technique for biomedical applications. *Mat Sci Eng C-Mater* **48**, 21-27 (2015).

71 Wang, H. X., Guan, S. K., Wang, X., Ren, C. X. & Wang, L. G. In vitro

degradation and mechanical integrity of Mg-Zn-Ca alloy coated with Ca-deficient hydroxyapatite by the pulse electrodeposition process. *Acta Biomater* **6**, 1743-1748 (2010).

72 Wang, H. X. *et al.* In vivo degradation behavior of Ca-deficient hydroxyapatite coated Mg-Zn-Ca alloy for bone implant application. *Colloid Surface B* **88**, 254-259 (2011).

73 Ratner, B. Polymeric implants. *Elsevier B.V.* **397-411** (2012).

74 Diez, M., Kang, M. H., Kim, S. M., Kim, H. E. & Song, J. Hydroxyapatite (HA)/poly-L-lactic acid (PLLA) dual coating on magnesium alloy under deformation for biomedical applications. *J Mater Sci-Mater M* **27** (2016).

75 Gu, X. N. *et al.* Surface modification of an Mg-1Ca alloy to slow down its biocorrosion by chitosan. *Biomed Mater* **4** (2009).

76 Xu, L. P. & Yamamoto, A. Characteristics and cytocompatibility of biodegradable polymer film on magnesium by spin coating. *Colloid Surface B* **93**, 67-74 (2012).

77 Xu, L. P. & Yamamoto, A. In vitro degradation of biodegradable polymer-coated magnesium under cell culture condition. *Appl Surf Sci* **258**, 6353-6358 (2012).

78 Wong, H. M. *et al.* A biodegradable polymer-based coating to control the performance of magnesium alloy orthopaedic implants. *Biomaterials* **31**, 2084-2096 (2010).

79 Barchiche, C. E., Rocca, E., Juers, C., Hazan, J. & Steinmetz, J. Corrosion resistance of plasma-anodized AZ91D magnesium alloy by electrochemical methods. *Electrochim Acta* **53**, 417-425 (2007).

80 Blawert, C., Dietzel, W., Ghali, E. & Song, G. L. Anodizing treatments for magnesium alloys and their effecton corrosion resistance in various environments. *Adv Eng Mater* **8**, 511-533 (2006).

81 Gray, J. E. & Luan, B. Protective coatings on magnesium and its alloys - a critical review. *J Alloy Compd* **336**, 88-113 (2002).

82 Hsiao, H. Y. & Tsai, W. T. Characterization of anodic films formed on AZ91D magnesium alloy. *Surf Coat Tech* **190**, 299-308 (2005).

83 Li, L. C., Gao, J. C. & Wang, Y. Evaluation of cyto-toxicity and corrosion behavior of alkali-heat-treated magnesium in simulated body fluid. *Surf Coat Tech* **185**, 92-98 (2004).

84 Lorenz, C. *et al.* Effect of surface pre-treatments on biocompatibility of magnesium. *Acta Biomater* **5**, 2783-2789 (2009).

85 Hoog, C. O., Birbilis, N. & Estrin, Y. Corrosion of pure Mg as a function of grain size and processing route. *Adv Eng Mater* **10**, 579-582 (2008).

86 Wang, H., Estrin, Y., Fu, H., Song, G. & Zuberova, Z. The effect of pre-processing and grain structure on the bio-corrosion and fatigue resistance of magnesium alloy AZ31. *Adv Eng Mater* **9**, 967-972 (2007).

87 Song, G. L. & Song, S. Z. A possible biodegradable magnesium implant material. *Adv Eng Mater* **9**, 298-302 (2007).

88 Song, Y. W., Shan, D. Y. & Han, E. H. Electrodeposition of hydroxyapatite coating on AZ91D magnesium alloy for biomaterial application. *Mater Lett* **62**, 3276-3279 (2008).

89 Xu, L. P., Zhang, E. L. & Yang, K. Phosphating treatment and corrosion properties of Mg-Mn-Zn alloy for biomedical application. *J Mater Sci-Mater M* **20**, 859-867 (2009).

90 Wang, Y., Wei, M. & Gao, J. C. Improve corrosion resistance of magnesium in simulated body fluid by dicalcium phosphate dihydrate coating. *Mat Sci Eng C-Bio S* **29**, 1311-1316 (2009).

91 Zhang, E., Xu, L. P. & Yang, K. Formation by ion plating of Ti-coating on pure Mg for biomedical applications. *Scripta Mater* **53**, 523-527 (2005).

92 Bigi, A. *et al.* The response of bone to nanocrystalline hydroxyapatite-coated Ti13Nb11Zr alloy in an animal model. *Biomaterials* **29**, 1730-1736 (2008).

93 Hiromoto, S. *et al.* Precipitation control of calcium phosphate on pure magnesium by anodization. *Corros Sci* **50**, 2906-2913 (2008).

94 Hiromoto, S. & Yamamoto, A. High corrosion resistance of magnesium coated with hydroxyapatite directly synthesized in an aqueous solution. *Electrochim Acta* **54**, 7085-7093 (2009).

95 Lakstein, D. *et al.* Enhanced osseointegration of grit-blasted, NaOH-treated and electrochemically hydroxyapatite-coated Ti-6Al-4V implants in rabbits. *Acta Biomater* **5**, 2258-2269 (2009).

96 Tomozawa, M., Hiromoto, S. & Harada, Y. Microstructure of hydroxyapatite-coated magnesium prepared in aqueous solution. *Surf Coat Tech* **204**, 3243-3247 (2010).

97 Kokubo, T. & Takadama, H. How useful is SBF in predicting in vivo bone bioactivity? *Biomaterials* **27**, 2907-2915 (2006).

98 Hahn, B. D. *et al.* Aerosol deposition of silicon-substituted hydroxyapatite coatings for biomedical applications. *Thin Solid Films* **518**, 2194-2199 (2010).

99 Abou Neel, E. A. *et al.* In vitro bioactivity and gene expression by cells cultured on titanium dioxide doped phosphate-based glasses. *Biomaterials* **28**, 2967-2977 (2007).

100 Kim, H. W., Georgiou, G., Knowles, J. C., Koh, Y. H. & Kim, H. E. Calcium phosphates and glass composite coatings on zirconia for enhanced blocompatibility. *Biomaterials* **25**, 4203-4213 (2004).

101 Yun, Y. *et al.* Biodegradable Mg corrosion and osteoblast cell culture studies. *Mat Sci Eng C-Mater* **29**, 1814-1821 (2009).

102 Zambonin, G. & Grano, M. Biomaterials in Orthopedic-Surgery - Effects of Different Hydroxyapatites and Demineralized Bone-Matrix on Proliferation Rate and Bone-Matrix Synthesis by Human Osteoblasts. *Biomaterials* **16**, 397-402 (1995).

103 Meyer, U., Büchter, A., Wiesmann, H., Joos, U. & Jones, D. Basic reactions of osteoblasts on structured material surfaces. *Eur Cell Mater* **9**, 39-49 (2005).

104 Hanzi, A. C., Gerber, I., Schinhammer, M., Loffler, J. F. & Uggowitzer, P. J. On the in vitro and in vivo degradation performance and biological response of new biodegradable Mg-Y-Zn alloys. *Acta Biomater* **6**, 1824-1833 (2010).

105 Faeda, R. S., Tavares, H. S., Sartori, R., Guastaldi, A. C. & Marcantonio, E.

Biological Performance of Chemical Hydroxyapatite Coating Associated With Implant Surface Modification by Laser Beam: Biomechanical Study in Rabbit Tibias. *J Oral Maxil Surg* **67**, 1706-1715 (2009).

106 Ramires, P. A. *et al.* Biological behavior of sol-gel coated dental implants. *J Mater Sci-Mater M* **14**, 539-545 (2003).

107 Berger, J. *et al.* Ultraviolet laser interference patterning of hydroxyapatite surfaces. *Appl Surf Sci* **257**, 3081-3087 (2011).

108 Li, X., Huang, J. & Edirisinghe, M. J. Novel patterning of nano-bioceramics: template-assisted electrohydrodynamic atomization spraying. *J R Soc Interface* **5**, 253-257 (2008).

109 Li, X. *et al.* A novel jet-based nano-hydroxyapatite patterning technique for osteoblast guidance. *J R Soc Interface* **7**, 189-197 (2010).

110 Munir, G. *et al.* The pathway to intelligent implants: osteoblast response to nano silicon-doped hydroxyapatite patterning. *J R Soc Interface* **8**, 678-688 (2011).

111 Puckett, S., Pareta, R. & Webster, T. J. Nano rough micron patterned titanium for directing osteoblast morphology and adhesion. *Int J Nanomed* **3**, 229-241 (2008).

112 Tamagawa, Y., Yatsuo, Y., Horikawa, H. & Iwasaki, M. Fine Patterning of Titanium Oxide Film Loaded with Hydroxyapatite Using Photopatterning and Anodic Oxidation. *Mater Trans* **51**, 2225-2229 (2010).

113 Yamaguchi, S., Yabutsuka, T., Hibino, M. & Yao, T. Generation of hydroxyapatite patterns by electrophoretic deposition. *J Mater Sci-Mater M* **19**, 1419-1424 (2008).

114 Zhao, C. C. *et al.* Designing ordered micropatterned hydroxyapatite bioceramics to promote the growth and osteogenic differentiation of bone marrow stromal cells. *J Mater Chem B* **3**, 968-976 (2015).

115 Wang, T. X. *et al.* Improve the Strength of PLA/HA Composite Through the Use of Surface Initiated Polymerization and Phosphonic Acid Coupling Agent. *J Res Natl Inst Stan* **116**, 785-796 (2011).

116 Suganuma, J. & Alexander, H. Biological Response of Intramedullary Bone

to Poly-L-Lactic Acid. *J Appl Biomater* **4**, 13-27 (1993).

117 Abboud, M., Turner, M., Duguet, E. & Fontanille, M. PMMA-based composite materials with reactive ceramic fillers .1. Chemical modification and characterisation of ceramic particles. *J Mater Chem* **7**, 1527-1532 (1997).

118 Wang, X. J., Li, Y. B., Wei, J. & de Groot, K. Development of biomimetic nano-hydroxyapatite/poly(hexamethylene adipamide) composites. *Biomaterials* **23**, 4787-4791 (2002).

119 Dorozhkin, S. V. Calcium orthophosphates. *J Mater Sci* **42**, 1061-1095 (2007).

120 Li, H. Y. & Chang, J. pH-compensation effect of bioactive inorganic fillers on the degradation of PLGA. *Compos Sci Technol* **65**, 2226-2232 (2005).

121 Liang, J. Z. Toughening and reinforcing in rigid inorganic particulate filled poly(propylene): A review. *J Appl Polym Sci* **83**, 1547-1555 (2002).

122 Urayama, H., Ma, C. H. & Kimura, Y. Mechanical and thermal properties of poly(L-lactide) incorporating various inorganic fillers with particle and whisker shapes. *Macromol Mater Eng* **288**, 562-568 (2003).

초 록

최근 마그네슘은 생체흡수성 재료에 대한 요구가 증가함에 따라 생체의료용 분야에 적합한 물질로 각광받고 있다. 인체에 무해하고 뼈와 유사한 기계적 강도를 지니고 있으며, 생체 내에서 분해가 가능하다는 점은 마그네슘의 가장 중요한 특징이다. 특히 상처받은 티슈가 회복됨에 따라 완전한 분해가 일어날 수 있다는 점은 주목할 만 하다. 하지만 이러한 긍정적인 특징에도 불구하고, 생체와 유사한 환경에서의 마그네슘의 빠른 부식속도는 임상 분야로의 실제적인 응용을 제한하고 있다. 그리하여 마그네슘의 부식 저항성을 조절하기 위한 수많은 연구가 진행되어 왔으며, 이들은 크게 합금화와 표면처리로 구분될 수 있다. 본 연구에서는 마그네슘의 표면처리를 심도 있게 다루었으며, 이는 표면처리 기법이 마그네슘의 부식저항성을 조절하는데 매우 효과적일 뿐 아니라 향상된 생체적합성 등의 부가적인 기능을 부여할 수 있다는 장점이 있기 때문이다. 하이드록시아파타이트 등의 생체적합성이 높은 물질을 코팅재료로 이용하면 부식 방지와 생체적합성 향상의 두 가지 목표를 모두 이룰 수 있다.

첫 번째 연구에서는 마그네슘 표면에 하이드록시아파타이트를 이용한 생체적합성과 부식저항성이 높은 코팅을 형성하고자 하였다.

하이드록시아파타이트는 칼슘과 인산염 재료가 포함된 수용액 내에서의 석출법을 통해 마그네슘의 표면에 코팅되었으며, 이는 재료의 생체 내, 그리고 생체 외의 부식저항성, 생체적합성, 그리고 뼈와의 반응성을 높이려는 데에 목적이 있었다. 바늘형태의 하이드록시아파타이트 결정으로 이루어진 코팅 층은 마그네슘 기판의 전 영역에 걸쳐 고르게 형성되었으며, 나사와 같은 복잡한 형상에도 잘 적용되었다. 이 하이드록시아파타이트 코팅 층은 생체 모방용액 내에서의 마그네슘의 부식속도를 효과적으로 낮추었다. 또한, 세포 부착, 증식, 분화 등의 생체 반응이 코팅을 한 시편에서 훨씬 향상된 수치를 나타내었다. 예비 동물실험에서도 역시 하이드록시아파타이트를 코팅한 시편에서 생체부식속도가 매우 낮게 제어되어, 향상된 기계적 안정성을 나타내었다. 그리고 하이드록시아파타이트가 코팅된 임플란트의 경우, 생체분해속도가 첫 6주간의 임플란트 기간 동안 효과적으로 제어되었으며, 이는 임플란트와 기존 뼈 사이에서의 새로운 뼈 형성양에 크게 기여하였다. 이러한 결과들을 통해, 하이드록시아파타이트를 마그네슘의 표면에 코팅하면 의료용 임플란트에 응용하기에 매우 용이하다는 것을 확인할 수 있다.

두 번째 연구에서는 표면 패터닝 공법을 도입하여, 생체적합성이 높고 부식을 막아 줄 뿐만 아니라 변형에도 효과적으로 견디는 코팅

층을 형성하고자 하였다. 첫 번째 연구에서 소개되었던 수용액 석출법과 포토리소그래피 공정을 적용하여 마이크로 단위로 패턴화된 하이드록시아파타이트와 폴리락틱에시드 코팅층을 마그네슘의 표면에 형성하였다. 10 마이크로미터의 지름을 가지는 하이드록시아파타이트 원형 패턴이 마그네슘의 표면에 잘 정렬되었으며, 이 원형 패턴 사이를 폴리락틱에시드가 채우고 있었다. 실제 임상과정과 유사한 환경을 구현하기 위하여, 하이드록시아파타이트와 폴리락틱에시드가 패턴화된 마그네슘에 5%의 인장변형을 가하였다. 하이드록시아파타이트나 폴리락틱에시드만 단독으로 코팅하였을 때에 비해, 패턴화된 코팅 층은 인장변형 하에서도 어떠한 균열이나 박리가 발생하지 않았으며, 이렇게 향상된 코팅 안정성은 마그네슘의 부식속도 제어에 효과적으로 기여하여 생체모방용액 내에서 부식산물인 수소기체가 거의 발생하지 않았다. 또한 하이드록시아파타이트나 폴리락틱에시드의 단독 코팅 층의 경우 인장변형 하에서 세포 부착이나 증식 등의 세포 반응성이 현저하게 떨어진 것에 반해 패턴화된 마그네슘은 매우 안정적으로 높은 세포 반응성을 유지하였다. 이러한 결과들을 통해, 하이드록시아파타이트와 폴리락틱에시드를 이용한 패턴을 마그네슘에 적용함으로써 실제 임상분야로의 실현가능성을 확인할 수 있었다.

세 번째 연구에서는 두 번째 연구를 통해 개발된

하이드록시아파타이트 패턴을 다른 재료, 예를 들면 폴리락틱에시드 등에 적용하는 방안에 대해 다뤘다. 하이드록시아파타이트 패턴이 폴리락틱에시드의 표면에 균일하게 정렬됨에 따라, 향상된 생체적합성은 자연스럽게 얻게 될 것이며 이 과정에서 폴리머 본연의 유연성은 영향을 받지 않을 것이다. 우선 두 번째 연구에 기술된 것과 같이 하이드록시아파타이트 패턴을 실리콘 기판 위에 형성 한 뒤, 이를 폴리락틱에시드 표면에 옮기는 방식으로 패턴을 형성하였다. 하이드록시아파타이트 분말을 섞은 폴리락틱에시드의 경우 재료의 강성도는 증가하고 전체 강도는 감소하는 등 기계적 물성이 전체적으로 저하된 것에 반해, 하이드록시아파타이트가 패턴화된 폴리락틱에시드는 순수 폴리락틱에시드와 비슷한 수준의 기계적 물성을 유지하였다. 또한 세포 부착과 증식 등의 세포 특성이 기존 폴리락틱에시드에 비해 월등히 향상되었다. 신기한 점은, 재료의 생체적합성이 패턴의 구조에 따라 다르게 나타났다는 것이다. 하이드록시아파타이트의 표면 노출 양을 고정하고 이 패턴의 지름 크기를 조절한 결과, 작은 지름을 가진 패턴에서 가장 향상된 생체적합성을 나타내었다. 이러한 결과들을 통해, 하이드록시아파타이트를 표면에 패턴화함으로써 재료의 세포특성을 효과적으로 조절할 수 있었음을 확인하였다.

주요어: 마그네슘, 하이드록시아파타이트 코팅, 폴리락틱에시드, 패터닝, 생체분해성, 생체적합성

학번: 2010-22756